SELECTION AND ENGINEERING OF DNA APTAMER BIOSENSORS FOR HIGH-THROUGHPUT SMALL-MOLECULE ENANTIOPURITY ANALYSIS

by

Trevor Alexander Feagin

A dissertation submitted to the faculty of
The University of Utah
in partial fulfillment of the requirements for the degree of

Doctor of Philosophy

Department of Chemistry

The University of Utah

December 2015

The University of Utah Graduate School

STATEMENT OF DISSERTATION APPROVAL

The dissertation of **Trevor Alexander Feagin**

has been approved by the following supervisory committee members:

Jennifer M. Heemstra	, Chair	**9/21/15** Date Approved
Joel M. Harris	, Member	**9/21/15** Date Approved
Haitao (Mark) Ji	, Member	**9/21/15** Date Approved
C. Dale Poulter	, Member	**9/21/15** Date Approved
Martin P. Horvath	, Member	**9/21/15** Date Approved

and by **Cynthia J. Burrows**, Chair/Dean of the Department/College/School of **Chemistry**

and by David B. Kieda, Dean of The Graduate School.

ABSTRACT

Nucleic acid aptamers are short oligonucleotides that can bind specifically to a wide range of targets, making them an analogue to the more widely known amino acid-based antibodies. Aptamers are selected from a random oligonucleotide library by a method called systematic evolution of ligands via exponential enrichment (SELEX), originally described in 1990. The purpose of this dissertation is to highlight new uses for aptamer biosensors, as well as new methods for their selection.

We envisioned that a high throughput enantiopurity assay using DNA aptamers (Chapter 2) would be especially powerful in the directed evolution of stereoselective enzymes. As a proof of concept, we used tyrosinamide to demonstrate our enantiopurity analysis method. However, as a compelling target for enzyme evolution, we were drawn to the molecule 2-chloromandelic acid (2-CMA), since it is a key intermediate in the synthesis of Clopidogrel (Plavix) and can be generated asymmetrically using engineered P450 enzymes. In order to select an aptamer for 2-CMA, we used several known bead-based SELEX methods (Chapter 3). While we were able to select for several aptamers using these methods, ultimately we found that conversion of these aptamers into structure switching biosensors was difficult. This inspired us to explore SELEX methods that could directly select for the required biosensor architecture. We initially explored bead-based structure-switching SELEX methodologies. These methods directly link the structure switching architecture to ligand binding. However, we found that we predominately obtained false positives using these methods.

Thus, we instead chose to explore capillary electrophoresis (CE) as our

separation method due to its high partitioning potential. Using a drag tag and complementary strand, we hypothesize that we will be able to directly select for structure switching aptamers using this method. This method offers the potential to remove the current bottleneck of our enantiopurity analysis method by allowing for rapid development of new structure-switching biosensors for targets of interest.

Chapter 4 describes the development of a scalable and cost-effective synthesis for the protected *N*-[2-(Fmoc)aminoethyl]glycine benzyl ester backbone for peptide nucleic acids (PNA). PNA has emerged as a promising alternative to the native nucleic acids DNA and RNA for a wide variety of applications, including antisense therapy and gene diagnostics.

To my Mom and Dad for their unwavering faith in me and my abilities and Vanessa Grace for holding me together and teaching me more than she could ever know

TABLE OF CONTENTS

APPENDICES

LIST OF ABBREVIATIONS

2-CMA	2-chloromandelic acid
A	adenine
Alm	alaninamide
BFS	bare fused silica
BHQ1	black hole quencher 1
C	cytosine
CAA	2-chlorophenylacetic acid
CD	circular dichroism
CE	capillary electrophoresis
CME	2-chloromandelic methyl ester
COA	2-chlorophenyloxalic acid
Cy3	cyanine 3
d	doublet (spectral)
DCM	dichloromethane
dd	doublet of doublet (spectral)
ee	enantiomeric excess
EOF	electroosmotic flow
FAM	fluorescein
FP	fluorescence polarization
g	gram(s)
G	guanine

Glm	glycinamide
h	hour(s)
HEX	hexachlorofluorescein
HPLC	high performance liquid chromatography
HTS	high-throughput screening
m	multiplet (spectral)
Me	methyl
MeOH	methanol
min	minute(s)
mol	mole(s)
MS	mass spectrometry
NMR	nuclear magnetic resonance
OEt	ethyl ester
p	pentet (spectral)
P450	Cytochrome P450 monooxygenase superfamily
PCR	polymerase chain reaction
PEG	polyethylene glycol
Phm	phenylalaninamide
PNA	peptide nucleic acid
ppm	parts per million
q	quartet (spectral)
Rf	retention factor (chromatography)
rt	room temperature
s	singlet (spectral)
(*S*)-CMA	(*S*)-2-chloromandelic acid

SELEX	systematic evolution of ligands by exponential enrichment
t	triplet (spectral)
T	thymine
TLC	thin layer chromatography
Tym	tyrosinamide

ACKNOWLEDGEMENTS

I am forever grateful for the incredible support from my research advisor, Prof. Jennifer M. Heemstra, without which I never would have realized this goal. Her support, guidance, inspiration, and enthusiasm for research and life helped me to grow as a scientist and person.

I would like to thank my committee members Prof. Joel Harris, Prof. Martin Horvath, Prof. Mark Ji, and Prof. Dale Poulter for their time, guidance, and support throughout my graduate career. I would also like to thank the Department of Chemistry and the University of Utah for providing me with financial support. I also extend my gratitude to the faculty and staff of the Department of Chemistry, especially Jo Hoovey and Katie Shelton.

I am grateful to the past and current members of the Heemstra group, Dr. Ashwani Sharma, Dr. Zhe Chen, Dr. Petre Simon, Tilani De Costa, Kirsten Meek, David Olsen, Amberlyn Peterson, Alex Rangel, Nick Spiropulos, Zhesen Tan, April Anamisis, Zach Headman, Alexandra Kent, and Evelyn Kimbrough. No one could have asked for a harder working, kinder, or more compassionate group with which to work.

I am thankful to have such a loving and supportive family. My brothers Chris, Ryan, Kevin, Ian, Toby, and Dustin have always been there for me, even in the darkest of times. I am particularly grateful to my parents, Dr. Steven and Norma Feagin, for the unconditional support and love that they always provided me with. They knew I could do it even when I didn’t. Last but not least, I am extremely grateful and indebted to Vanessa Chavez for being my best friend, partner, and for always being there for me.

CHAPTER 1

APTAMERS AS AFFINITY REAGENTS AND BIOSENSORS

Introduction

Nucleic acids encode the genetic information for all living organisms, and are unrivaled in their capacity to store and transmit this information. DNA in particular is highly stable, and mere picograms of material can store an entire genome. Additionally, nucleic acids have powerful self-recognition properties arising from Watson-Crick base pairing (Figure 1.1). By exploiting the unique recognition ability of DNA, researchers have developed DNA nanostructures that are capable of self-assembly into lattice structures.[1-2] Moreover, DNA-templated reactions have been used for a myriad of tasks, including small-molecule and protein detection. Further, the self-recognition ability of DNA has been shown to be an effective tool for the detection of abasic sites and other mutations within DNA. However, all of these systems have traditionally depended only upon the affinity of two complementary DNA strands for one another.

The excellent molecular recognition capabilities of nucleic acids can also be used for detecting non-nucleic acid targets, enabling the design of analytical biosensors. These biosensors are generally composed of an aptamer recognition element and a transducer, which converts physical or chemical changes into a measurable signal.

Aptamers are short nucleic acid sequences selected to have affinity for specific targets through an *in vitro* evolution process referred to as Systematic Evolution of Ligands via EXponential enrichment (SELEX) (Figure 1.2).[3-5] Since the discovery that nuc-

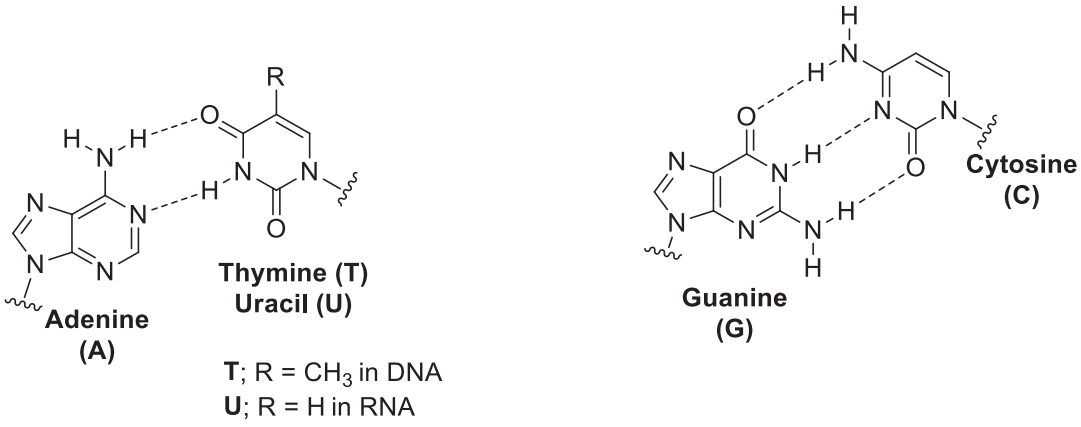

Figure 1.1. Watson-Crick base pairing.

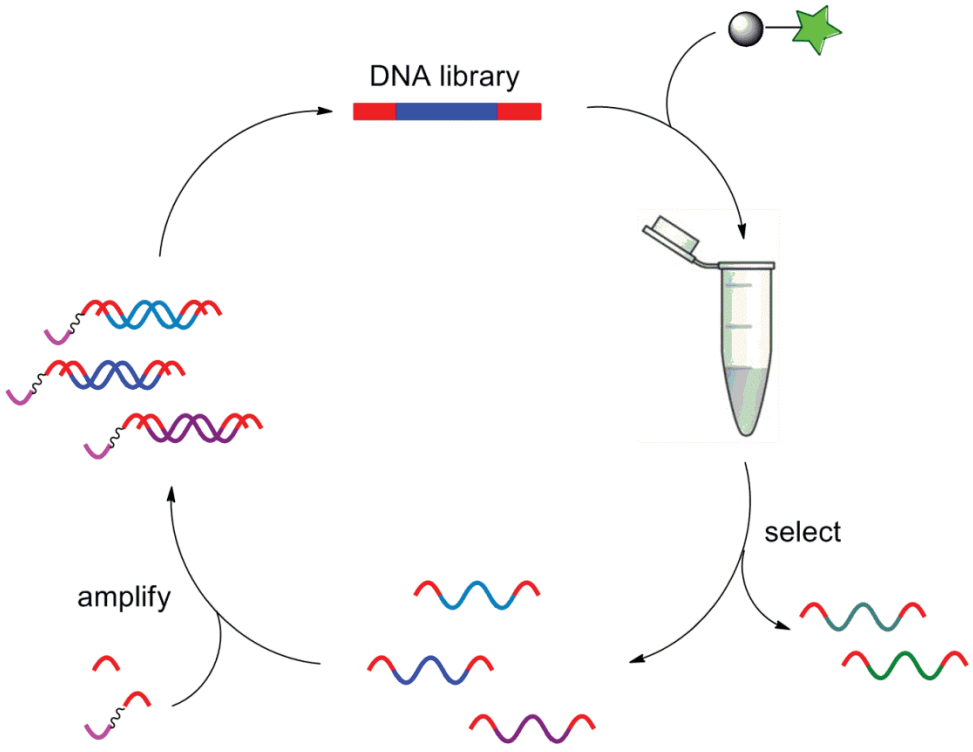

Figure 1.2. Target-bound SELEX cycle. Target (green star) is bound to a solid support and incubated with a random library containing primer binding sites. Target-bound library is collected and amplified through PCR using a PEG-T_{20}-modified reverse primer. Denaturing poly acrylamide gel electrophoresis is used for strand separation. The enriched library is now ready for another round or sequencing.

leic acids can serve as affinity reagents for non-nucleic acid targets, over 1000 papers have been published on their many uses in the detection of ligands, ranging from whole cells to small molecules. Aptamers are emerging as the affinity reagent of choice in many fields due to their ease of use, cost effectiveness, and reproducibility of their chemical synthesis and *in vitro* selection processes. Further, the versatility of these molecules has led to their rapid incorporation in new technologies. The state of the field regarding analytical applications of nucleic acid aptamers has been extensively reviewed.[6]

Nucleic Acid Aptamers

Aptamer-based biosensors can be classified by their mode of detection, which encompasses a variety of platforms, including fluorescence, colorimetric, electrochemical and mass-sensitive readouts.[6-7] The majority of these detection methods rely upon a conformational change of the aptamer upon target binding to induce signal transduction. This dissertation will predominately focus on fluorescence-based detection and the challenges involved in transforming an affinity reagent into a functioning biosensor.

Fluorescence-based aptamer assays typically involve fluorophore and quencher moieties that can undergo a change in their spatial orientation upon binding of the target molecule. Fluorescence detection is widely employed due to its rapid signal output, wide fluorophore variety, sensitivity, and ease of fluorophore attachment. Traditional molecular beacons utilize nucleic acid probes end-labeled with a fluorophore and quencher, which form hairpin structures resulting in quenching of the florescence. Upon hybridization with a complementary sequence, the beacon undergoes a conformation change that increases the distance between the fluorophore and quencher, resulting in an increase in fluorescence. Inspired by this design, Ellington and coworkers designed a thrombin-binding molecular aptamer beacon, for the detection of thrombin (Figure 1.3).[8] In the presence of thrombin, the aptamer undergoes a conformational change, resulting in an

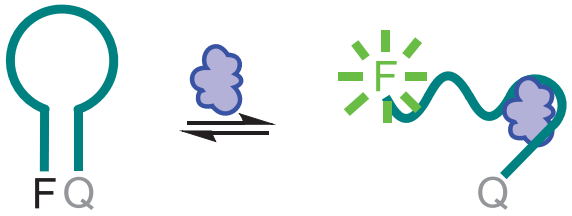

Figure 1.3. Molecular aptamer beacon. Introduction of target leads to a conformational change, resulting in an increase in fluorescence intensity.

increase in fluorescence signal. This system was able to detect thrombin at concentrations of less than 10 nM, showing that the process of converting the aptamer into a molecular beacon did not significantly decrease the binding affinity. However, this approach is far from generalizable, as many aptamers adopt random conformations in solution and the preorganization of the hairpin can therefore have detrimental effects on target binding. An alternate approach presented by Landry and coworkers utilized probes known as reverse aptamer beacons (Figure 1.4).[9] In this system, an aptamer sensitive to cocaine was end-labeled with a fluorophore and quencher. In the absence of target, the aptamer was shown to favor a random orientation in solution, and thus exhibited high fluorescence. Incubation with cocaine promoted aptamer folding, resulting in fluorescence quenching and the detection of cocaine down to 10 μM in blood serum. An extension of this system can be seen in recently developed split-aptamer biosensors.

Split-aptamers consist of two nucleic acid strands that only associate in the presence of a specific target. The two fragments can be labeled with a fluorophore and quencher, and in the absence of target, they will remain free in solution. Upon incubation with the desired target, the two fragments will assemble, resulting in fluorescence quenching. Szostak and coworkers demonstrated the first example of a split-aptamer for the detection of ATP (Figure 1.5).[10] Using structure prediction, the original ATP aptamer

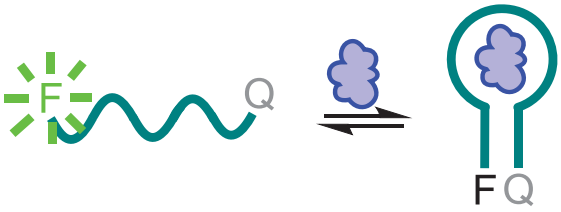

Figure 1.4. Reverse molecular aptamer beacon. Introduction of target leads to a conformational change resulting in formation of a structure stem loop producing a decrease in fluorescence intensity.

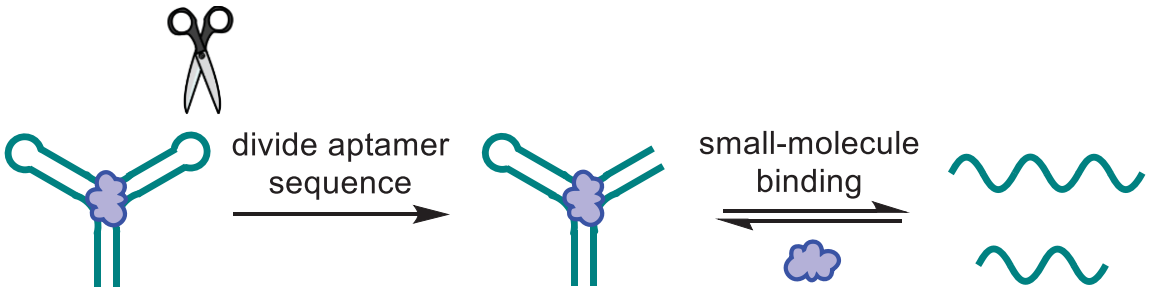

Figure 1.5. Design and function of a split-aptamer. The two split-aptamer fragments associate only in the presence of the target molecule.

was modified and split within a loop region to create this unique architecture. Limitations for split-aptamer systems stem from the delicate thermodynamic balance required to eliminate nonspecific assembly of the fragments. This limitation results in weakly forming complexes that generally have poor affinity for the target molecule, decreasing their sensitivity and thus their utility as analytical sensors. The Heemstra lab has pioneered a potential solution to this challenge by incorporating a covalent proximity ligation event upon the target-induced association of the split-aptamer fragments (Figure 1.6).[11] This system greatly increases the utility of split-aptamer technology through signal amplification, as each target molecule can induce the ligation of several aptamer-fragment pairs. Unfortunately, rational design of split-aptamers is a difficult task due to the complex binding and structural organization requirements needed to achieve selective assembly in the presence of the target.

In 2001, Li and coworkers recognized that none of the available approaches were generalizable to create aptamer biosensors for a wide variety of targets. Consequently they introduced the structure-switching aptamer as a potential solution to circumvent this issue. Structure-switching aptamers generally consist of a short displacement strand that is complementary to a region of an aptamer. The aptamer can be labeled with a fluorophore, while the displacement strand is functionalized with a quencher. In the absence of the target, the two strands hybridize, leading to low fluorescence. Upon introduction of the target molecule, the aptamer undergoes a conformational change that displaces the quencher strand, leading to dose-dependent fluorescence recovery (Figure 1.7). Li and coworkers showed the first proof of concept for structure-switching biosensors using the known ATP and thrombin aptamers.[12] This approach was seen as a highly generalizable method for converting any known aptamer into a biosensor, and structure-switching biosensor platforms have shown great promise for aptamers

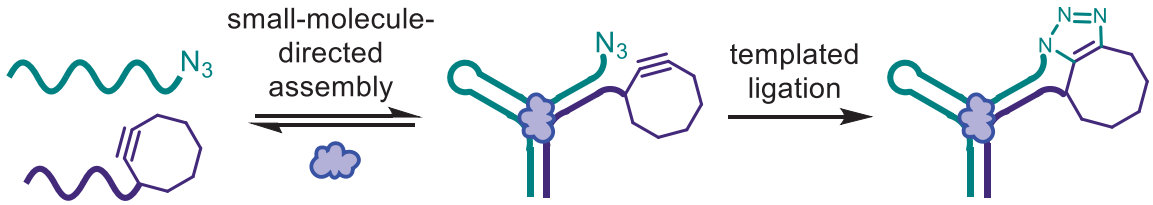

Figure 1.6. Split-aptamer covalent proximity ligation using strain promoted azide-alkyne click chemistry.

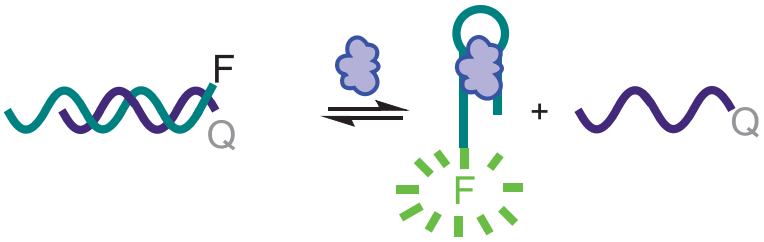

Figure 1.7. Structure-switching aptamer biosensor.

that undergo large conformational changes upon target binding. Unfortunately, while larger targets, like proteins, typically produce significant conformational changes upon binding to aptamers, small molecules generally lead to relatively small changes in the structure of the aptamer upon binding. This is likely due to the limited number of recognition elements and lack of physical bulk of small-molecule targets, which obviates the need for complex folding upon aptamer binding. As a result, only a handful of small-molecule-binding aptamers have been successfully converted to structure-switching biosensors in the 13-year time period since this system was first introduced.

Small-molecule-binding aptamers

The first law of directed evolution states that "You get what you screen for."[13] When performing traditional aptamer selections, the primary goals are high specificity and selectivity. These goals are often met for targets of all sizes, producing very robust affinity reagents. While it has become trivial to select aptamers that can perform as affinity reagents, converting these aptamers to biosensors remains a critical challenge. As previously described, the requirement of a significant conformational change is evident in all of the previously described sensor formats. Conformational changes are common for protein-binding aptamers, due to the target being larger than the aptamer, but it is only by chance that a small-molecule-binding aptamer undergoes a significant change in conformation upon target binding. The paucity of small-molecule-binding structure-switching aptamer sensors in the literature is testament to the challenges inherent in generating this architecture using traditional selection approaches.

According to the first law of directed evolution, the SELEX process must require a significant conformational change upon target binding to ensure that the resulting aptamers will display this property. Morse and coworkers proposed a novel selection method known as "structure-switching SELEX" that fulfills this requirement.[14] This method us-

es a short capture strand attached to a magnetic bead that is complementary to the 5' primer binding site of a random RNA library (Figure 1.8). This method only enriches sequences that are displaced from the capture strand upon target binding, thereby directly selecting for the structure-switching architecture. The requirement of displacement upon target binding was shown to simultaneously select for specificity, selectivity, and induction of an appropriate conformational change. Using this method, RNA aptamers selected for tobramycin were easily converted to structure-switching biosensors. Capture-SELEX is an alternative approach using DNA that was later demonstrated by Strehlitz and coworkers.[15] Instead of forcing the 5' primer binding site to be involved in aptamer binding like the Morse design, they placed the docking region within the random region of the library (Figure 1.9). This design was anticipated to allow for greater diversity in the library by distancing the aptamer binding events from the fixed primer binding sites of the library. This method was successfully used to select several aptamers for kanamycin A. Unfortunately, the authors did not test the ability of the aptamers to function as structure-switching biosensors, instead determining the binding affinities through a competitive elution approach. This competitive elution assay was performed similarly to the selections, by annealing each aptamer to magnetic beads coated in capture strand, followed by incubation with kanamycin A and quantification of the disassociation events via fluorescence. While our lab was able to successfully repeat the competitive elution assay from this paper, we were unable to successfully convert any of the aforementioned aptamers for kanamycin A to structure-switching biosensors. However, these selection methods provide a promising stepping stone for our efforts to reliably generate aptamers having the unique privileged structure-switching architecture.

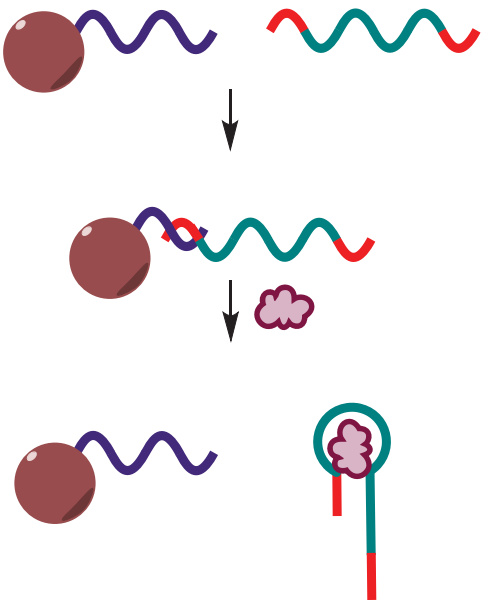

Figure 1.8. Library design for structure-switching SELEX.

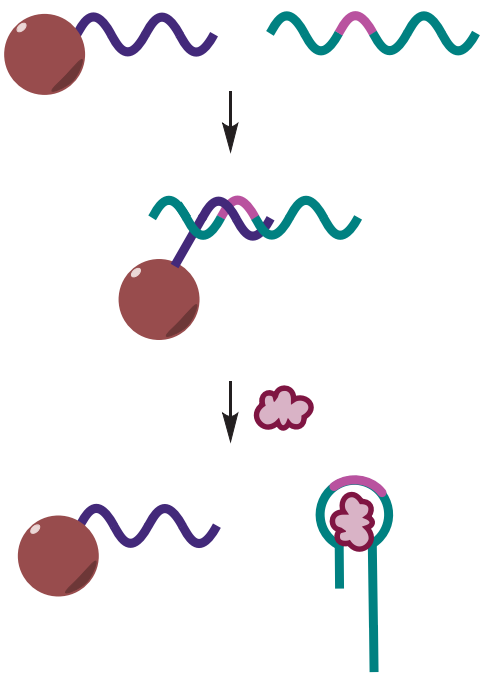

Figure 1.9. Library design for Capture-SELEX.

Objectives of This Dissertation

Since the discovery of Watson-Crick base pairing and the powerful recognition capabilities of nucleic acids, scientists have strived to realize the full potential of these fascinating biological molecules. Aptamers, which resulted from this scientific movement, are poised to overtake antibodies as the preferred choice for many biosensing applications. Unlike antibodies, aptamers can be chemically synthesized giving little to no batch-to-batch variation. Additionally, aptamers are selected through an *in vitro* process, allowing for a wider range of targets to be used. Although great strides have been made in the field of aptamer biosensor development for large targets, there is still a void in the literature for small-molecule-binding analogs. While new technologies for aptamer biosensors progress, their utility hinges on finding a generalizable, rapid, and robust method for their selection. This dissertation primarily focuses on advancing aptamer technologies and furthering the aptamer field as a whole by addressing this key limitation.

Chapter 2

Chapter 2 describes a novel screening method that explores a new application for structure-switching aptamer biosensors. This was accomplished through the use of orthogonal L- and D-DNA structure-switching biosensors to simultaneously measure both concentration and enantiopurity of mixtures of tyrosinamide enantiomers. Engineered enzymes can perform a myriad of chemical transformations with high enantioselectivity, but they must be discovered through extensive screening of enormous mutant libraries. The Heemstra lab recognized this as the key bottleneck to the progression of the field of biocatalysis, and therefore worked to design a rapid, simple method to increase the rate at which libraries may be screened.

Chapter 3

We hypothesized that if a SELEX method could be validated using an extremely small molecule with a limited number of functional groups, then this method would likely be capable of producing structure-switching aptamers for nearly any target. We investigated this in Chapter 3 by selecting aptamers for the small molecule (S)-2-chloromandelic acid (2-CMA) through modifications of known structure-switching SELEX methods and introduction of novel separation techniques utilizing capillary electrophoresis (CE). Our interest in 2-CMA was two-fold: first, it is an extremely difficult target for structure-switching aptamer selections and second, 2-CMA can be asymmetrically synthesized through the use of an enzymatic reaction that has yet to be made commercially viable due to insufficient stereoselectivity. The growing interest in new methods to efficiently screen enzyme-catalyzed reactions for enantiopurity makes 2-CMA a compelling target for our studies.

Chapter 4

The Heemstra lab is also interested in the development of technologies utilizing non-native nucleic acid backbones. Peptide nucleic acids (PNA) are of particular interest to the biological community due to their high nuclease stability and affinity for DNA and RNA. In working with PNA, we recognized a deficiency in the literature for a simple, scalable synthetic route to generate the protected backbone. As such, Chapter 4 demonstrates a novel synthetic route to synthesize the protected PNA backbone molecule.

References

(1) Seeman, N. C. DNA Engineering and Its Application to Nanotechnology. Trends Biotechnol. 1999, 17, 437–443.

(2) Seeman, N. C. Nucleic Acid Junctions and Lattices. J. Theor. Biol. 1982, 99, 237-247.

(3) Ellington, A. D.; Szostak, J. W. In Vitro Selection of RNA Molecules That Bind Specific Ligands. Nature 1990, 346, 818-822.

(4) Robertson, D. L.; Joyce, G. F. Selection in Vitro of an RNA Enzyme That Specifically Cleaves Single-Stranded DNA. Nature 1990, 344, 467-468.

(5) Tuerk, C.; Gold, L. Systematic Evolution of Ligands by Exponential Enrichment: RNA Ligands to Bacteriophage T4 DNA Polymerase. Science 1990, 249, 505-510.

(6) Liu, J.; Cao, Z.; Lu, Y. Functional Nucleic Acid Sensors. Chem. Rev. 2009, 109, 1948-1998.

(7) Song, S.; Wang, L.; Li, J.; Fan, C.; Zhao, J. Aptamer-Based Biosensors. Trends Anal. Chem. 2008, 27, 108-117.

(8) Hamaguchi, N.; Ellington, A.; Stanton, M. Aptamer Beacons for the Direct Detection of Proteins. Anal. Biochem. 2001, 294, 126-131.

(9) Stojanovic, M. N.; de Prada, P.; Landry, D. W. Aptamer-Based Folding Fluorescent Sensor for Cocaine. J. Am. Chem. Soc. 2001, 123, 4928-4931.

(10) David E. Huizenga, J. W. S. A DNA Aptamer That Binds Adenosine and Atp. Biochemistry 1995, 34, 656-665.

(11) Sharma, A. K.; Heemstra, J. M. Small-Molecule-Dependent Split Aptamer Ligation. J. Am. Chem. Soc. 2011, 133, 12426-12429.

(12) Nutiu, R.; Li, Y. Structure-Switching Signaling Aptamers. J. Am. Chem. Soc. 2003, 125, 4771-4778.

(13) Schmidt-Dannert, C.; Arnold, F. H. Directed Evolution of Industrial Enzymes. Trends Biotechnol. 1999, 17, 135-136.

(14) Morse, D. P. Direct Selection of RNA Beacon Aptamers. Biochem. Biophys. Res. Comm. 2007, 359, 94-101.

(15) Stoltenburg, R.; Nikolaus, N.; Strehlitz, B. Capture-Selex: Selection of DNA Aptamers for Aminoglycoside Antibiotics. J. Anal. Met. Chem. 2012, 2012, 14.

CHAPTER 2

ENANTIOSELECTIVE APTAMER BIOSENSORS FOR THE HIGH-THROUGHPUT SCREENING OF ENZYME-MEDIATED REACTIONS[1]

Introduction

Biological systems are exquisitely adept at producing small organic molecules with high stereoselectivity, as different stereoisomers of a molecule can illicit markedly different biological effects.[1] Achieving high stereoselectivity plays an equally important role in many applications of synthetic organic chemistry, as the target molecules are often intended to interact with biological systems, for example in the case of small-molecule therapeutics. Asymmetric catalysis has proven to be a revolutionary technology for the stereoselective synthesis of small molecules,[2] and high-throughput screening (HTS) can be used to accelerate the optimization of reaction conditions for a particular synthetic transformation.[3-10] In HTS, reaction conditions including catalyst, solvent, and temperature can be sampled combinatorially, and the implementation of robotics enables a large number of reactions to be run in parallel. However, the analysis of these reaction mixtures for yield and stereoselectivity remains a severe bottleneck that hinders the discovery of improved catalysts and reaction conditions.

Chemical reactions that produce a mixture of enantiomers pose an especially

---

[1]Adapted under the terms of the Standard ACS AuthorChoice/Editors' Choice usage agreement from Feagin, T. A.; Olsen, D. P. V.; Headman, Z. C.; Heemstra, J. M. High-Throughput Enantiopurity Analysis Using Enantiomeric DNA-Based Sensors. *J. Am. Chem. Soc.* **2015** *137,* 4198

challenging analysis problem, as enantiomers have nearly identical physical properties. The current gold standard for measuring yield and enantiopurity is chiral high performance liquid chromatography (HPLC). However, even under optimized conditions, HPLC is only capable of analyzing approximately 800 samples per day.[11-12] A large number of alternative analysis platforms have been explored, including gas chromatography (GC),[13] capillary electrophoresis (CE),[14-16] circular dichroism (CD),[17-19] infrared thermography,[20] mass spectrometry (MS),[21-22] and enzymatic methods.[23] Notably, new MS methods have been developed that enable the analysis of up to 10,000 samples per day,[22] but even this level of throughput is not sufficient to scan the vast libraries of reaction mixtures that can plausibly be generated in catalyst development and reaction optimization.[3] Moreover, many of these methods can accurately analyze enantiopurity, but provide little information regarding reaction yield.

In contrast to the analysis platforms listed above, fluorescence-based methods have potential to enable exceptionally high throughput, as a 1,536-well plate can be analyzed in less than 1 minute.[24] A number of laboratories have reported elegant approaches for fluorescence-based enantiopurity analysis of small molecules containing specific functional groups, such as α-hydroxycarboxylates, diols, and carboxylic acids.[25-27] We envisioned the development of a complementary approach in which a single small-molecule target (or small handful of structurally similar targets) can be rapidly analyzed for enantiopurity, but without the requirement for specific functional groups. While this approach may find limitations for use in the development of new reaction methodologies, where large substrate scope is beneficial, it is ideal for use in reaction development for high-value compounds, such as pharmaceuticals and their synthetic intermediates. In the latter case, a tremendous amount of effort is focused on the development of optimized reaction conditions for a single molecule or small subset of molecules, and thus achieving high throughput takes priority over substrate scope.

Our approach to high-throughput enantiopurity analysis relies on molecular recognition of the target molecule using a DNA aptamer. Aptamers are short nucleic acid sequences that can be generated *in vitro* to bind a wide range of targets including small molecules, proteins, and cell types.[28-30] Importantly, because aptamers are generated *in vitro*, negative selections can be utilized to increase substrate selectivity, and aptamers have been reported which bind to one enantiomer of a small molecule with greater than 10,000:1 selectivity over the opposite enantiomer.[31] In utilizing aptamers for high-throughput enantiopurity measurement, the first key element to our approach is the concept of reciprocal chiral substrate selectivity. DNA is a chiral molecule, and thus if a native D-DNA aptamer binds selectively to one enantiomer of a small molecule, then by definition, the same aptamer sequence synthesized from non-native L-DNA (referred to as the Spiegelmer from the German word “Spiegel” meaning “mirror”)[32-35] will bind to the opposite enantiomer of the small molecule with identical selectivity and affinity (Figure 2.1a-b).

The second key element to our approach is the ability of nucleic acid aptamers to transduce the presence of a specific molecule into a dose-dependent fluorescence output. This can be achieved in a number of formats,[36] and for our enantiopurity analysis approach, we chose to utilize what is arguably the most straightforward of these formats, the structure-switching biosensor.[37-38] In the structure-switching biosensor format, a short complementary strand is hybridized to the aptamer via Watson-Crick base pairing. However, in the presence of the target molecule, the aptamer preferentially binds to the target, displacing the complementary strand. If the aptamer and complementary strand are labeled with a fluorophore and quencher respectively, then the target ligand will produce a dose-dependent increase in fluorescence signal.

Applying the concept of reciprocal chiral substrate selectivity to structure-switching biosensors, we designed a system in which the D- and L-DNA biosensors are

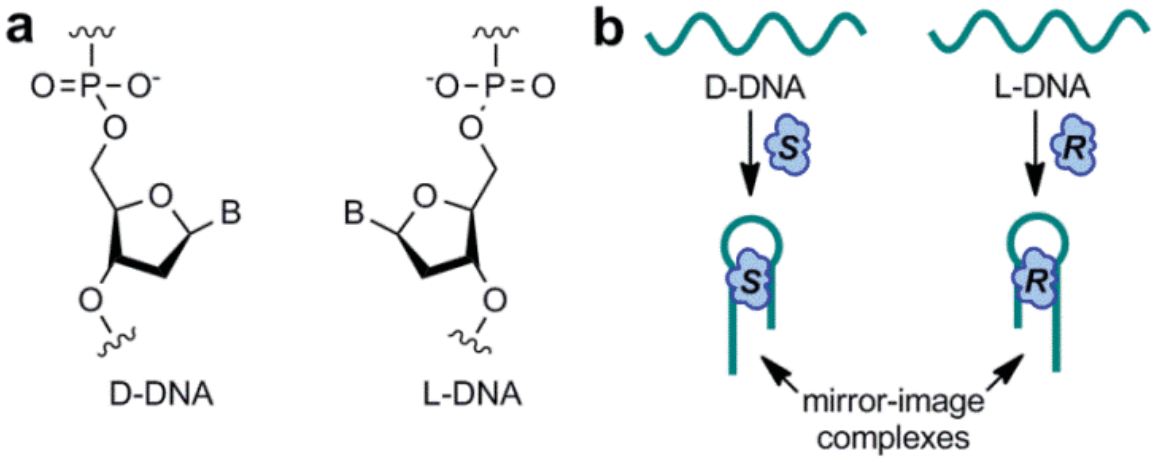

Figure 2.1. DNA enantiomers (a) Chemical structures of native D-DNA and enantiomeric L-DNA (Spiegelmer). (b) In accordance with the principle of reciprocal chiral substrate selectivity, D- and L-DNA aptamers will bind to opposite enantiomers of a small-molecule target with equal affinity and selectivity to give mirror-image complexes.

synthesized having orthogonal fluorophores (Figure 2.2a). These enantiomeric sensors can then be added together to a solution of the target molecule, and two-color fluorescence measurement used to provide the concentration of each enantiomer of the target, in turn providing both yield and enantiopurity. We note that upon addition of different fluorophores to the D- and L-DNA biosensors, these complexes are no longer perfect enantiomers. However, we find that this subtle difference in chemical structure has only a minor impact on the performance of the biosensors, and does not alter their ability to behave according to the concept of reciprocal chiral substrate selectivity. Thus, while the D- and L-DNA biosensors in our study are not true enantiomers, for simplicity we will refer to them as enantiomeric.

Using the previously reported structure-switching biosensor for L-tyrosinamide (L-Tym), (Figure 2.2b)(Table 2.1),[39] we demonstrate here the ability to rapidly and accurately measure both enantiopurity and concentration for mixtures of L- and D-Tym. To demonstrate the utility of this approach, we apply our enantiomeric biosensors to the optimization of reaction conditions for the synthesis of D-Tym. We demonstrate that our fluorescence-based approach not only allows rapid screening of multiple conditions and reaction time-points, but has potential to enable near real-time analysis. We also provide mathematical analysis to suggest that structure-switching biosensors having only modest binding selectivity can also be used for fluorescence-based enantiopurity measurement. Together, this research provides a novel method for the high-throughput analysis of enantiopurity that can be adapted for use with a diverse array of small-molecule targets and has potential to enable screening of ~10^5-10^6 reaction mixtures per day. Achieving this high level of throughput in a generalizable format is anticipated to significantly accelerate reaction optimization for the synthesis of high-value chiral small molecules.

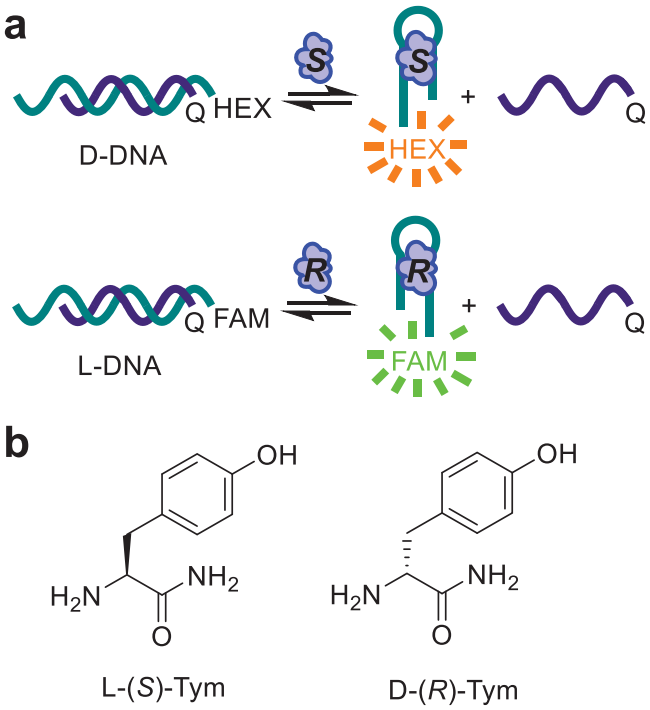

Figure 2.2. Biosensor design and target (a) Enantiomeric structure-switching biosensors are functionalized with orthogonal fluorophores, enabling simultaneous quantification of both enantiomers of the target molecule. HEX = hexachlorofluorescein; FAM = fluorescein. (b) Chemical structures of L- and D-Tym.

Table 2.1. Sequences of the aptamer and complementary strands tested during biosensor optimization. The underlined region of the aptamer indicates the complementary strand binding site.

Name	Sequence (5'-3')
aptamer	FAM/HEX-TGGAGCTTGGATTGATGTGGTGTGTGAGTGCGGTGCCC
CS-09	CACATCAAT-BHQ1
CS-10	CACATCAATC-BHQ1
CS-11	CACATCAATCC-BHQ1
CS-12	CACATCAATCCA-BHQ1

Results and Discussion

To demonstrate the utility of our enantiopurity analysis method, we utilized the previously reported DNA aptamer for L-Tym. This aptamer was first reported by Gatto and coworkers in 2001,[40] and in 2011, was elaborated into an structure-switching biosensor by Peyrin and coworkers.[39] The structure-switching biosensor developed by Peyrin was utilized for L-Tym detection by fluorescence polarization (FP), so the aptamer was unfunctionalized, and the complementary strand was labeled with a fluorophore. For our biosensing format, we instead functionalized the termini of the aptamer and complementary strand with a fluorophore and quencher, respectively, to enable small-molecule quantification using a standard fluorescence plate reader.

Identifying an appropriate fluorophore pair

For our orthogonal fluorophores to be used on the D- and L-DNA aptamers, we initially chose fluorescein (FAM) and cyanine 3 (Cy3). However, initial results showed that the Cy3 biosensor had a K_{sens} value (defined as the ligand concentration at which half of the aptamer strands are dehybridized from their complementary strands) 2-fold higher than that of the FAM biosensor. Similar results demonstrating the differential impact of cationic and anionic dyes on aptamer-complementary strand binding have been reported by Peyrin and coworkers.[39] Therefore, in refining our enantiomeric dual biosensors, we sought to use dyes having similar chemical properties, as this was hypothesized to result in biosensors having similar K_{sens} values. We found that hexachlorofluorescein (HEX) and FAM were an ideal fluorophore pair for our dual biosensors, as these fluorophores have very similar electronic and structural properties, and have excitation/emission maxima of 524/572 nm (HEX) and 490/520 nm (FAM), making them spectrally orthogonal. Furthermore, Black Hole quencher 1 (BHQ1) effectively quenches both FAM and HEX, minimizing the difference in chemical modifications. To validate the

orthogonality of our fluorescent biosensors, we carried out an experiment in which solutions were prepared having the D-DNA aptamer functionalized with HEX, the L-DNA aptamer functionalized with FAM, or an equal mixture of the two aptamers. All samples were analyzed for fluorescence intensity using excitation/emission wavelengths of 490/520 nm and 524/572 nm, and we observed significant signal above background for each biosensor using its target wavelengths, but no signal was detectible above background when using the off-target wavelengths (Table 2.2). Thus, we decided to utilize HEX-BHQ1 and FAM-BHQ1 as our fluorophore-quencher pairs in all subsequent structure-switching biosensors.

Biosensor design and optimization

Our first consideration in biosensor optimization was to screen buffer conditions for those that provided the highest selectivity and lowest fluorescence background. We used the conditions reported by Peyrin as a starting point for optimization, but found that for our assay, a higher ionic strength was beneficial. This optimized binding buffer (10 mM Tris-HCl, 100 mM NaCl, 5 mM KCl, 2 mM MgCl2, 1 mM CaCl2, pH 7.5) was used for all of the following experiments.

It is well established that the length and binding position of the complementary strand can have a large impact on the hybridization and ligand binding characteristics of structure-switching biosensors,[41] and a number of complementary strand sequences have previously been tested for use with the L-Tym aptamer in CE and FP experiments.[16, 39] Based upon these previous reports, we synthesized and tested four BHQ1-labeled complementary strands having various lengths (Table 2.1). Each of these complementary strands were incubated with HEX-labeled L-Tym (D-DNA) aptamer and increasing concentrations of L-Tym. After allowing 20 minutes for equilibration, the percent displacement (%D) for each biosensor was calculated using equation 1.1 in which F

is the measured fluorescence, F_0 is the fluorescence of the biosensor in the absence of ligand, and F_m is the fluorescence of the aptamer alone.

(Eq 2.1) $$\%D = \left(\frac{F-F_0}{F_m-F_0}\right) * 100$$

We compared %D values for the different complementary strand sequences to determine which sequence provided the greatest signal-to-noise ratio across a wide range of ligand concentrations. Of those tested, we found that CS-09 showed the best signal-to-noise ratio at 25 ºC (Figure 2.3).

The concentrations and stoichiometry of the aptamer and complementary strand can also have a dramatic impact on K_{sens}, as these factors influence the position of equilibrium for hybridization of the two DNA strands, which is in direct competition with the equilibrium of ligand binding. Therefore, to optimize aptamer and complementary strand concentrations and stoichiometry, we first prepared 6 solutions of the D-DNA biosensor having a 1:1 aptamer:complementary strand stoichiometry, but having concentrations of each strand varying from 30 nM to 1 μM. A binding isotherm for hybridization of the aptamer and complementary strand was produced by plotting the concentration versus percent displacement (Figure 2.4).

At lower concentrations, high background fluorescence was observed, presumably because equilibrium favors dehybridization of the aptamer and complementary strand. However, calculations from our binding isotherm indicated that at 500 nM, approximately 90% of the aptamer strands were hybridized to a complementary strand. We reasoned that this approximate level of hybridization would be suitable for our enantiopurity assay, as the majority of biosensors are assembled, minimizing background and maximizing potential signal gain. However, the presence of a small number of disassembled biosensors suggests that the mixture is perched at an equilibrium where small perturbations in the energetics of the system (e.g., through the introduction of target

Table 2.2. Demonstrating orthogonality of FAM and HEX. Table shows values for relative fluorescence intensity.

excitation/emission wavelength	FAM	FAM/HEX	HEX
490/520 nm	72589	75052	81
524/572 nm	228	79944	88050

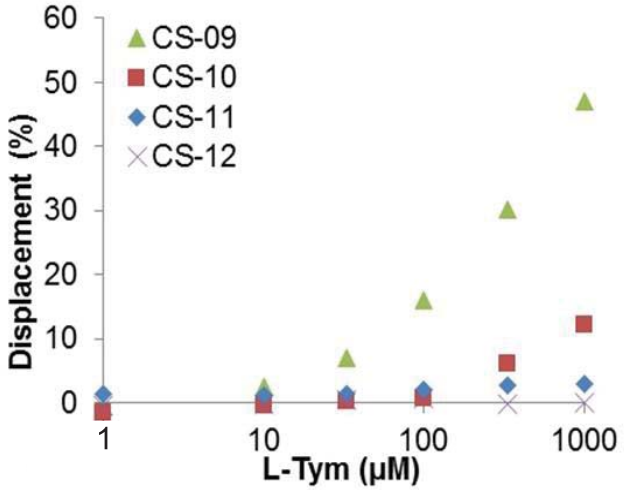

Figure 2.3. Complementary strand length strongly impacts the responsiveness of the structure-switching biosensor. CS-09 was chosen for all subsequent enantiopurity analysis experiments.

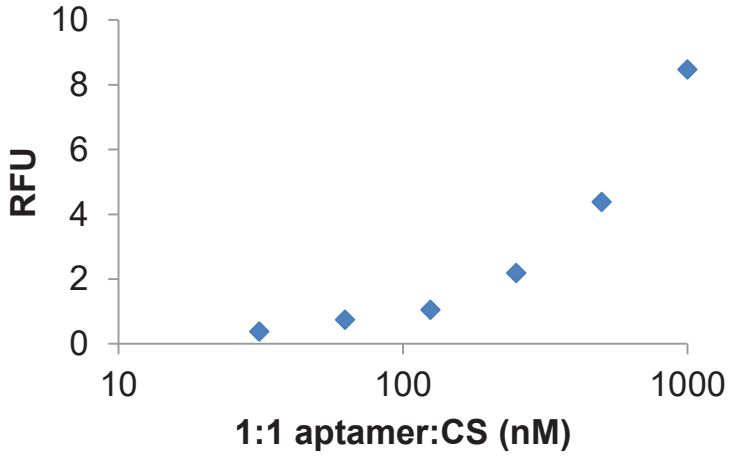

Figure 2.4. Optimizing concentration for aptamer and complementary strand.

ligand) are likely to produce large shifts in the ratio of assembled:disassembled biosensors, and thus fluorescence signal.

In addition to optimizing concentration, we also systematically investigated the effect of aptamer:complementary strand stoichiometry on signal-to-background ratio. Similar to overall concentration, varying the stoichiometry of the aptamer and complementary strand shifts the equilibrium for assembly of the biosensor, and thus impacts both background and signal gain. Five samples were prepared having 500 nM aptamer and a 1:1, 1:1.5, 1:2, 1:2.5, or 1:3 aptamer:complementary strand ratio. Each sample was tested with increasing L-Tym concentrations, and we found that the 1:2.5 ratio provided the highest level of reproducibility. While 1:1 to 1:2.0 gave greater overall signal response, they were found to be less reproducible than 1:2.5 producing higher noise at low target concentrations (Figure 2.5). Thus, we identified 500 nM aptamer and 1.25 μM complementary strand as the ideal concentrations for use in our enantiopurity assays.

Enantioselectivity and specificity of biosensors

Having optimized the sequences and concentrations of the structure-switching biosensors, we next turned to analyzing target binding selectivity. First, the biosensors were individually tested for binding to L- and D-Tym. The data in Figure 2.6a-b illustrate that the biosensors bind to Tym with a high degree of enantioselectivity, as fluorescence signal was observed for the target enantiomer at concentrations as low as 3-10 μM, but no binding of the off-target enantiomer was detected up to 1 mM. To test the effect of side chain structure on aptamer binding, glycinamide (Glm), racemic alaninamide (Alm), and both L- and D-phenylalaninamide (L-Phm and D-Phm) were incubated with the biosensors and fluorescence intensity measured (Figure 2.6c-d). Glm and Alm were chosen because they are the least-functionalized non-chiral and chiral amino amides, respectively. Thus, binding information for these molecules would reveal the role of the phenyl

side chain and chiral center in aptamer recognition. No signal was observed for either of these targets at concentrations up to 1 mM, suggesting that the phenyl side chain is critical to aptamer binding. In contrast, L- and D-Phm were found to bind enantioselectively to the structure-switching biosensors, showing a similar trend to L- and D-Tym, but with a weaker binding affinity. We interpret this result to indicate that the hydroxyl functionality of Tym likely interacts with the aptamer via a hydrogen bonding interaction, and that this interaction strengthens, but is not critical to target binding. Finally, the importance of the amino amide functionality was investigated using L- and D-tyrosine ethyl ester (L-Tyr-OEt and D-Tyr-OEt). As selectivity for Tym over Tyr-OEt is necessary for the reaction monitoring experiments described below, we were pleased to observe no signal for L- or D-Tyr-OEt at concentrations up to 1 mM. Collectively, these data indicate that the chirality, phenyl side chain, and amide functionality all play critical roles in binding of the aptamer to the target, and the presence of a hydroxyl group on the phenyl ring enhances the strength of the aptamer-target binding interaction.

In principle, enantiomeric D- and L-DNA biosensors should bind to opposite enantiomers of a given small-molecule target with identical K_{sens} values. However, the data in Figure 2.6 show that the L-DNA biosensor consistently gives slightly smaller % displacement values compared to the D-DNA biosensor.

We hypothesize that this difference arises from the fact that our biosensors are not perfectly enantiomeric. The FAM and HEX fluorophores, while carefully selected, have different electronic properties, which can impact binding of the aptamer to the displacement strand, leading to differences in target-dependent displacement. However, it is important to note that we use calibration curves as described below to solve for the concentration of each enantiomer. Thus, these subtle differences in biosensor response will not impact the accuracy of our enantiopurity measurements.

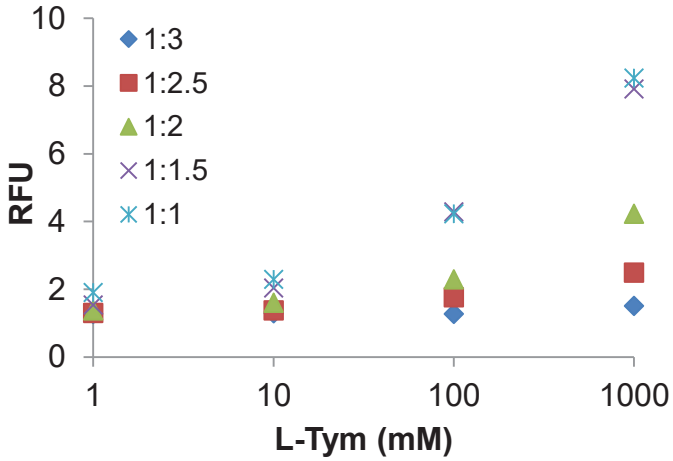

Figure 2.5. Optimizing stoichiometry for aptamer and complementary strand.

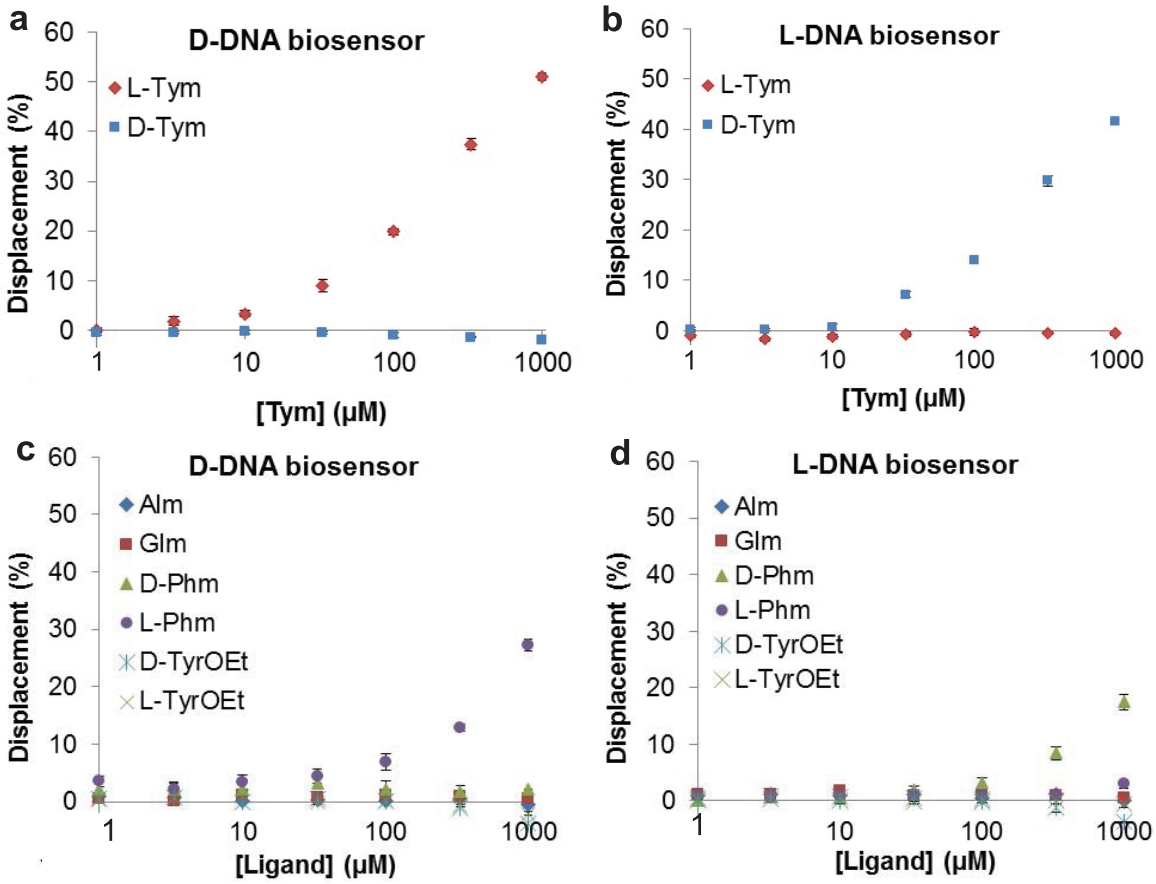

Figure 2.6. Fluorescence response of (a) D-DNA and (b) L-DNA biosensors to L- and D-Tym. Fluorescence response of (c) D-DNA and (d) L-DNA biosensors to structurally related compounds. All data represent an average of three trials.

Enantiopurity analysis for mixtures of L- and D-Tym

As seen in Figure 2.6a-b, the fluorescence response of the structure-switching biosensors follows a Langmuir isotherm. This is to be expected, as the fluorescence signal results from an equilibrium binding interaction between the aptamer and the target. Thus, we reasoned that by maintaining substrate concentrations below saturation, we could construct calibration curves to enable quantitative analysis of unknown samples. Importantly, the use of % displacement instead of raw fluorescence intensity enables the calibration curve to be applied across samples analyzed on different days and potentially on different pieces of instrumentation.

To construct the calibration curves, the L- and D-DNA biosensors were combined together in a single solution and incubated with varying concentrations of L- and D-Tym. In each solution, the total Tym concentration was held at constant at 500 μM, and the D:L ratio of the Tym was systematically varied from 100:0 to 0:100. Each solution was analyzed using excitation/emission wavelengths of 490/520 nm and 524/572 nm to determine % displacement of the FAM and HEX biosensors, respectively (Figure 2.7a). We were encouraged to observe that in both of the solutions containing only a single enantiomer of Tym (0 and 100% L-Tym in Figure 2.7a), the off-target biosensor showed no detectable signal. This further validates the excellent binding selectivity of the aptamer and the lack of fluorescence cross-talk between the FAM and HEX fluorophores. The resulting calibration curves were each fit to a Langmuir binding isotherm using OriginPro. The K_{sens} values for the D- and L-DNA structure-switching biosensors were calculated to be 442 ± 28 μM and 464 ± 29 μM, respectively. These values are significantly higher than the K_{sens} of 160 μM reported for the Peyrin fluorescence polarization biosensor, likely due to the higher ionic strength of the binding buffer used in our experiments. However, given our proposed application of organic reaction monitoring, where typical substrate concentrations are in the high mM range, the higher K_{sens} values for our biosensors were

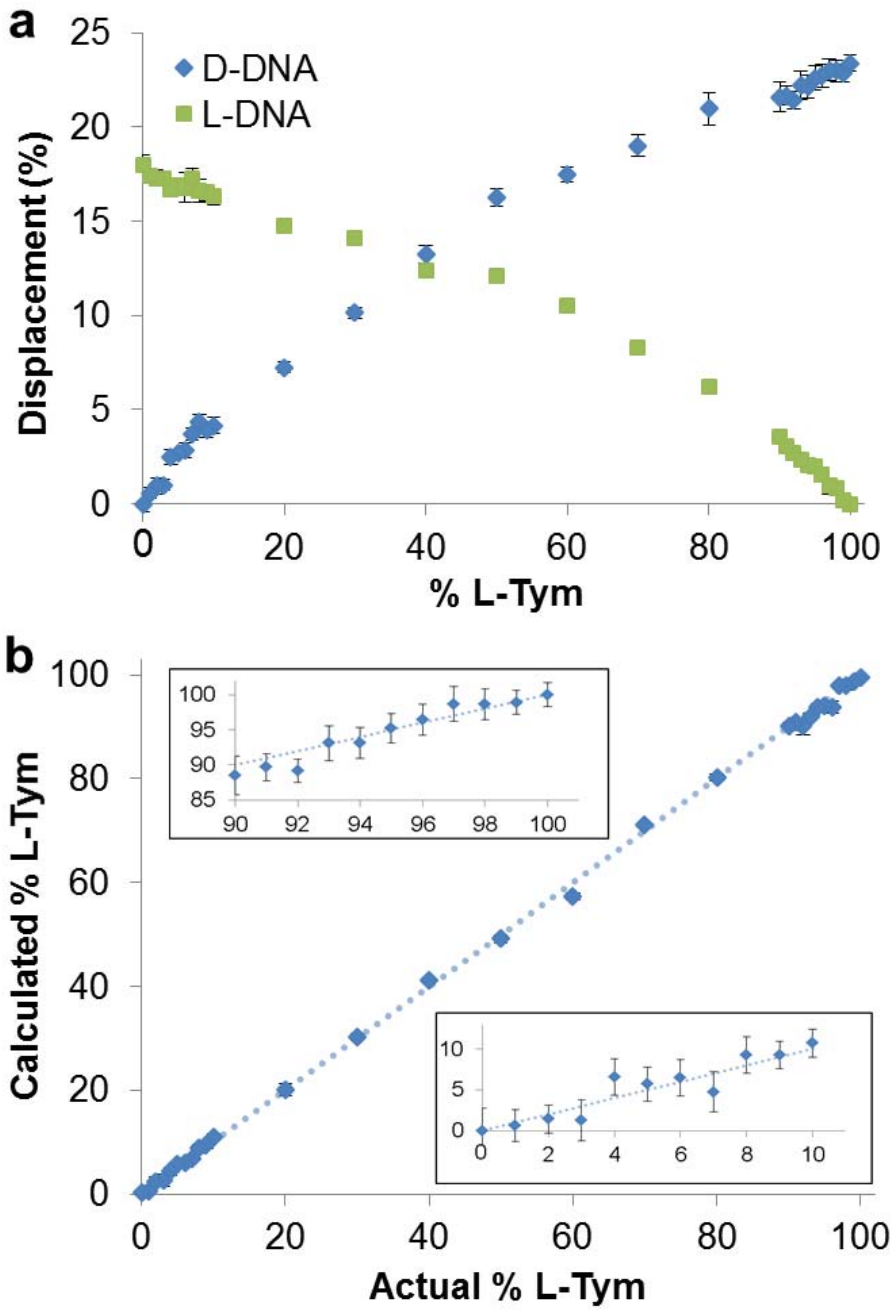

Figure 2.7. Dual biosensor results (a) Enantiopurity analysis of samples having varying ratios of L/D-Tym. All samples had a total Tym concentration of 500 μM. Curves were fit to langmuir isotherms. Equations and R^2 values can be found in Appendix A. (b) Comparison of calculated vs actual % L-Tym.

not anticipated to be problematic.

To test the accuracy of our calibration curve fitting, we used the resulting Langmuir equation to independently calculate the % L for each Tym mixture. Figure 2.7b compares the calculated vs. actual values of % L-Tym. The deviation between calculated and actual values of % L-Tym ranged from 0-2.2%, with an average deviation of 0.66%. The error bars on each measurement are calculated from the standard deviation of 3 independent fluorescence experiments, and range from 0.17-1.64% with an average error of 0.71%. Together, these data establish a high level of accuracy and reproducibility for our enantiopurity analysis method.

Analysis of reaction conditions and progress

To validate the utility of our enantiopurity analysis method, we chose to apply it to optimization and monitoring of the synthesis of Tym from Tyr-OEt. The importance of reaction optimization for this particular transformation became apparent during our initial experiments using the Tym biosensors. We had set out to synthesize D-Tym using a literature protocol, but observed anomalous results when our “D-Tym” was tested with the structure-switching biosensors. Analysis of our small-molecule product using chiral chromatography revealed that a significant degree of racemization had occurred using the reaction conditions reported in the literature (stirring in NH_4OH for 48 hours at 4 ºC).[42] We hypothesized that this racemization could be suppressed by reducing reaction time, but this would come with the trade-off of reduced yields, and thus optimization would be of high utility.

One unique benefit of calculating enantiopurity from the absolute concentration of each enantiomer is that it also enables simultaneous monitoring of reaction yield. Moreover, our method requires only that a sample from a reaction mixture be diluted into buffer containing the enantiomeric structure-switching biosensors, incubated to allow for

equilibration, and analyzed on a fluorescence plate reader. In our experiments, these manipulations required approximately 25 minutes, but this time could likely be significantly reduced by shortening the equilibration period. Thus, our method has potential to allow for near real-time monitoring of reaction mixtures.

To demonstrate the utility of our biosensors for monitoring the conversion of D-Tyr-OEt to D-Tym, we reacted D-Tyr-OEt with ammonium hydroxide at four temperatures ranging from 10-50 °C. While these temperatures are higher than those in the initially reported literature conditions, we reasoned that these conditions warranted investigation, as it was possible that racemization could be minimized by utilizing shorter reaction times, without negatively impacting yield. For each reaction, 100 µL aliquots were removed at 16 time points over the course of 2 hours, diluted to 10 mL with binding buffer containing both structure-switching biosensors, and analyzed using a fluorescence plate reader. The % displacement was calculated for each biosensor, and these values were used to independently solve for the concentration of each enantiomer of Tym using our calibration curves.

A plot of the % yield of each enantiomer as a function or time for each of our four reaction temperatures is shown in Figure 2.8. These data reveal that while increasing the temperature of the reaction increases the rate of product formation, it also increases the rate of epimerization. However, by reducing the reaction temperature to 10 ºC, D-Tym can be generated in modest, though reasonable, yield with no observable epimerization after 2 hours.

To validate the accuracy of our enantiopurity measurements, we employed chiral HPLC to analyze all of the samples from the reaction carried out at 50 ºC. We initially attempted to identify HPLC conditions that would enable baseline resolution of L- and D-Tym, but despite surveying a large number of solvent systems with multiple chiral columns, we were unable to achieve sufficient resolution. However, we were able to

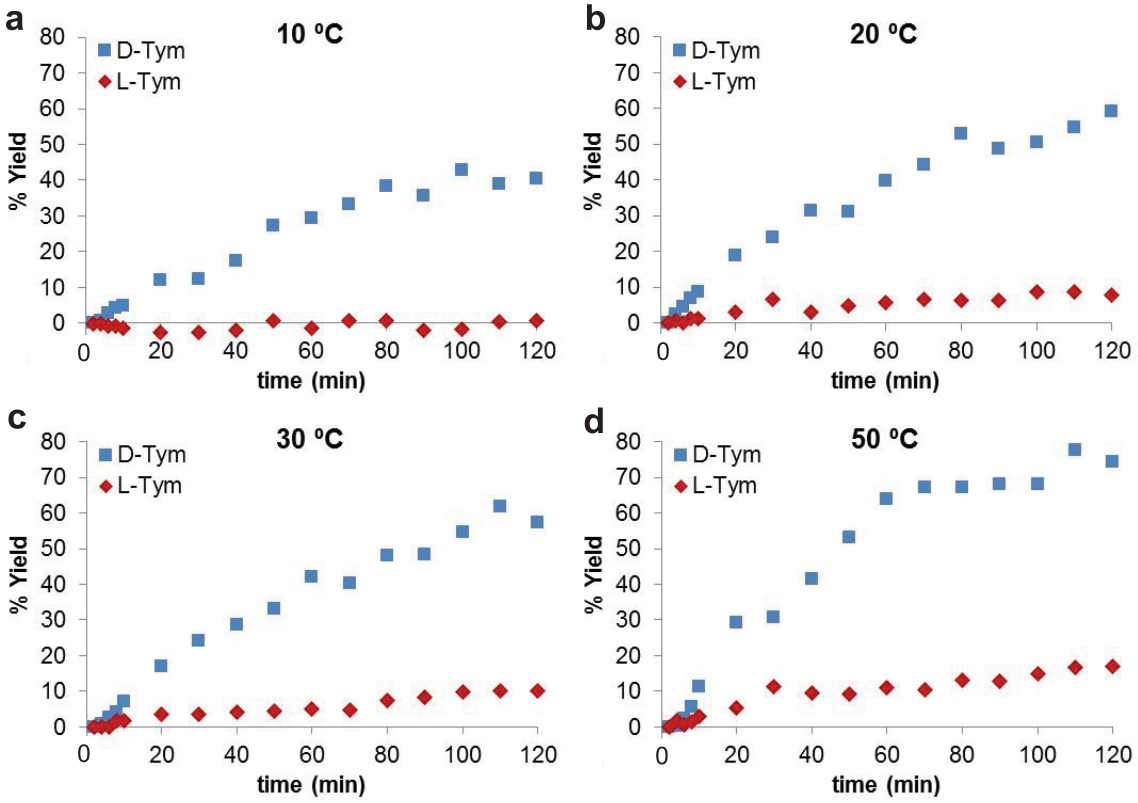

Figure 2.8. Monitoring the yield of D- and L-Tym during reaction of D-Tyr-OEt with ammonium hydroxide at (a) 10 °C, (b) 20 °C, (c) 30 °C, and (d) 50 °C.

achieve good resolution of L- and D-Tyr. Thus, we first used HPLC to separate all Tym from Tyr-OEt, then hydrolyzed the Tym to Tyr using H-form Dowex for 24 hours at 100 ºC. Finally, we were able to determine the ratio of L- and D-Tyr using an Astec Chirobiotic T 25 cm X 4.6 mm, 5 µm column. To ensure that no racemization occurred during the hydrolysis, we tested this protocol using a mixture L/D-Tym containing 10% L enantiomer, and measured 9.98% L-Tyr in the final HPLC. The data in Table 2.3 compare the % L-Tym for the reaction samples as measured by HPLC and using the biosensors, and show an average difference of 1.5% L-Tym, thus validating the accuracy of our reaction monitoring experiments.

We highlight that analysis of all of the samples in our study required approximately 1 minute of scanning on a plate reader when using our fluorescent biosensors, but would have required approximately 17 hours using chiral HPLC, even without the additional hydrolysis and manipulations required specifically for Tym. Thus, this initial reaction monitoring study demonstrates that we can rapidly generate data regarding both yield and enantiopurity for multiple reaction conditions, and that these data can be used to identify optimized conditions for a synthetic transformation in significantly less time than would be required using HPLC.

Enantiopurity analysis using structure-switching biosensors having moderate enantioselectivity

The extremely high enantioselectivity of the Tym structure-switching biosensor enables quantification of individual enantiomers of the target with negligible off-target signal. However, not all aptamers possess such high enantioselectivity, and thus we sought to develop a mathematical model that would enable the measurement of enantiopurity using structure-switching biosensors that have only moderate enantioselectivity. Figure 2.9 shows a calculated representation of the signal that would be observed for

Table 2.3. Validation of reaction monitoring results using HPLC. Samples were utilized from the 50 °C reaction.

Time (min)	% L-Tym (biosen-sors)	% L-Tyr (HPLC)	deviation
6	6.9	10.3	3.5
8	9.7	4.9	4.8
10	10.2	7.6	2.6
20	6.9	4.6	2.2
30	13.1	11.0	2.1
40	8.9	7.1	1.7
50	6.3	5.3	1.0
60	6.2	5.0	1.3
70	5.2	3.7	1.5
90	7.0	5.7	1.3
100	8.4	6.8	1.5

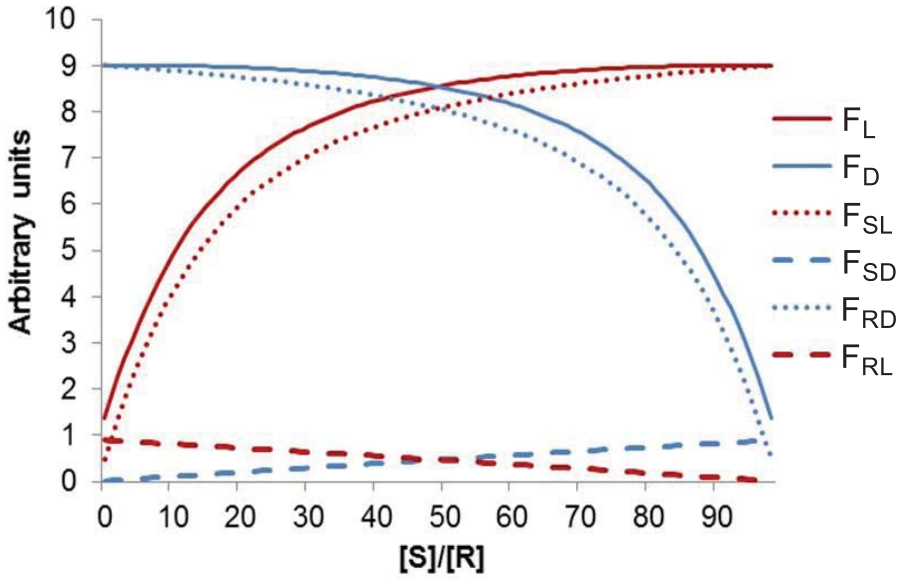

Figure 2.9. Modeling of fluorescence signal arising from a combination of on-target and off-target binding interactions.

enantiomeric structure-switching biosensors that bind to a target with 100:1 enantioselectivity. In this graph, the dotted lines represent signal arising from each of the biosensors binding to its target enantiomer, and the dashed lines represent signal arising from the off-target enantiomer. The solid line is the sum of these two signals and represents the total relative fluorescence intensity that would be observed for each of the biosensors (F_D and F_L). The values of F_D and F_L can be used in equation 2.2 to solve for small-molecule enantiopurity.

As shown in Figure 2.10, K_1 and K_2 are the on-target and off-target K_{sens} values, respectively, for the L-DNA biosensor, and K_4 and K_3 are the on-target and off-target K_{sens} values, respectively, for the D-DNA biosensor (specific pairing of the D- and L-DNA biosensors with *S*- and *R*-enantiomers of target was arbitrarily chosen for this model). These values can be obtained empirically by measuring the fluorescence response of each biosensor with varying concentrations of each ligand, then fitting these data to the Langmuir equation. A_{tot} is the total aptamer biosensor concentration. Using this equation, the ratio of enantiomers in a mixture can be determined even if a significant (ca. 1%) amount of off-target binding is observed. The primary limitation to this alternative calculation method is that it can only provide a ratio of the two enantiomers, and not their total concentration. To determine the concentrations of the two enantiomers, equation 2.3 can be used. Equation 2.3 requires the creation of a calibration curve relating absolute fluorescence of each enantiomer to concentration. The use of these two equations greatly increases the flexibility of this system.

Derivation of equation 2.2 for enantiopurity analysis using aptamers having moderate selectivity

Key:

A^L= L-DNA aptamer biosensor

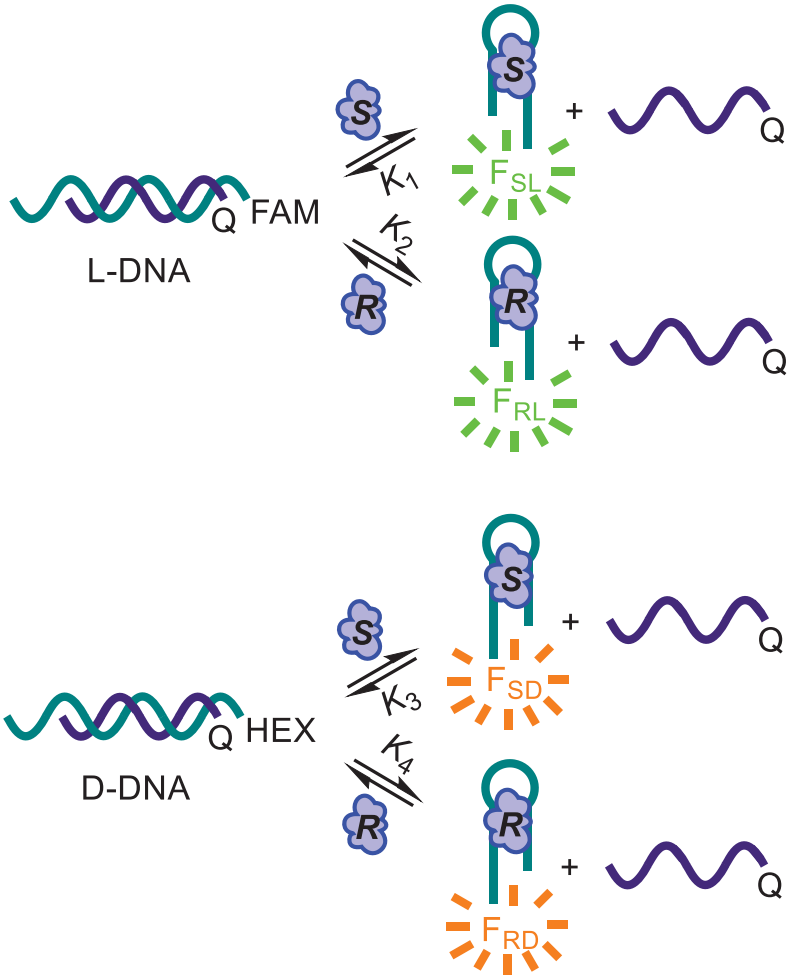

Figure 2.10. Equilibria involved in on-target and off-target interactions. Specific pairing of the D- and L-DNA biosensors with *S*- and *R*-enantiomers of target was arbitrarily chosen for this model.

A^D= D-DNA aptamer biosensor

A_{tot}= Total aptamer biosensor

R_i= Initial *R*-enantiomer

S_i= Initial *S*-enantiomer

R·A= *R*-enantiomer bound to aptamer biosensor

S·A= *S*-enantiomer bound to aptamer biosensor

F_L= Total fluorescence from L-DNA biosensor

F_D= Total fluorescence from D-DNA biosensor

Given the mechanism below for binding of D- and L-DNA biosensors to *S*- and *R*-enantiomer of target:

$$\mathrm{R \cdot A^L} \overset{\mathrm{K_2}}{\leftarrow} \mathrm{R + A^L + S} \overset{\mathrm{K_1}}{\rightarrow} \mathrm{S \cdot A^L}$$

$$\mathrm{R \cdot A^D} \overset{\mathrm{K_4}}{\leftarrow} \mathrm{R + A^D + S} \overset{\mathrm{K_3}}{\rightarrow} \mathrm{S \cdot A^D}$$

The equilibrium constants will be defined as follows:

$$\mathrm{K_2} = \frac{[\mathrm{R \cdot A^L}]}{[\mathrm{R}][\mathrm{A^L}]} \; \mathrm{K_1} = \frac{[\mathrm{S \cdot A^L}]}{[\mathrm{S}][\mathrm{A^L}]}$$

$$\mathrm{K_4} = \frac{[\mathrm{R \cdot A^D}]}{[\mathrm{R}][\mathrm{A^D}]} \; \mathrm{K_3} = \frac{[\mathrm{S \cdot A^D}]}{[\mathrm{S}][\mathrm{A^D}]}$$

Given that aptamer may exist free, or bound to either enantiomer of target:

$$[\mathrm{A^L_{tot}}] = [\mathrm{A^L}] + [\mathrm{R \cdot A^L}] + [\mathrm{S \cdot A^L}]$$

$$[\mathrm{A^D_{tot}}] = [\mathrm{A^D}] + [\mathrm{R \cdot A^D}] + [\mathrm{S \cdot A^D}]$$

Then substituting for the concentration of aptamer-target complexes gives:

$$[A^{L}_{tot}] = [A^{L}] + K_2[R][A^{L}] + K_1[S][A^{L}]$$

$$[A^{D}_{tot}] = [A^{D}] + K_4[R][A^{D}] + K_3[S][A^{D}]$$

Using an excess of ligand, complex arising from off-target binding is negligible compared to total target, and thus:

$$[R] \approx [R_i] - [R \cdot A^{D}]$$

$$[S] \approx [S_i] - [S \cdot A^{L}]$$

Substituting for [R] and [S] and factoring out [A] gives:

$$\frac{[A^{L}_{tot}]}{[A^{L}]} = K_1[S_i] - K_1[S \cdot A^{L}] - K_2[R \cdot A^{D}] + K_2[R_i] + 1$$

$$\frac{[A^{D}_{tot}]}{[A^{D}]} = K_4[R_i] - K_4[R \cdot A^{D}] - K_3[S \cdot A^{L}] + K_3[S_i] + 1$$

Solving for $[R_i]$ and $[S_i]$ gives:

$$[R_i] = \frac{\frac{[A^{D}_{tot}]}{[A^{D}]} - K_3[S_i] + K_3[S \cdot A^{L}] + K_4[R \cdot A^{D}] - 1}{K_4}$$

$$[S_i] = \frac{\frac{[A^{L}_{tot}]}{[A^{L}]} - K_2[R_i] + K_2[R \cdot A^{D}] + K_1[S \cdot A^{L}] - 1}{K_1}$$

Substituting $[R_i]$ and $[S_i]$ into one another allows for both equations to be expressed in terms of a single enantiomer:

$$[R_i] = \frac{\frac{K_1[A^{D}_{tot}]}{[A^{D}]} - \frac{K_3[A^{L}_{tot}]}{[A^{L}]} + K_1K_4[R \cdot A^{D}] - K_2K_3[R \cdot A^{D}] + K_1K_3[S \cdot A^{L}] - K_1K_3[S \cdot A^{L}] + K_3 - K_1}{(K_1K_4 - K_2K_3)}$$

$$[S_i] = \frac{\frac{K_4[A^L_{tot}]}{[A^L]} - \frac{K_2[A^D_{tot}]}{[A^D]} + K_1K_4[S \cdot A^L] - K_2K_3[S \cdot A^L] + K_2K_4[R \cdot A^D] - K_2K_4[R \cdot A^D] + K_2 - K_4}{(K_1K_4 - K_2K_3)}$$

Simplification of the previous equations gives:

$$[R_i] = \frac{\frac{K_1[A^D_{tot}]}{[A^D]} - \frac{K_3[A^L_{tot}]}{[A^L]} + K_1K_4[R \cdot A^D] - K_2K_3[R \cdot A^D] + K_3 - K_1}{(K_1K_4 - K_2K_3)}$$

$$[S_i] = \frac{\frac{K_4[A^L_{tot}]}{[A^L]} - \frac{K_2[A^D_{tot}]}{[A^D]} + K_1K_4[S \cdot A^L] - K_2K_3[S \cdot A^L] + K_2 - K_4}{(K_1K_4 - K_2K_3)}$$

Recalling that:

$$[A^L] = [A^L_{tot}] - [S \cdot A^L] - [R \cdot A^L]$$

$$[A^D] = [A^D_{tot}] - [S \cdot A^D] - [R \cdot A^D]$$

and that total fluorescence is representative of the sum of on-target and off-target interactions for a given aptamer, the following equations can be generated in which x and y are scaling factors relating concentration to relative fluorescence intensity. The values of x and y can be experimentally determined using a calibration curve.

$$[S \cdot A^L] + [R \cdot A^L] = xF_L$$

$$[S \cdot A^D] + [R \cdot A^D] = yF_D$$

Following the earlier assumption that the off-target contribution to the signal is negligible compared to on-target:

$$[S \cdot A^L] \approx xF_L$$

$$[R \cdot A^D] \approx yF_D$$

Substitution of fluorescence intensity in place of concentrations for aptamer-target complexes gives equation 2.2:

$$\frac{[\mathrm{S_i}]}{[\mathrm{R_i}]} = \frac{\frac{\mathrm{K_4}[\mathrm{A_{tot}^L}]}{[\mathrm{A_{tot}^L}] - x\mathrm{F_L}} - \frac{\mathrm{K_2}[\mathrm{A_{tot}^D}]}{[\mathrm{A_{tot}^D}] - y\mathrm{F_D}} + \mathrm{K_2} - \mathrm{K_4} + \mathrm{K_1K_4}(x\mathrm{F_L}) - \mathrm{K_2K_3}(x\mathrm{F_L})}{\frac{\mathrm{K_1}[\mathrm{A_{tot}^D}]}{[\mathrm{A_{tot}^D}] - y\mathrm{F_D}} - \frac{\mathrm{K_3}[\mathrm{A_{tot}^L}]}{[\mathrm{A_{tot}^L}] - x\mathrm{F_L}} + \mathrm{K_3} - \mathrm{K_1} + \mathrm{K_1K_4}(y\mathrm{F_D}) - \mathrm{K_2K_3}(y\mathrm{F_D})}$$

Derivation of equation 2.3 for enantiopurity analysis using aptamers having moderate selectivity

Key:

R_i= Initial *R*-enantiomer

S_i= Initial *S*-enantiomer

F_L= Total fluorescence from L-DNA biosensor

F_L^S= Total fluorescence from L-DNA biosensor from S-enantiomer

F_L^R= Total fluorescence from L-DNA biosensor from R-enantiomer

F_D= Total fluorescence from D-DNA biosensor

F_D^S= Total fluorescence from D-DNA biosensor from S-enantiomer

F_D^R= Total fluorescence from L-DNA biosensor from R-enantiomer

Each signal can be represented by the following components:

$$F_L^S = \frac{[S_i]}{K_1 + [S_i]};\ F_D^S = \frac{[S_i]}{K_2 + [S_i]};\ F_L^R = \frac{[R_i]}{K_3 + [R_i]};\ F_D^R = \frac{[R_i]}{K_4 + [R_i]}$$

Therefore the total signal of the L and D biosensors can be expressed as:

$$F_L = \frac{[S_i]}{K_1 + [S_i]} + \frac{[R_i]}{K_3 + [R_i]}$$

$$F_D = \frac{[S_i]}{K_2 + [S_i]} + \frac{[R_i]}{K_4 + [R_i]}$$

Rearrangement gives the following two linear equations:

$$F_L - 2 = \frac{[S_i]}{K_1} + \frac{[R_i]}{K_3}$$

$$F_D - 2 = \frac{[S_i]}{K_2} + \frac{[R_i]}{K_4}$$

These can be solved using the following determinants:

$$[S_i] = \frac{\begin{vmatrix} F_L - 2 & \frac{1}{K_3} \\ F_D - 2 & \frac{1}{K_4} \end{vmatrix}}{\begin{vmatrix} \frac{1}{K_1} & \frac{1}{K_3} \\ \frac{1}{K_2} & \frac{1}{K_4} \end{vmatrix}} \quad [R_i] = \frac{\begin{vmatrix} \frac{1}{K_1} & F_L - 2 \\ \frac{1}{K_2} & F_D - 2 \end{vmatrix}}{\begin{vmatrix} \frac{1}{K_1} & \frac{1}{K_3} \\ \frac{1}{K_2} & \frac{1}{K_4} \end{vmatrix}}$$

Conclusions

In summary, we describe here a novel method for the rapid and high-throughput analysis of both small-molecule concentration and enantiopurity. This method relies on the ability of structure-switching nucleic acid biosensors to transduce the presence of a small-molecule target into a dose-dependent fluorescence output, and the ability of enantiomeric structure-switching biosensors to simultaneously quantify both enantiomers of the target molecule. Using our enantiomeric biosensors, we demonstrate the ability to measure the % L-enantiomer in a genuine reaction mixture with an average error of 1.5% relative to values determined by HPLC analysis. Additionally, we demonstrate the utility of our method by applying it towards optimization of reaction conditions for the synthesis of D-Tym. Finally, we have generated a mathematical model to demonstrate that enantiopurity analysis is also feasible using aptamer biosensors that possess only mod-

erate enantioselectivity.

Our initial demonstration of this enantiopurity analysis method required significant optimization of the structure-switching biosensor concentration and stoichiometry, as well as identification of the ideal range of target concentrations. However, with the knowledge gained from these experiments, these optimizations could be rapidly performed on a new aptamer system, enabling use of our method to analyze the enantiopurity of a wide range of potential small-molecule targets. Fluorescence-based measurement techniques such as the one described here have potential to enable orders-of-magnitude higher throughput relative to the standard HPLC analysis methods. Thus, we envision that enantiomeric aptamer-based sensors will prove to be a powerful tool for the high-throughput analysis of reaction outcomes, enabling rapid optimization of reaction.

Materials and Methods

General methods

Unless otherwise noted, all starting materials were obtained from commercial suppliers and used without further purification. All DNA was purchased from the University of Utah DNA/Peptide Synthesis Core Facility. All absorbance and fluorescence values were recorded using a Biotek Synergy Mx microplate reader.

Modifiers used for DNA synthesis

Fluorescein and hexachlorofluroscein dyes were installed using phosphoramidites from Glen Research. Black Hole quencher 1 was installed using CPG cartridges from Glen Research. L-DNA was prepared using phosphoramidites from ChemGenes.

Preparation of biosensor stocks

Binding buffer (10 mM Tris-HCl, 100 mM NaCl, 5 mM KCl, 2 mM MgCl2, 1 mM CaCl2, pH 7.5) was used for all DNA stock solutions. DNA biosensors were prepared by generating a solution containing 1 μM aptamer and 2.5 μM complementary strand in binding buffer. This solution was incubated at 90 °C for 10 minutes then rapidly cooled and stored at 4 °C. Prior to use, the solution was allowed to warm to room temperature.

Enantiopurity measurement

A sample of 50 μL containing varying concentrations of L- and D-Tym was combined with 50 μL of the biosensor stock solution described above to give a 100 μL sample having concentrations of 500 nM aptamer and 1.25 μM complementary strand. These samples were then transferred to a Costar 96-well black flat bottom polystyrene plate. The plates were covered and incubated at 25 °C for 20 minutes and subsequently scanned for fluorescence intensity using excitation/emission wavelengths of 490/520 nm (FAM) and 524/572 nm (HEX). Fluorescence values were standardized using a control solution containing only fluorophore-labeled aptamer.

Reaction progress

All reactions were carried out in 200 μL PCR tubes using a Bio-Rad PTC-1148 thermocycler for temperature control. D-tyrosine ethyl ester was added to 100 μL of NH_4OH to a final concentration of 10 mM. Reactions were quenched by diluting the reaction mixture into of 9.9 mL of binding buffer containing the biosensors at specified time points. Samples were then analyzed as described above.

HPLC validation

We were unable to achieve baseline separation of L- and D-Tym using a commercially available HPLC column, and thus, we developed the following method for purification, hydrolysis, and analysis of our reaction mixtures. Samples from the reaction carried out at 50 °C were lyophilized and desalted. The L/D-Tym was separated from the remaining unreacted Tyr-OEt by HPLC using 60:40 water:MeOH (Agilent ZORBAX Eclipse XDB-C18, 5 μm, 9.4 x 250 mm). Collected fractions were lyophilized and resuspended in 100 μL water. The solutions were then added to H-form Dowex and reacted for 24 hours at 100 °C to hydrolyze the tyrosinamide to tyrosine. Dowex was removed using 0.2 μm centrifuge spin filters (Millipore UFC30GV00) and the L/D-Tyr was purified by HPLC using 60:40 water:MeOH (Agilent ZORBAX Eclipse XDB-C18, 5 μm, 9.4 x 250 mm). The Tyr fraction was then analyzed by chiral HPLC (Astec Chirobiotic T 25 cm x 4.6 mm) using 20:80 water:MeOH with 0.02% formic acid. Enantiomeric ratios were calculated by integration of peak areas and compared to those measured using the DNA biosensors.

References

(1) Ariens, E. J. Stereochemistry, a Basis for Sophisticated Nonsense in Pharmacokinetics and Clinical Pharmacology. *Eur. J. Clin. Pharmacol.* **1984**, *26*, 663-668.

(2) Jacobsen, E. N.; Pfaltz, A.; Yamamoto, H., Comprehensive Asymmetric Catalysis. Springer: New York, **2004**.

(3) Reetz, M. T. Laboratory Evolution of Stereoselective Enzymes: A Prolific Source of Catalysts for Asymmetric Reactions. Angew. Chem. Int. Edit. **2011**, 50, 138-174.

(4) Reetz, M. T. Directed Evolution of Enantioselective Enzymes as Catalysts for Organic Synthesis. *Adv. Catal.* **2006**, *49*, 1-69.

(5) Jaeger, K. Directed Evolution of Enantioselective Enzymes for Organic Chemistry. *Curr. Opin. Chem. Biol.* **2000**, *4*, 68-73.

(6) Reetz, M. T.; Zonta, A.; Schimossek, K.; Jaeger, K.-E.; Liebeton, K. Creation of Enantioselective Biocatalysts for Organic Chemistry by in Vitro Evolution. *Angew. Chem. Int. Edit.* **1997**, *36*, 2830-2832.

(7) Knowles, W. S.; Sabacky, M. J. Catalytic Asymmetric Hydrogenation Employing a Soluble, Optically Active, Rhodium Complex. *Chem. Commun. (London)* **1968**, 1445.

(8) McNally, A.; Prier, C. K.; MacMillan, D. W. Discovery of an Alpha-Amino C-H Arylation Reaction Using the Strategy of Accelerated Serendipity. *Science* **2011**, *334*, 1114-1117.

(9) Szewczyk, J. W.; Zuckerman, R. L.; Bergman, R. G.; Ellman, J. A. A Mass Spectrometric Labeling Strategy for High-Throughput Reaction Evaluation and Optimization: Exploring C−H Activation. *Angew. Chem. Int. Edit.* **2001**, *40*, 216-219.

(10) Finn, M. G. Emerging Methods for the Rapid Determination of Enantiomeric Excess. *Chirality* **2002**, *14*, 534-540.

(11) Reetz, M. T.; Wilensek, S.; Zha, D.; Jaeger, K.-E. Directed Evolution of an Enantioselective Enzyme through Combinatorial Multiple-Cassette Mutagenesis. *Angew. Chem. Int. Edit.* **2001**, *40*, 3589.

(12) Sajonz, P.; Schafer, W.; Gong, X.; Shultz, S.; Rosner, T.; Welch, C. J. Multiparallel Microfluidic High-Performance Liquid Chromatography for High-Throughput Normal-Phase Chiral Analysis. *J. Chromatogr. A* **2007**, *1145*, 149-154.

(13) Subramanian, G., *Chiral Separation Techniques: A Practical Approach. 3rd Ed.* Wiley-VCH: Weinheim, **2006**.

(14) Kang, J.; Wistuba, D.; Schurig, V. Recent Progress in Enantiomeric Separation by Capillary Electrochromatography. *Electrophoresis* **2002**, *23*, 4005-4021.

(15) Gubitz, G.; Schmid, M. G. Chiral Separation by Chromatographic and Electromigration Techniques. A Review. *Biopharm. Drug Dispos.* **2001**, *22*, 291-336.

(16) Zhu, Z.; Ravelet, C.; Perrier, S.; Guieu, V.; Roy, B.; Perigaud, C.; Peyrin, E. Multiplexed Detection of Small Analytes by Structure-Switching Aptamer-Based Capillary Electrophoresis. *Anal. Chem.* **2010**, *82*, 4613-4620.

(17) Drake, A. F.; Grould, J. M.; Mason, S. F. Simultaneous Monitoring of Light-Absorption and Optical Activity in the Liquid Chromatography of Chiral Substance. *J. Chromatogr. A* **1980**, *202*, 239-245.

(18) Nieto, S.; Lynch, V. M.; Anslyn, E. V.; Kim, H.; Chin, J. High-Throughput Screening of Identity, Enantiomeric Excess, and Concentration Using Mlct Transitions in Cd Spectroscopy. *J. Am. Chem. Soc.* **2008**, *130*, 9232-9233.

(19) Jo, H. H.; Lin, C. Y.; Anslyn, E. V. Rapid Optical Methods for Enantiomeric Excess Analysis: From Enantioselective Indicator Displacement Assays to Exciton-Coupled Circular Dichroism. *Accounts Chem. Res.* **2014**, *47*, 2212-2221.

(20) Reetz, M. T.; Hermes, M.; Becker, M. H. Infrared-Thermographic Screening of the Activity and Enantioselectivity of Enzymes. *Appl. Microbiol. Biot.* **2001**, *55*, 531–536.

(21) Sawada, M.; Takai, Y.; Yamada, H.; Hirayama, S.; Kaneda, T.; Tanaka, T.; Kamada, K.; Mizooku, T.; Takeuchi, S. Chiral Recognition in Host-Guest Complexation Determined by the Enantiomer-Labeled Guest Method Using Fast Atom Bombardment Mass Spectrometry. *J. Am. Chem. Soc.* **1995**, *117*, 7726-7736.

(22) Schrader, W.; Eipper, A.; Pugh, D. J.; Reetz, M. T. Second-Generation Ms-Based High-Throughput Screening System for Enantioselective Catalysts and Biocatalysts. *Can. J. Chemistry* **2002**, *80*, 626-632.

(23) Abato, P.; Seto, C. T. Emdee: An Enzymatic Method for Determining Enantiomeric Excess. *J. Am. Chem. Soc.* **2001**, *123*, 9206-9207.

(24) Synergy Neo Hts Multi-Mode Microplate Reader. Http://Www.Biotek.Com/Products/Microplate_Detection/Synergy_Neo_Hts_Multimode_Microplate_Reader.Html (10/30/2012).

(25) Shabbir, S. H.; Regan, C. J.; Anslyn, E. V. Molecular Recognition and Self-Assembly Special Feature: A General Protocol for Creating High-Throughput Screening Assays for Reaction Yield and Enantiomeric Excess Applied to Hydrobenzoin. *Proc. Natl. Acad. Sci. USA* **2009**, *106*, 10487-10492.

(26) Leung, D.; Kang, S. O.; Anslyn, E. V. Rapid Determination of Enantiomeric Excess: A Focus on Optical Approaches. *Chem. Soc. Rev.* **2012**, *41*, 448-479.

(27) Pu, L. Enantioselective Fluorescent Sensors: A Tale of Binol. *Accounts Chem. Res.* **2012**, *45*, 150-163.

(28) Tuerk, C.; Gold, L. Systematic Evolution of Ligands by Exponential Enrichment: RNA Ligands to Bacteriophage T4 DNA Polymerase. *Science* **1990**, *249*, 505-510.

(29) Robertson, D. L.; Joyce, G. F. Selection in Vitro of an RNA Enzyme That Specifically Cleaves Single-Stranded DNA. *Nature* **1990**, *344*, 467-468.

(30) Ellington, A. D.; Szostak, J. W. In Vitro Selection of RNA Molecules That Bind Specific Ligands. *Nature* **1990**, *346*, 818-822.

(31) Geiger, A.; Burgstaller, P.; Von der Eltz, H.; Roeder, A.; Famulok, M. RNA Aptamers That Bind L-Arginine with Sub-Micromolar Dissociation Constants and High Enantioselectivity. *Nucleic Acids Res.* **1996**, *24*, 1029-1036.

(32) Klussmann, S.; Nolte, A.; Bald, R.; Erdmann, V. A.; Furste, J. P. Mirror-Image RNA That Binds D-Adenosine. *Nat. Biotechnol.* **1996**, *14*, 1112-1115.

(33) Williams, K. P.; Liu, X. H.; Schumacher, T. N.; Lin, H. Y.; Ausiello, D. A.; Kim, P. S.; Bartel, D. P. Bioactive and Nuclease-Resistant L-DNA Ligand of Vasopressin. *Proc. Natl. Acad. Sci. USA* **1997**, *94*, 11285-11290.

(34) Nolte, A.; Klussmann, S.; Bald, R.; Erdmann, V. A.; Furste, J. P. Mirror-Design of L-Oligonucleotide Ligands Binding to L-Arginine. *Nat. Biotechnol.* **1996**, *14*, 1116-1119.

(35) Vater, A.; Klussmann, S. Toward Third-Generation Aptamers: Spiegelmers and Their Therapeutic Prospects. *Curr. Opin. Drug Di. De.* **2003**, *6*, 253-261.

(36) Liu, J.; Cao, Z.; Lu, Y. Functional Nucleic Acid Sensors. *Chem. Rev.* **2009**, *109*, 1948-1998.

(37) Jhaveri, S. D.; Kirby, R.; Conrad, R.; Maglott, E. J.; Bowser, M.; Kennedy, R. T.; Glick, G.; Ellington, A. D. Designed Signaling Aptamers That Transduce Molecular Recognition to Changes in Fluorescence Intensity. *J. Am. Chem. Soc.* **2000**, *122*, 2469-2473.

(38) Jhaveri, S.; Rajendran, M.; Ellington, A. D. In Vitro Selection of Signaling Aptamers. *Nat. Biotechnol.* **2000**, *18*, 1293-1297.

(39) Zhu, Z.; Schmidt, T.; Mahrous, M.; Guieu, V.; Perrier, S.; Ravelet, C.; Peyrin, E. Optimization of the Structure-Switching Aptamer-Based Fluorescence Polarization Assay for the Sensitive Tyrosinamide Sensing. *Anal. Chim. Acta.* **2011**, *707*, 191-196.

(40) Vianini, E.; Palumbo, M.; Gatto, B. In Vitro Selection of DNA Aptamers That Bind L-Tyrosinamide. *Bioorgan. Med. Chem.* **2001**, *9*, 2543–2548.

(41) Nutiu, R.; Li, Y. Structure-Switching Signaling Aptamers. *J. Am. Chem. Soc.* **2003**, *125*, 4771-4778.

(42) Yi, G.; Yong-xia, Z.; Xin, J.; Xue-zhong, Z.; Yi, W.; Li, X. Chemo-Enzymatic Synthesis of Z-Asp-Val-Tyr-Nh2—a Precursor Tripeptide of Thymopentin. *Chem. Res. Chinese U.* **2010**, *26*, 942-947.

CHAPTER 3

SELECTION OF APTAMER BIOSENSORS FOR THE HIGH-THROUGHPUT SCREENING OF ENZYME-MEDIATED REACTIONS

Introduction

Enzymes provide an excellent example of the power of natural selection, as they are capable of catalyzing nearly all of the chemical reactions needed for life, ranging from highly complex syntheses to simple modifications of small molecules.[1] At the interface between chemistry and biology lies a field termed chemical biology, in which scientists often try to mimic nature's designs. Harnessing some of nature's power can produce far better catalysts than could be created in the laboratory. Unfortunately, natural enzymes cannot catalyze as many exotic reactions as synthetic catalysts can. However, inspired by the power of evolution, *in vitro* selection can be used to improve natural enzymes and even create new ones. Using techniques such as saturation mutagenesis and error-prone PCR, scientists are evolving exciting new enzymes having extremely high selectivity and specificity. [2-4]

Enzymes from the Cytochrome P450 monooxygenases (P450) superfamily have been gaining popularity as efficient and environmentally friendly catalysts for organic synthesis.[5] These heme-containing enzymes can facilitate a broad range of reactions, and typically have high regioselectivity and stereoselectivity. P450 enzymes are found in all domains of life and are used for the detoxification of many drugs, accounting for almost 75% of all metabolic reactions related to bio-activation and drug metabolism.[6] Most

importantly, they are highly tolerant of mutations within the active site, greatly expanding the possible substrate scope.[7-9] Recent results by Zhao and co-workers have demonstrated that a single mutation within the active site of a wild-type P450 could invert enantioselectivity from the *S*-enantiomer to the *R*-enantiomer with 42% enantiomeric excess (ee).[10] Further modifications led to an increased *R*-enantioselectivity of 83% ee. This was found via individual randomization of 17 amino acids through site-saturation mutagenesis. Arnold and co-workers reported that a variant of P450 BM-3 could be evolved through site-saturation mutagenesis to perform enantioselective hydroxylation at the alpha position of small aromatic compounds.[9] Later work demonstrated that a single modification at phenylalanine 87 (F87) of this P450 BM-3 variant was capable of increasing reactivity nearly 10-fold.[11] Developing enzyme libraries has become increasingly facile due to new techniques in directed evolution,[12] and the limitations now lie in screening the enormous enzyme libraries produced.[13-14]

The probability of discovering novel or improved enzymes using directed evolution increases with library size. However, the amount of time required to screen a library also greatly increases with size, making library screening a limiting factor in enzyme discovery. Sequence space can be defined mathematically as $N = \frac{19^M X!}{(X-M)!M!}$, where X represents the total residues in the enzyme, N the maximum theoretical diversity, and M the total number of mutations.[15] An enzyme library where twenty amino acids are randomly mutated would produce a library of ~10^{26} potential sequences. As a result, screening efficiency dictates the maximum number of sites that can be randomized, and must be taken into account when designing libraries.[1] The most recent, and currently most powerful screening method utilizes mass spectrometry to determine the ee of a given reaction. This method has the ability to screen thousands of samples daily, greatly increasing the enzyme sequence space that can be covered. Unfortunately, this method is limited

to a small subset of molecules, usually requires isotopic labeling, and would still require months to scan the potential sequence space created by five random mutations. Chapter 2 of this dissertation introduced an alternative method using nucleic acid biosensors to create a high-throughput screening method that has the potential to screen up to one million samples per day.

Aptamers are nucleic acid sequences that are capable of binding to a variety of small-molecule and protein targets. They have been adapted for use in a wide variety of tasks throughout chemistry and biology. Aptamers have emerged as a promising alternative to antibodies as they show little batch-to-batch variation and can be engineered through an *in vitro* selection process called Systematic Evolution of Ligands by EXponential Enrichment (SELEX) (Figure 3.1).[16-17] Using SELEX, aptamers can be selected to discriminate between ligands that are structurally similar. They can also bind to a diverse range of ligands with micromolar to nanomolar dissociation constants (K_d), making them well-suited for the creation of biosensors. DNA aptamers generally have tertiary structures with a variety of stems and loops. Using structure prediction software such as Mfold[18], it is possible to hypothesize where the binding site may be, allowing for a displacement strand to be designed, allowing for the construction of a structure-switching biosensor. The majority of structure-switching biosensors have been described in depth by Lu and coworkers (Figure 3.2).[19] However, the vast majority of aptamers do not have the privilaged architeture required to allow for target-responsive displacement. As such, the overarching goal of the research described in this chapter is to develop an efficient method for selecting enantioselective small-molecule-binding aptamers that can function as structure-switching biosensors.

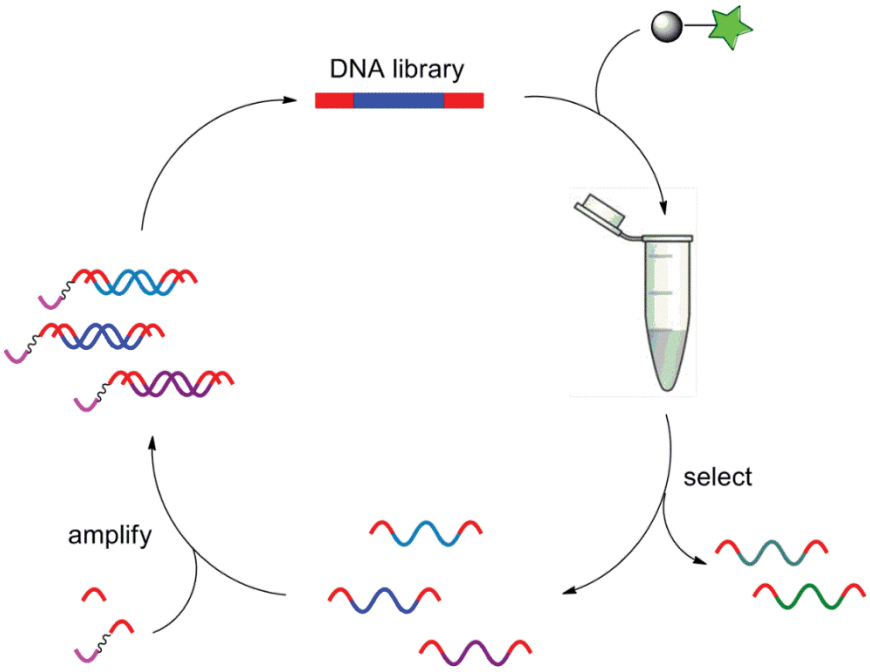

Figure 3.1. SELEX allows for the enrichment of randomized libraries to perform selected functions. Modified primers are used for quantification and separation of sense and anti-sense strands to complete each round.

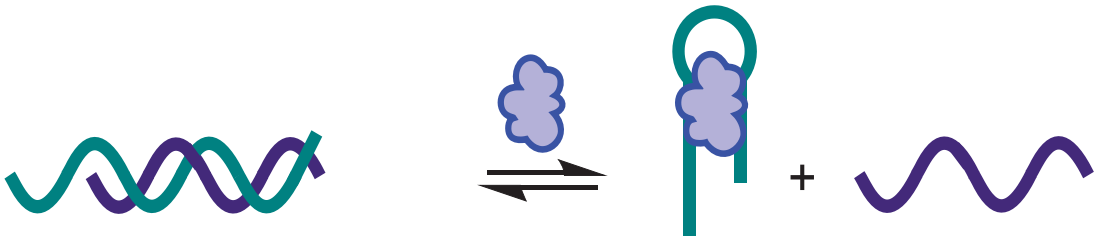

Figure 3.2. Structure-switching biosensor. Aptamer and displacement strand are shown in green and purple, respectively. Upon incubation with the target molecule, the aptamer binds and displaces the displacement strand.

Results and Discussion

Selecting an enantioselective aptamer for the small molecule (*S*)-2-chloromandelic acid

The research in this chapter explores a variety of methods for generating DNA aptamers and biosensors to the small molecule 2-chloromandelic acid (2-CMA) (Figure 3.3). This target was chosen because 2-CMA is an intermediate for the blockbuster cholesterol-lowering drug clopidogrel (Plavix).[19] The stereocenter at the alpha position of 2-CMA can be set through an enzyme catalyzed reaction, which would allow for the aptamer that is selected to be used for enzyme screening. Currently, the best enzyme can only confer an ee of 82%. We hypothesized that through the use of our enantioselective high-throughput screening method, we could greatly increase the number of mutants screened and therefore find an enzyme capable of producing higher enantiopurity.

FluMag-SELEX with immobilized target

SELEX produces aptamer sequences via multiple rounds of selection from a random library of oligonucleotides. The FluMag method for SELEX was chosen as the starting point for the design of this experiment as it relies on the convenient attachment of the small molecule of interest to magnetic beads.[20] (*S*)-2-chloromandelic acid ((*S*)-CMA) was used to create a synthetic analog to allow for attachment to the magnetic beads (Scheme 3.1).

Six nmols (~10^{15} sequences) of a DNA library consiting of 40 random nucleotides flanked by primer binding sites was used to begin SELEX. Subsequent rounds used approximately 200 pmols of DNA from the previous round. The (*S*)-CMA analog was attached to amine functionalized magnetic beads, and was incubated with the library. The beads were then exposed to several washes to remove any weak binding library

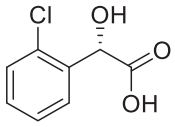

Figure 3.3. (*S*)-2-chloromandelic acid

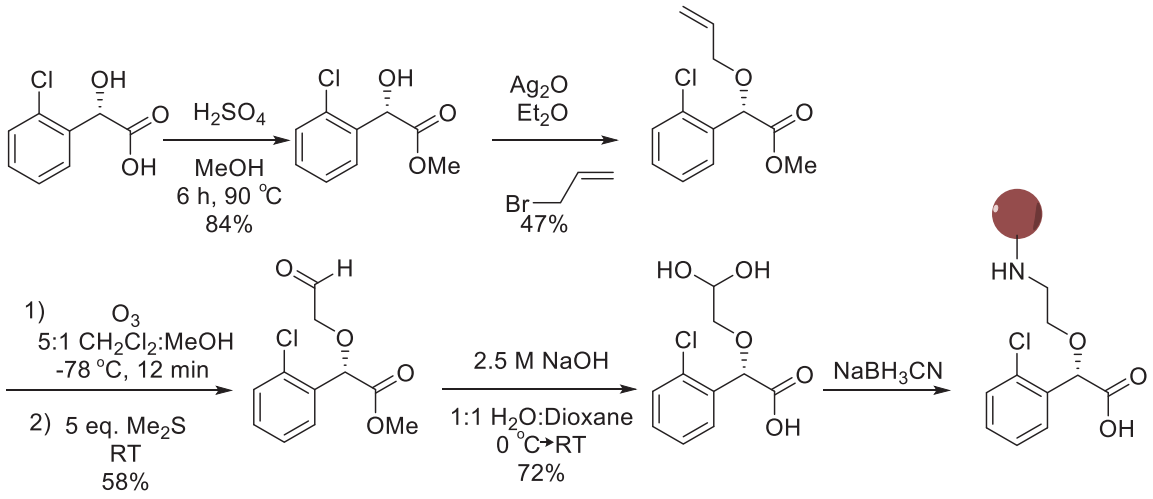

Scheme 3.1. Synthesis of a (*S*)-2-chloromandelic acid adduct for magnetic bead attachment. This route allowed for the retention of stereochemistry at the benzylic carbon. Attachment through the hydroxyl group was anticipated to allow for greater specificity in selections by retaining the pi-stacking ability of the ring. Reductive amination was used to attach the molecule to a free amine on the magnetic beads.

members, followed by incubation with free (*S*)-CMA to elute any potential aptamers. Quantification of the percent library bound for each round was measured via absorbance at 260 nm and cyanine 3 (Cy3) fluorescence emmision at 570 nm (Figure 3.4). The eluted DNA was amplified using the polymerase chain reaction (PCR) with modified primers. The forward primer contained a polyethylene glycol (PEG) linker and an A_{20} extension, and the reverse primer contained a Cy3 fluorophore. This allowed for separation of the double stranded DNA via denaturing polyacrylamide gel electrophoresis (PAGE). The DNA bands corresponding to the single stranded DNA library were cut out and recovered for use in the next round. Negative selections were performed against nonfunctionalized beads before rounds 5 and 9 to remove any library members that nonspecifically bound to the beads.

After twelve rounds, the pool of DNA was highly enriched with sequences that bound tightly to the small molecule. The library was then amplified using nonmodified primers and inserted into TOP 10 competent *E. coli* cells using a TOPO cloning kit. These were plated on LB/agar plates and incubated overnight. Eight successful colonies were chosen and grown overnight in enriched media. The cells were lysed and the plasmid DNA was recovered and sequenced at the University of Utah DNA sequencing core facility. Using Multalign free software, all sequences were aligned and the three with the highest level of conserved regions were selected (Figure 3.5). Competitive elution experiments provided the best method of studying the binding affinity for the aptamers. It was determined that of the three aptamers, aptamer 2.2 had the greatest affinity for (*S*)-CMA. Using structural predictions from Mfold, we minimized the sequence of aptamer 2.2 from 76 bases to 55 (2.2*t*) (Figure 3.6). 2.2*t* retained the main series of stem loops that existed in the most stable Mfold structure of the original 76mer. 2.2*t* was then tested using competitive elution experiments with (*S*)-CMA, (*R*)-CMA, non-

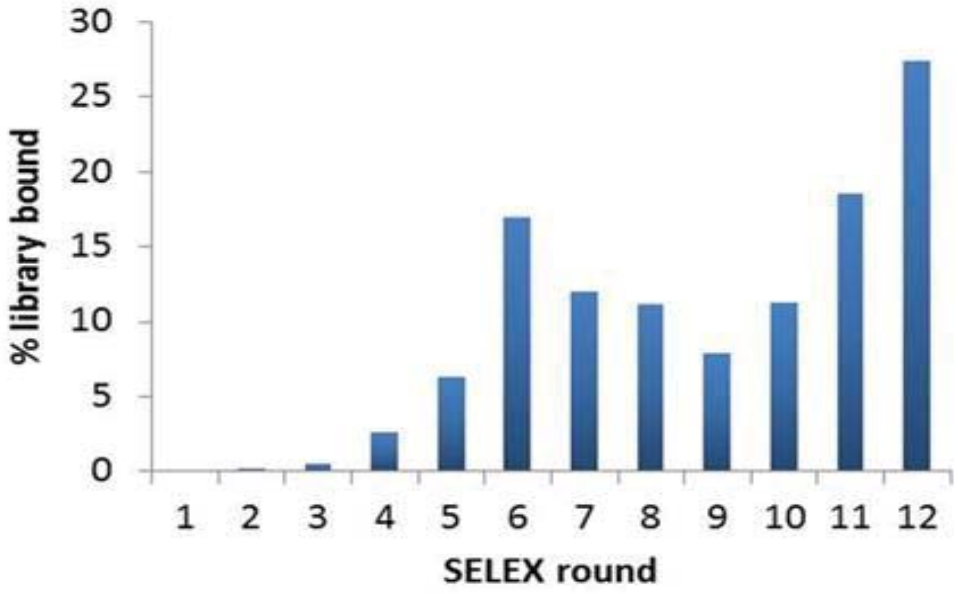

Figure 3.4. Enrichment data from 12 rounds of FluMag selections.

```
           1       10        20        30        40        50        60        70        78
           |--------+---------+---------+---------+---------+---------+---------+-------|
         1 AGATTGCACTTACTATCTTA--AAGTTTTTCCGTCACATCGTAGGGTAGACATTGCGTCCAATTGAATAAGCTGGTAT
         3 AGATTGCACTTACTATCTTA--AAGTTTTTCCGTCACATCGTAGGGTAGACATTGCGTCCAATTGAATAAGCTGGTAT
       4.1 AGATTGCACTTACTATCTTA--AAGTTTTTCCGTCACATCGTAGGGTAGACATTGCGTCCAATTGAATAAGCTGGTAT
       2.1 AGATTGCACTTACTATCTTA--GCGTTGCGCAGAATAATAGGAAAGCTAAGGGTCTGTGGAATTGAATAAGCTGGTAT
       2.2 AGATTGCACTTACTATCTCA--GCGTCGCGCAGAATAATAGGAAAGCTAAGGGTCTGTGGAATTGAATAAGCTGGTAT
       7.2 AGATTGCACTTACTATCTCA--GCGTCGCGCAGAATAATAGGAAAGCTAAGGGTCTGTGGAATTGAATAAGCTGGTAT
       4.2 AGATTGCACTTACTATCTCA--GCGTCGCGCAGAATAATAGGAAAGCTAAGGGTCTGTGGAATTGAATAAGCTGGTAT
       5.1 AGATTGCACTTACTATCTCA--GCGTCGCGCAGAATAATAGGAAAGCTAAGGGTCTGTGGAATTGAATAAGCTGGTAT
       2.3 AGATTGCACTTACTATCTCA--GCGTCGCGCAGAATAATAGGAAAGCTGAGGGTCTGTGGAATTGAATAAGCTGGTAT
       4.3 AGATTGCACTTACTATCTCA--GCGTCGCGCAGAATAATAGGAAAGCTGAGGGTCTGTGGAATTGAATAAGCTGGTAT
       7.1 AGATTGCACTTACTATCTCA--G-GTCGCGCAGAATAATAGGAAAGCTAAGGGTCTGTGGAATTGAATAAGCTGGTAT
       2.4 AGATTGCACTTACTATCTCAA-ACGGGATTGGCCCAGCTAATGCAGATGTCC-CACGCCCAATTGAATAAGCTGGTAT
       4.4 AGATTGCACTTACTATCTCAA-ACGGGATTGGCCCAGCTAATGCAGATGTCC-CACGCCCAATTGAATAAGCTGGTAT
       7.3 AGATTGCACTTACTATCTCTACACAACCATTGTCCT-CTTATGACCCCTTCC-CTTGCCCAATTGAATAAGCTGGTAT
       7.4 AGATTGCACTTACTATCTCGC--ATGCTGTCCACACACTAATCCGAGTCTCCTCTTGGCCAATTGAATAAGCTGGTAT
       5.2 AGATTGCACTTACTATCTATCGGACACATT--ACTTGCTTTTTGACCCCCCGTACG-CTAATTGAATAAGCTGGTAT
Consensus  AGATTGCACTTACTATCTca...cg.c..tc..c.t.cTa.t..agct..cc.t.tG.ccAATTGAATAAGCTGGTAT
```

Figure 3.5. Alignment of sequences from round 12. Sequence 1, 2.2, and 2.4 were selected for further testing.

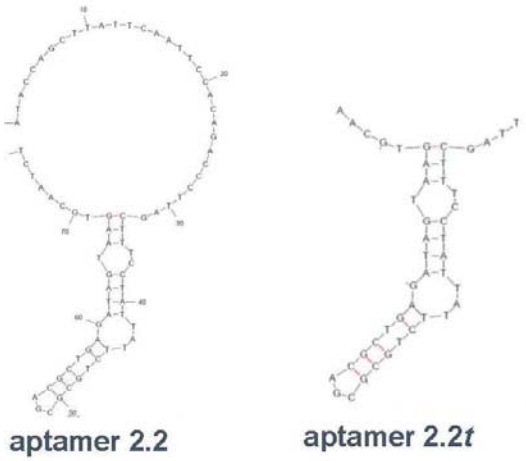

Figure 3.6. Mfold predicted structure of aptamer 2.2 was used to minimize the sequence to aptamer 2.2*t*.

functionalized beads, and three structurally similar control molecules (Figure 3.7). While aptamer 2.2*t* only shows modest enantioselectivity, this was not suprising as no negative selections against (*R*)-CMA were preformed. However, we were encouraged to see that aptamer 2.2 did not bind significantly to any of the structurally similar molecules.

Determining whether a superior aptamer can be selected through the use of a biased library or a random library with stringent negative selections

Using aptamer 2.2t, we explored the possibility of increasing enantioselectivity through the use of a biased library and a series of negative selections against (*R*)-CMA. Aptamer 2.2t was used as the starting point to create a biased library for use in the selections. Using Mfold to create structural predictions, six bases were chosen that were believed to be possibly the ligand binding sites. A biased library was synthesized by placing a 70% bias on the original base and 10% on each of the other 3 bases during synthesis at these 6 sites (Figure 3.8). Two separate SELEX trials were performed, one

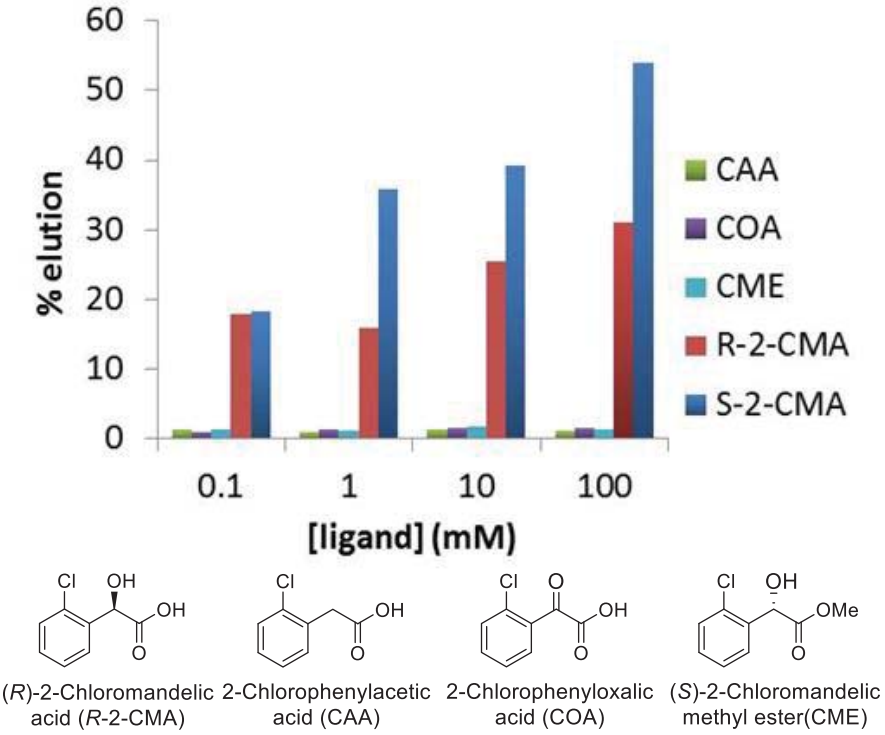

Figure 3.7. Competitive elution experiments using aptamer 2.2*t*.

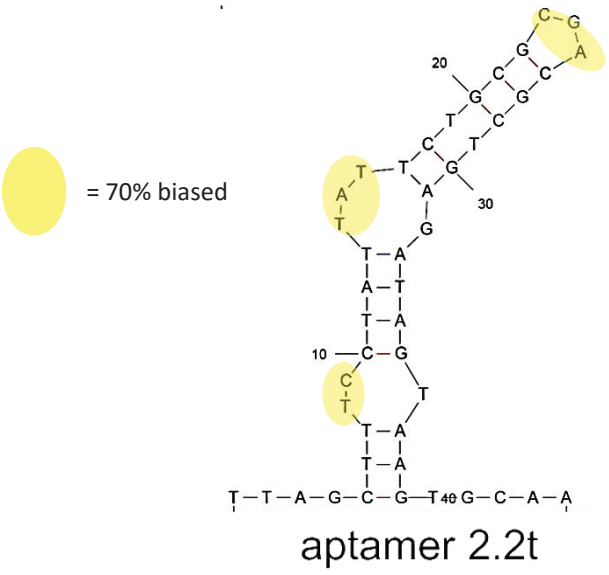

Figure 3.8. Biased regions of aptamer 2.2*t* chosen based upon Mfold structural predictions.

using the newly created biased library and the other using the DNA pool from round 4 of the original FluMag-SELEX experiment.

A negative selection method for increasing the enantioselectivity of selected aptamers was also tested. In the final 4 rounds, the aptamer library was heat denatured (70 ºC), (*R*)-CMA was added to a concentration of 100 µM, and then the solution was cooled to allow the DNA to refold. Next, the beads were washed thoroughly, and bound DNA sequences heat eluted as before. This allowed for the removal of sequences that bound more strongly to the (*R)*-CMA than (*S*)-CMA.

After 8 rounds, sufficient enrichment was seen for both the biased and random libraries (Figure 3.9). Both libraries were cloned and sequenced using the previously described methods. Using Multalign free software, all sequences were aligned and grouped into families (Figure 3.10). One sequence from each family was selected for further testing. Competitive elution experiments again provided the best method of studying the binding affinity and selectivity of the aptamers. It was determined that aptamer BH6 showed the best binding characteristics. Aptamer BH6 was minimized using Mfold to give BH6*t* (Figure 3.11). Competitive elutions were performed on BH6*t* using (*S*)-CMA, (*R*)-CMA, nonfunctionalized beads, and one structurally similar molecule 2-chlorophenyl acetic acid (CAA). It can be seen that BH6*t* not only binds tightly to (*S*)-CMA but also shows very high enantioselectivity and specificity against (*R*)-CMA and CAA (Figure 3.12). The high level of selectivity of BH6*t* speaks to the power of negative selections in the SELEX process. It is interesting to note that while aptamer BH6*t* was selected form the biased library, it showed no structural similarities to aptamer 2.2*t*. This suggests that there is no benefit to beginning with a structurally biased library, as nature is more efficient at selecting the best structure for the specific task.

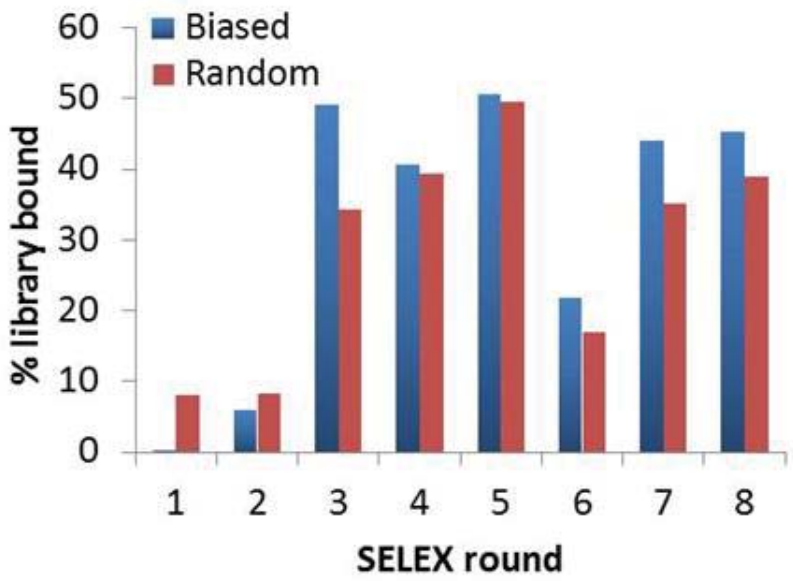

Figure 3.9. Enrichment of biased and random library over 8 rounds of selections.

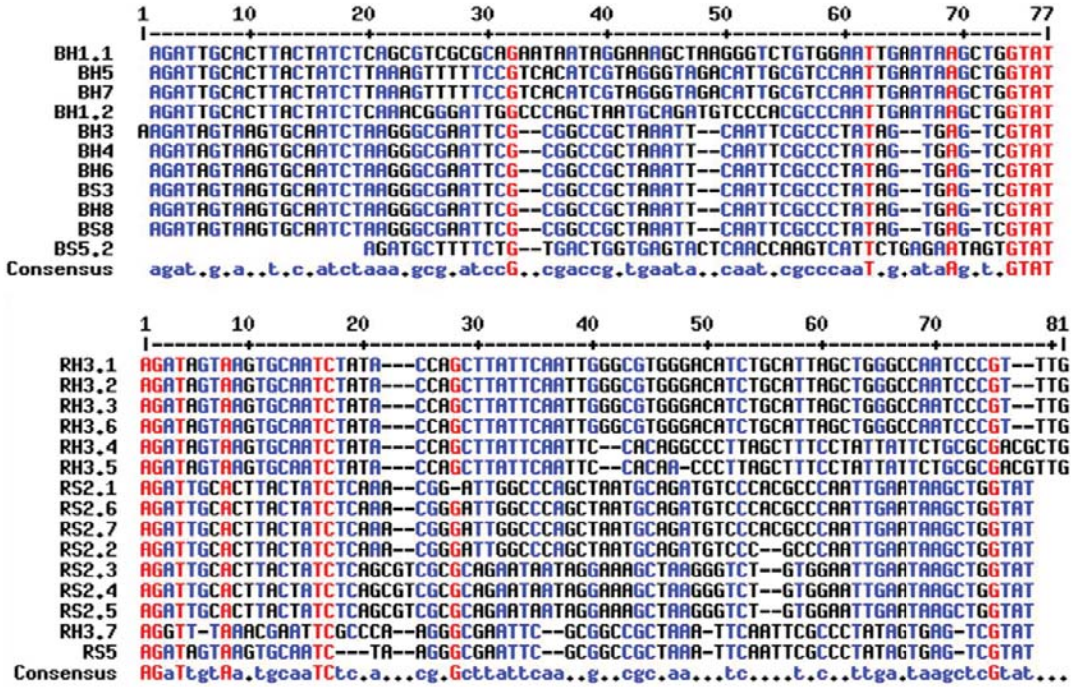

Figure 3.10. Alignment of sequences after 8 rounds of selections. Alignment was created using the free online software Multalign. Blue and red bases show 70% and 100% conservation, respectively. Sequences emerging from the biased and random libraries are on the top and bottom, respectively.

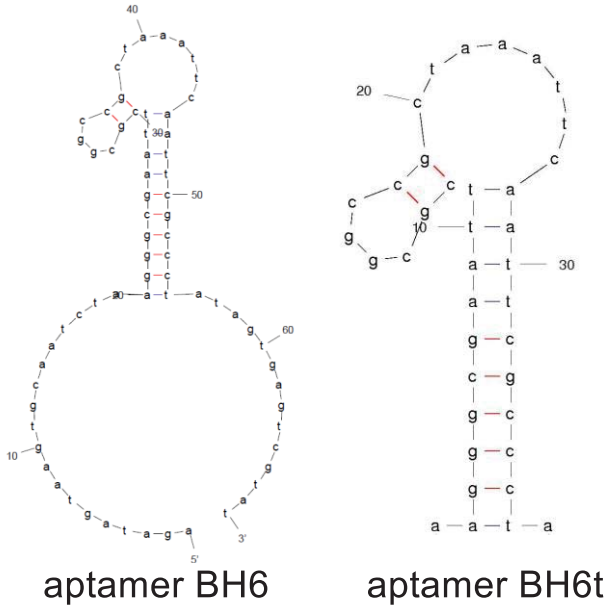

Figure 3.11. Mfold predicted structure of aptamer BH6 was used to minimize the sequence to aptamer BH6*t.*

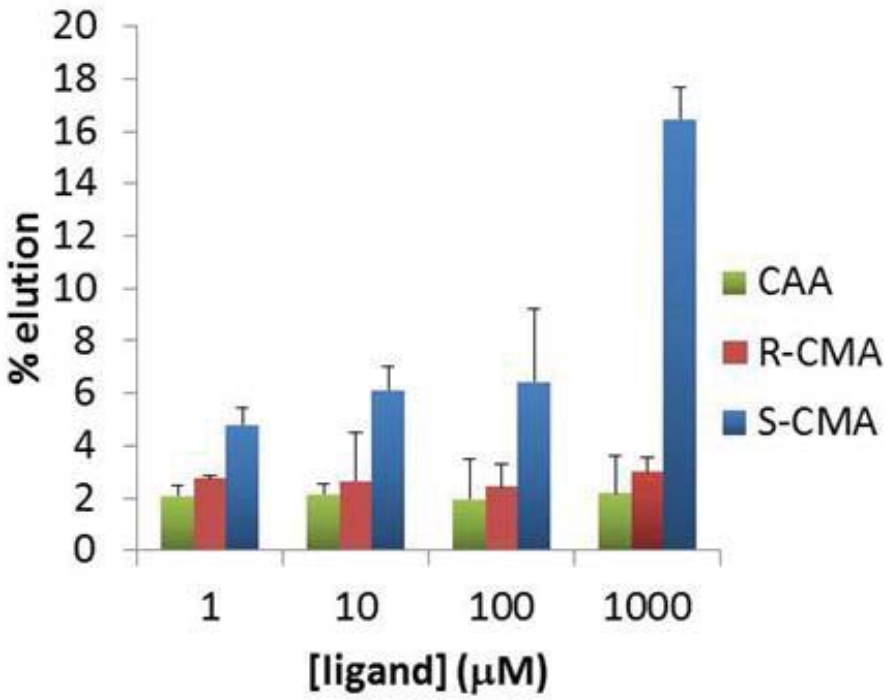

Figure 3.12. Competitive elution experiment with aptamer BH6*t.*

Aptamer BH6*t* conversion to a biosensor

In order to design a structure-switching aptamer biosensor, a displacement strand must be created. The displacement strand needs to be in close proximity to the active site so that it can be displaced upon ligand binding. However, it must not disrupt the function of the binding site. We designed a series of displacement strands based on proposed active sites deduced from Mfold. Varying lengths and invasion positions were tested for structure-switching function. Unfortunately, after exhausting all of these options, it was determined that aptamer BH6*t* would not function as a structure-switching biosensor. This highlighted the necessity for the development of better methods to directly select aptamers with the privileged architecture required for use as structure-switching biosensors.

Methods for the direct selection of structure-switching biosensors

In response to the difficulties that we encountered in engineering structure-switching biosensors from aptamers, we began to explore SELEX methods that would allow for the direct selection of aptamers that have the desired structure-switching capabilities. One such method developed by the Strehlitz lab,[21] Capture-SELEX, utilizes a special library that contains a constant docking sequence within the randomized region of the library. This docking sequence is complementary to a docking strand that is attached to magnetic beads via a streptavidin-biotin interaction. This design allows for selection using free ligand as opposed to selecting for bead-bound target adducts. Upon incubation with the target, sequences that displace from the docking strand can be collected through magnetic separation. Importantly, this directly selects for the structure-switching architecture we desire, as upon target binding, only those sequences that release from the docking strand are isolated. However, all of the known structure-switching SELEX methods have been performed with larger targets with many functional handles,

e.g. aminoglycosides. Our lab wanted to test whether these methods could be used to select for more difficult small molecules such as (*S*)-CMA.

Structure-switching SELEX Trial 1

We began selections for (*S*)-CMA using the identical sequence and procedure outlined by the Stehlitz group.[21] M-270 streptavidin beads were conjugated with 3' biotin labeled capture strands. For the first round, 2.5 nmols of library was annealed to the capture strand labeled beads. This was accomplished through a snap cool of the library followed by a 3-hour incubation at room temperature with nutation. The beads were thoroughly washed until background elution was constant. Negative selections for the (*R*)-CMA were performed for every round in an attempt to select only highly enantioselective aptamers. This was accomplished by incubation of the library bound beads with 1mM (*R*)-CMA for 30 minutes at room temperature with gentle nutation. The beads were then washed and incubated with 1mM (*S*)-CMA for 30 minutes with gentle nutation followed by collection of the supernatant. Sequences eluted in the positive selections were PCR amplified, strand separated by denaturing PAGE, extracted, and incubated with fresh capture strand labeled magnetic beads to begin the next round. This process was carried out through 8 rounds, at which point enrichment was observed.

Following round 8, we chose to further increase the stringency of selections by decreasing the concentration of positive target until we once again observed enrichment. We hypothesized that this would allow for enrichment of only the strongest binding aptamers. The (*S*)-CMA elutions were lowered to 10 μM (*S*)-CMA while the negative (*R*)-CMA elutions remained at 1 mM. Once enrichment was seen, an additional negative selection using 1 mM acetic acid was introduced (Figure 3.13). This negative selection was used to remove any aptamers that were simply binding to the acid moiety instead of conferring specificity to the entire (*S*)-CMA structure. After 14 rounds, the library was

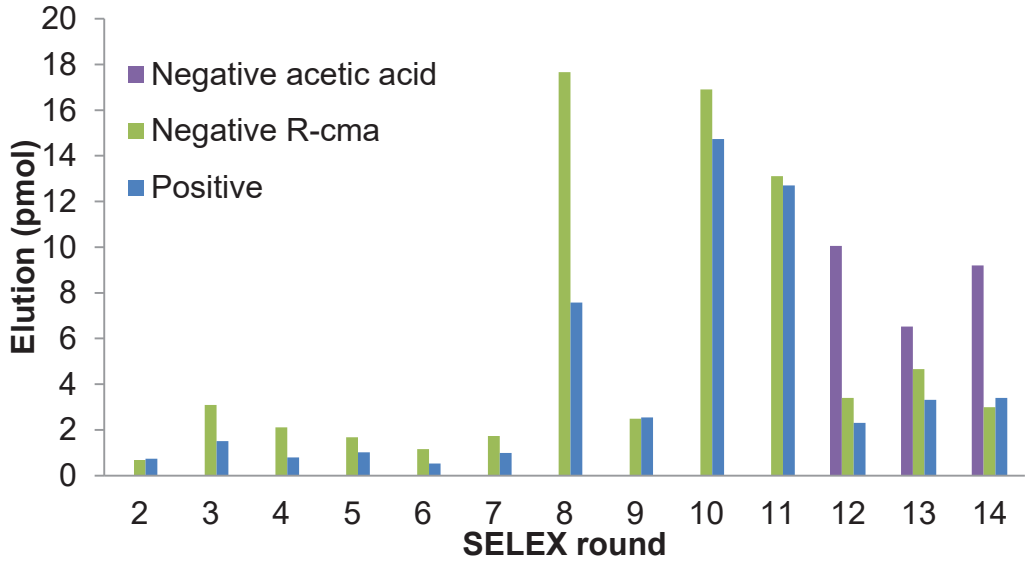

Figure 3.13. Enrichment of library for trial 1 of structure-switching SELEX.

cloned using a TOP 10 competent *E. coli* cell line. The resulting plasmids were sent for Sanger sequencing and sequences were grouped into families using Multialin (Figure 3.14).

A total of 4 sequences were chosen for further testing. The sequences represented each of the four major consensus families from Multialin. The ligand dependent displacement was tested for each sequence by annealing the FAM labeled aptamer sequence with BHQ1 functionalized capture strand, resulting in a quenching of the FAM signal. Upon incubation with (*S*)-CMA, any sequences that undergo a structural change to displace the capture strand would exhibit a large increase in the FAM signal. However, it was found that none of the eight sequences provided substantial fluorescence recovery upon exposure to up to 1 mM (*S*)-CMA. We hypothesized that stringency of the selections may have been too high, leading to enrichment of sequences based on factors other than affinity to (*S*)-CMA.

To test whether the addition of the second negative selection using acetic acid

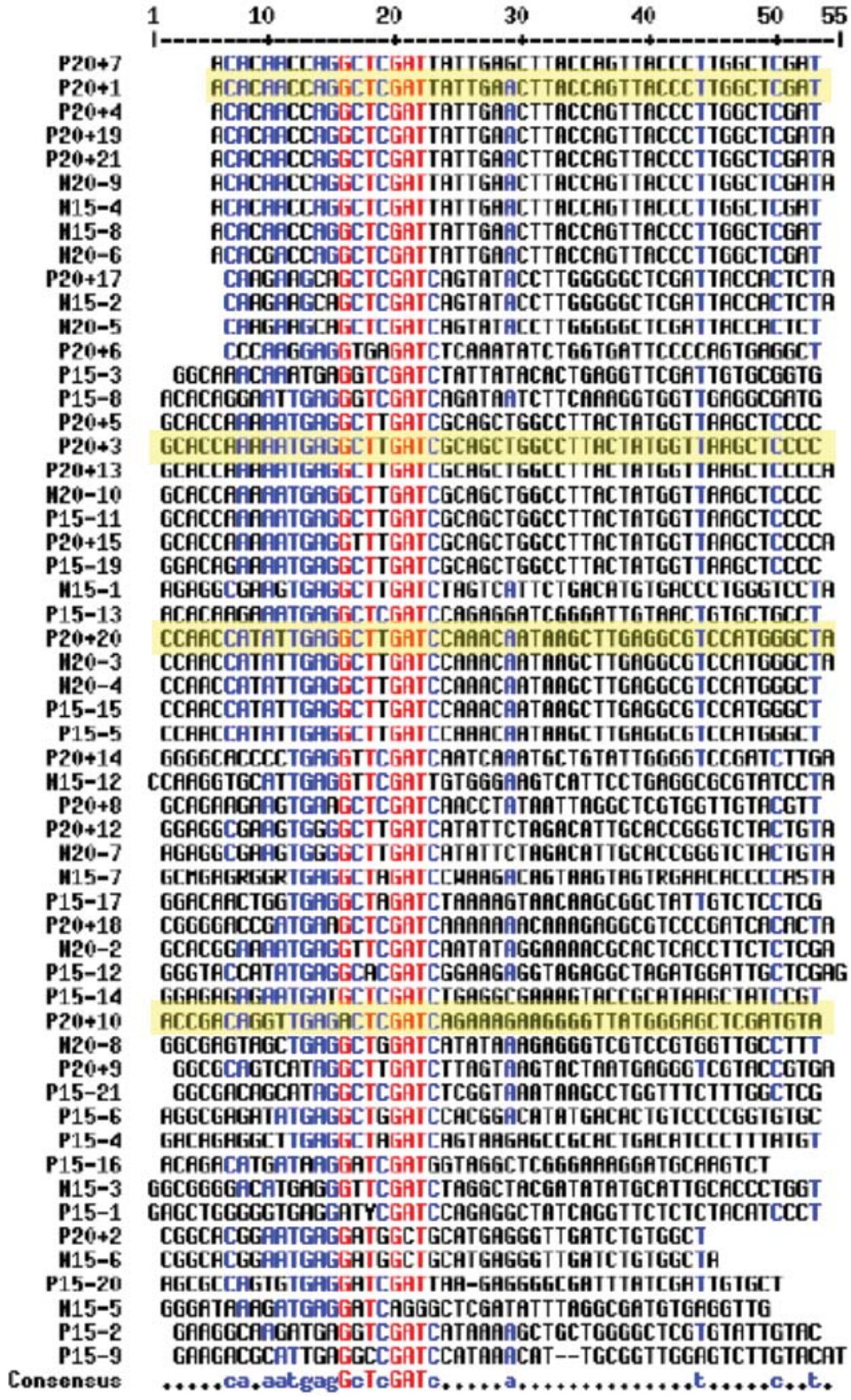

Figure 3.14. Sequence alignment after 14 rounds of selections. Alignment was created using the free online software Multalign. Blue and red bases show 70% and 100% conservation, respectively. Highlighted aptamers were selected for further analysis.

was too harsh, resulting in loss of potential aptamers, we went back to the round 11 library and carried out 9 more rounds using only positive selections. After the 9 rounds were completed, we again cloned and sequenced the library. Upon alignment, we found 8 more unique families. We tested one sequence from each family for target dependent displacement, but once again found that we had not successfully selected a functional aptamer biosensor. This led us to attempt a second cycle of capture-SELEX using a new library.

Structure-switching SELEX Trial 2

Morse and coworkers preformed a displacement style SELEX similar to capture-SELEX but with a different capture strand binding position.[22] In their version, the capture strand was complementary to the 5' region of the library. Using this library, we performed selections similar to those in the previous trial with the exclusion of the negative selection steps. We chose to greatly decrease the stringency of the selections to maximize our chances of successfully selecting a biosensor.

M-270 streptavidin beads were conjugated with 3' biotin labeled capture strands. For the first round, 2.5 nmols of library was annealed to the capture strand labeled beads. This was accomplished through a snap cool of the library followed by a 3-hour incubation at room temperature with nutation. The beads were thoroughly washed 10 times for 5 minutes each wash. Each wash was collected and the amount of library quantified to determine the amount of library that was successfully annealed to the beads. The beads were then incubated with 1 mM (*S*)-CMA for 30 minutes followed by collection of the supernatant. The (*S*)-CMA elution was then PCR amplified and strand separated by denaturing PAGE. The band corresponding to the library was excised, extracted, and incubated with fresh capture strand labeled magnetic beads to begin the next round. This process was carried out until slight enrichment of the library was seen

at round 17 (Figure 3.15). After 17 rounds, the library was tested with a bead elution approach.

Fresh capture strand labeled beads were incubated with the round 17 library and separated into 3 tubes. The 3 tubes were each incubated with buffer, (*R*)-CMA, or (*S*)-CMA at 1 mM. The percent elution for each was calculated using a fluorescence plate reader and found to be the same within error for all 3 samples. This led us to believe that this cycle had failed to produce any aptamers that would function as structure-switching biosensors. We hypothesized that the preselection washes were too harsh and thereby removed too much of the library. This led us to attempt a third cycle of selections using fewer preselection washes.

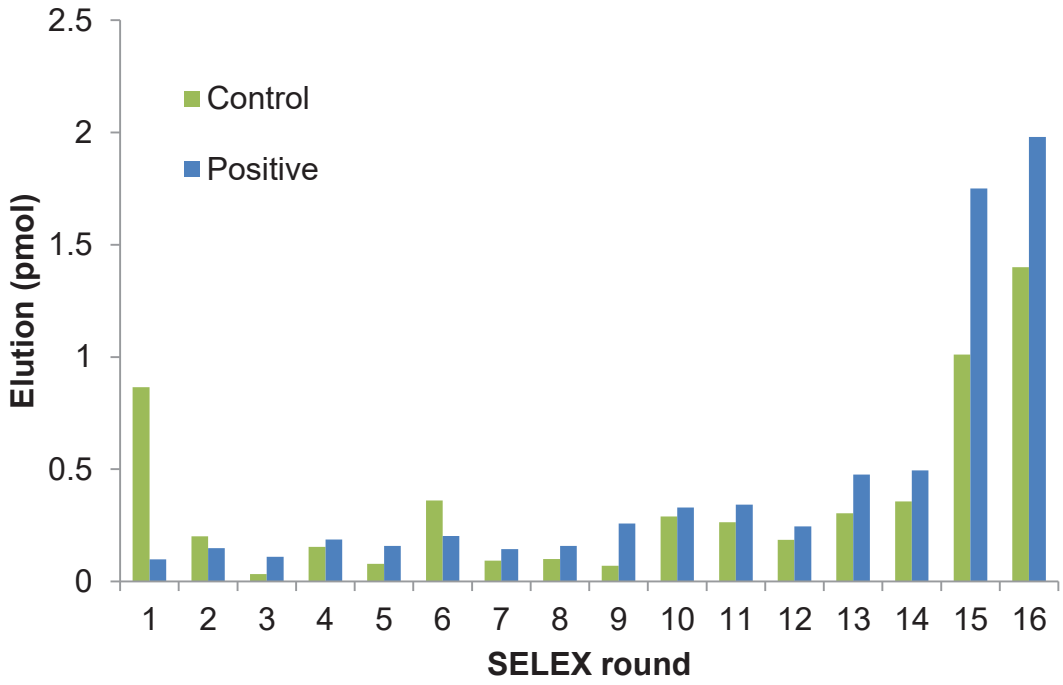

Figure 3.15. Enrichment of library for trial 2 of structure-switching SELEX. Control and positive elutions were performed using buffer and (*S*)-CMA, respectively.

Structure-switching SELEX Trial 3

Trial 3 was carried out identically to trial 2 using the Morse library, except that the preselection washes were decreased in number from 10 to 5 washes. A total of 10 rounds were performed in this trail, at which time no clear enrichment of the library was observed (Figure 3.16). Although little to no enrichment was seen at this point, we decided to test the library using the bead elution approach. Fresh capture strand labeled beads were incubated with the round 10 library and separated into 3 tubes. The 3 tubes were each incubated with either buffer, (*R*)-CMA or (*S*)-CMA at 1 mM. It was found that the percent displacement for the samples were again all within error. This led us to believe that this SELEX trial was going to suffer the same fate as the previous trial. We abandoned this trial and chose to test the trial 1 library again with less stringent preselection washes to determine whether this Strehlitz library would work under these conditions.

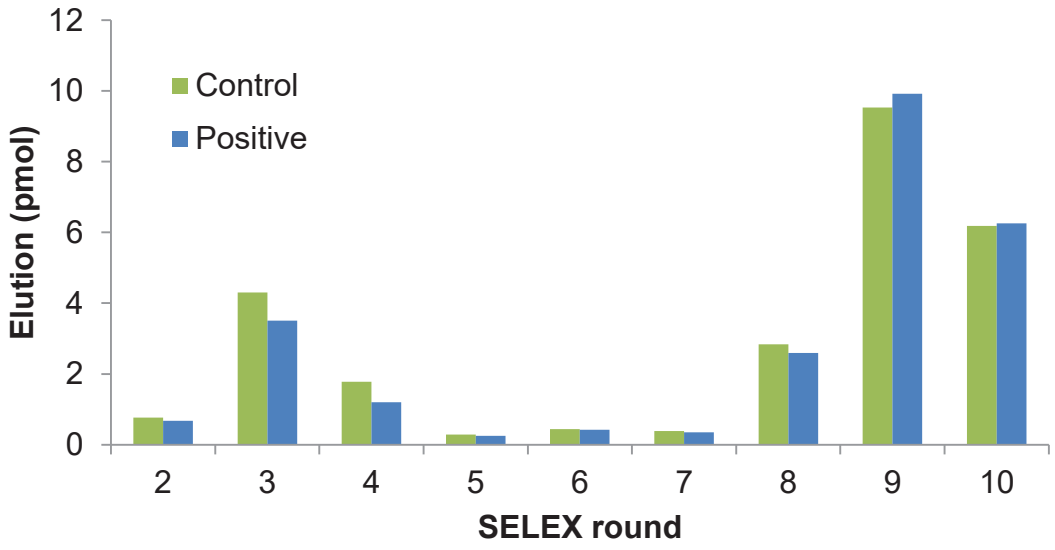

Figure 3.16. Enrichment of library for trial 3 of structure-switching SELEX. Control and positive elutions were performed using buffer and (*S*)-CMA, respectively.

Structure-switching SELEX Trial 4

Trial 4 was performed in the same way as trial 3 except we used the Strehlitz library and chose to do 2 positive elutions with (*S*)-CMA to determine if the less stringent preselection washes or the additional positive selection would affect our outcome. We hypothesized that the second positive elution step would allow for more potential aptamers to be collected. We performed 10 rounds and saw a small enrichment of the library (Figure 3.17). We were encouraged by the enrichment at this point so we tested the library using the bead elution approach. Fresh capture strand labeled beads were incubated with the round 10 library and separated into 3 tubes. The 3 tubes were each incubated with either buffer, (*R*)-CMA or (*S*)-CMA at 1 mM. We once again found that the percent elutions of the three samples were all within error.

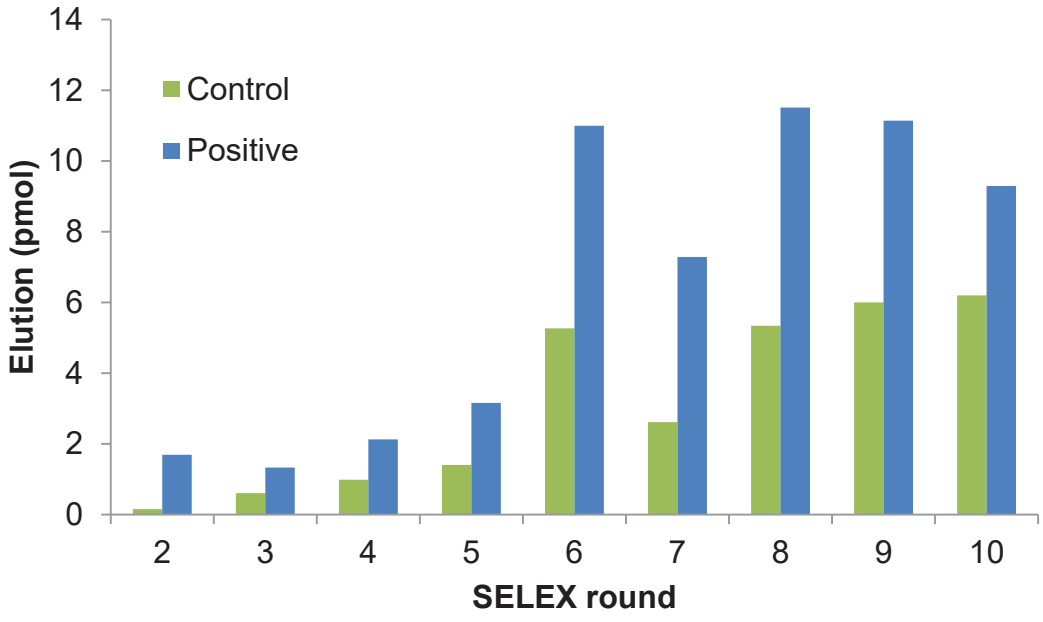

Figure 3.17. Enrichment of library for trial 4 of structure-switching SELEX. Control and positive elutions were performed using buffer and (*S*)-CMA, respectively.

Structure-switching SELEX Trial 5

For trial 5, we chose to test the Morse library using the same protocol employed in trial 4, except the 5 preselection washes were carried out for 30 seconds instead of 5 minutes. We also chose to select for a new target. We changed the target to (*S*)-2-chloromandelic methyl ester ((*S*)-CME). There were two important reasons for the switch in our target. First, the cytochrome P450 enzymes from the Arnold lab accept phenylacetic esters as substrates, but not phenylacetic acids. Thus, having a sensor for the ester would put us in better position to screen P450 variants. Second, our colleagues in the Burrows group at the University of Utah had shared with us unpublished work in which they had great difficulty selecting for targets that contained a carboxylic acid group. We began selections using the new target (*S*)-CME, and after 9 rounds of selection, we had seen no significant enrichment, but chose to test the library to see if any sequences that bound to (*S*)-CME had emerged (Figure 3.18). We tested the library using the bead elution method and again found no significant difference between the 3 samples.

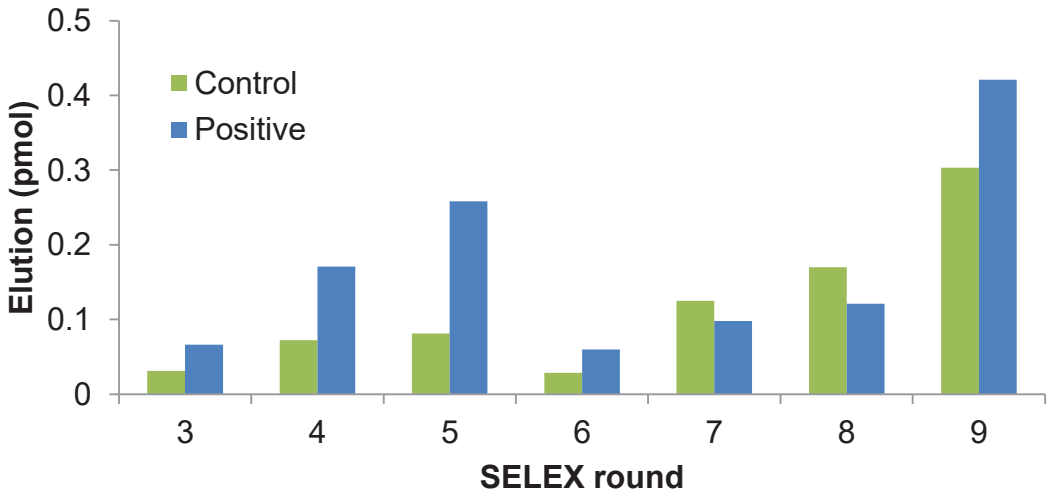

Figure 3.18. Enrichment of library for trial 5 of structure-switching SELEX. Control and positive elutions were performed using buffer and (*S*)-CME, respectively.

Structure-switching SELEX Trial 6

Trial 6 was carried out in the same way as trial 5 except we only performed a single preselection wash for 15 minutes. We hypothesized that in the previous trials, the extensive washing of the library-bound beads was thinning out the library too much and only leaving us with limited sequences that bound tightly to the capture strand. We performed 13 rounds and were encouraged to see enrichment (Figure 3.19). We then used the bead elution method to test the library but once again saw that the library did not displace in the presence of the target. Following this trial, we felt that these methods were not amenable to the selection of structure-switching aptamers for very small molecules and therefore chose to look into a more powerful method for the selection of small-molecule-binding structure-switching aptamers. The major limiting factor to bead-based SELEX methods is the high background from nonspecific elution in each round, leading to the need to perform >10 rounds of selections to successfully obtain an aptamer. Our search for more powerful methods hinged on finding a separation method able to increase the partitioning of bound and unbound sequences.

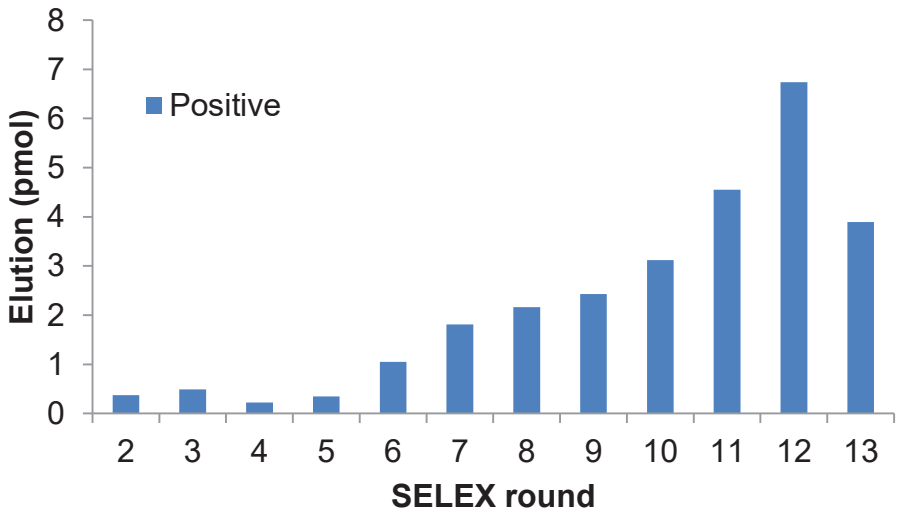

Figure 3.19. Enrichment of library for trial 6 of structure-switching SELEX.

Capillary electrophoresis structure-switching aptamer SELEX

Capillary electrophoresis (CE) has been successfully used to select for traditional aptamers in as little as one round.[23] The power of CE lies in its incredibly efficient partitioning ability. However, the major limitation of CE is that the target must be of high enough molecular weight to cause a shift in mobility when bound to a library member. This limitation severely hinders the applicability of CE SELEX for small-molecule aptamer selections. We discovered that many groups had successfully circumvented this problem and used CE to separate low molecular weight targets by appending a drag tag (high molecular weight molecule) to one of the molecules. Therefore, we hypothesized that by designing a CE structure-switching SELEX method with a drag tag on the capture strand, we could select structure-switching aptamers for smaller targets.

We first attempted selections using a displacement strand modified with a PEG spacer and a T_{20} (PT20) as a drag tag (Figure 3.20). We began optimization of the separation but found that the standard bare fused silica (BFS) capillary would not work with our system. In capillary electrophoresis, there are three dominating forces that lead to migration within the column (Figure 3.21). First, the electromotive force is dictated by the charge density of the molecules. In our case, we were running in reverse phase, allowing for negatively charged molecules to traverse the column toward the positive terminal. The second force is drag, which is related to the size and structure of the molecules. Finally, electroosmotic flow (EOF) is the flow of the bulk solvent towards the negative terminal. EOF is caused by the negatively charged silanol groups on the walls of the BFS capillaries. We found that the EOF increased both migration time and broadened peak width, leading to very poor separation of the molecules. Elimination of the EOF is possible through the use of a high pH (>9.4) buffer, or through modification of the capillary walls. High pH will interfere with DNA folding, so this was not an option for

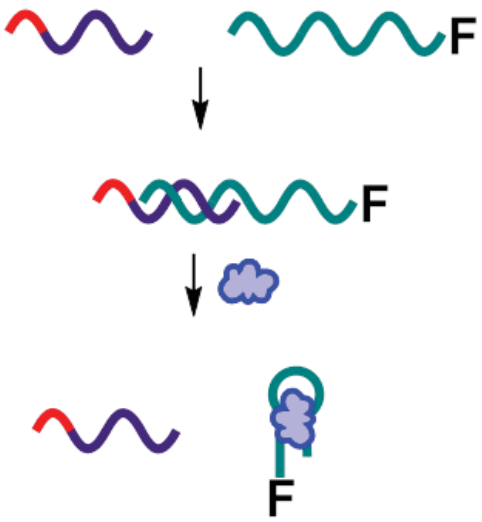

Figure 3.20. Library and capture strand PT20 design for CE SELEX. Red/purple = PT20; Green = library; F = fluorescein

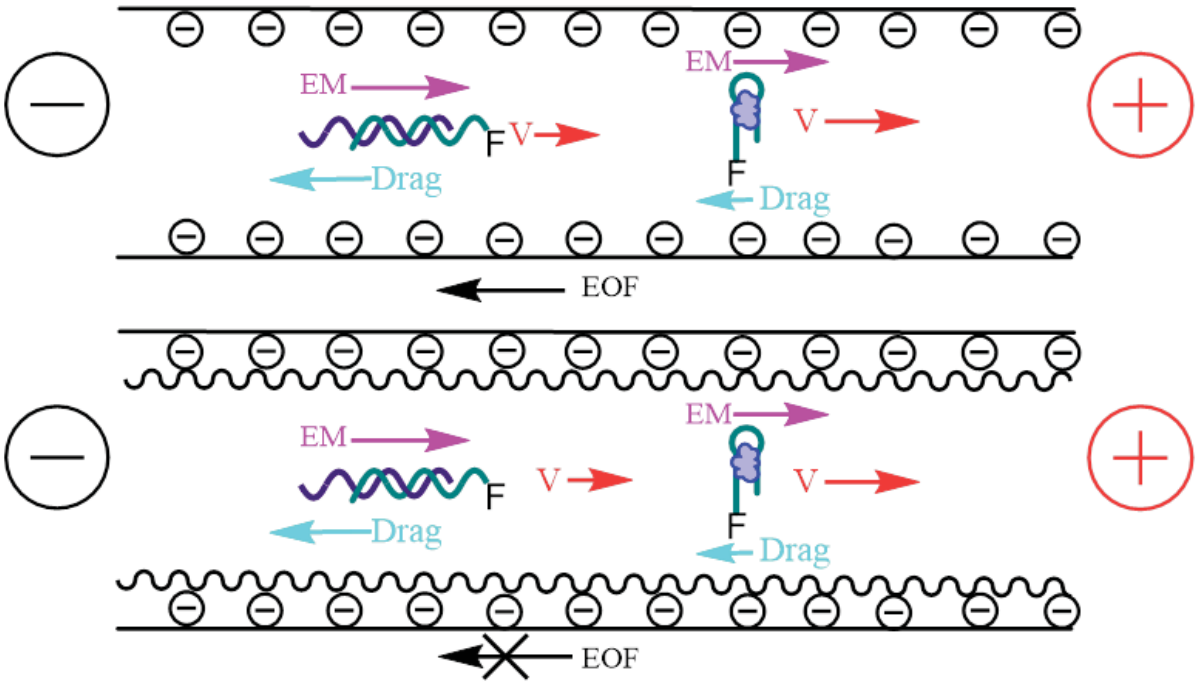

Figure 3.21. Comparison of the effects a BFS capillary (top) and a CEP capillary (bottom) have on the migration of a structure-switching SELEX library.

our system. We chose to use a CEP capillary that is functionalized with a layer of PEG on the walls, which eliminates the EOF.

Next, we optimized the ionic strength of the buffers used in the system. High ionic strength or the presence of divalent ions leads to limited separation as well as joule heating within the capillary. This becomes important for structure-switching SELEX, as the displacement strand must anneal to the library strongly enough to prevent nonspecific dissociation, while being labile enough to displace upon target binding. For instance, we were able to achieve baseline separation of the aptamer library from PT20 by decreasing the ionic strength to 10 μM monovalent ions, but we found that over 50% of the complex nonspecifically disassociated in solutions with such a low ionic strength.

These results led us to explore displacement strands modified with bulkier drag tags to increase separation, allowing the use of higher ionic strengths. We first explored the use of proteins as drag tags. The displacement strand was synthesized having a 3' biotin and attached to streptavidin, avidin, or neutravidin drag tag constructs. These were each tested in various ionic strength solutions to find the maximum concentration of monovalent ions that would still provide sufficient separation. The separation of the complexes was not as good as we had expected, and we hypothesized that this was due to the tetrameric nature of these protein tags. For example, each streptavidin has four biotin binding sites, thereby allowing for attachment of up to 4 capture strands and library members. This diversity led to very broad peaks and still required very low ionic strengths to provide sufficient separation. We found again that to achieve baseline separation, the ionic strength had to be reduced to <10 μM monovalent ions to achieve sufficient separation, resulting in an unacceptable level of nonspecific dissociation (Figure 3.22).

We next explored monovalent streptavidin to decrease the peak width, thereby allowing for higher ionic strengths to be used. This protein was expressed from plasmids

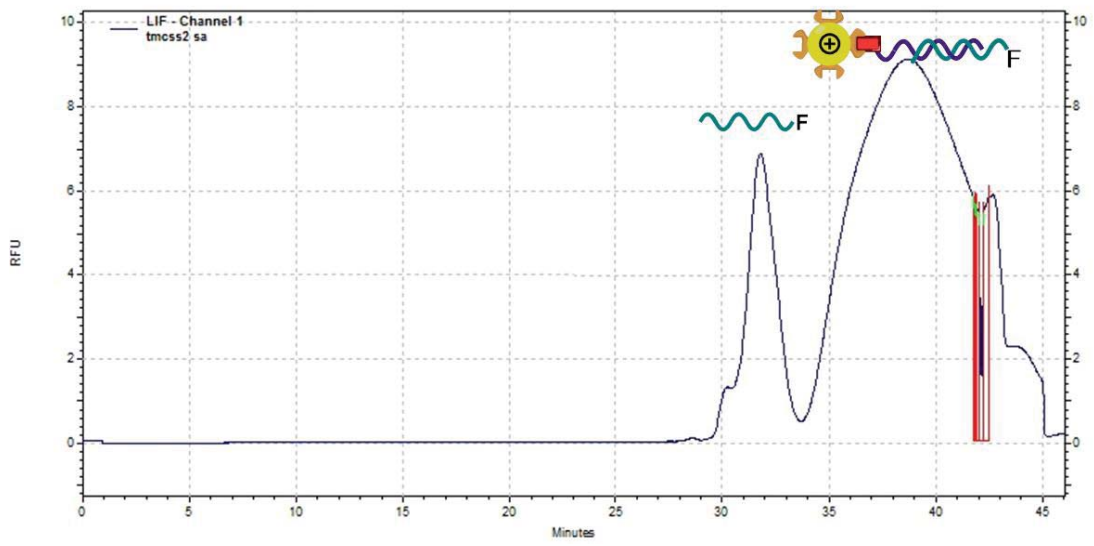

Figure 3.22. Electropherogram showing separation of free library and bound library. Baseline separation was achieved at low ionic strength but this led to high nonspecific dissociation of complex. Streptavidin is shown as binding only one biotin for simplicity.

acquired through ADDGENE. However, we found that this process was very laborious and after expression and purification, we obtained very little protein. The difficulty of obtaining a sufficient amount of protein for selection led us to abandon this method as we aim to develop a simple, widely applicable selection strategy. Therefore, the time and effort required to produce the monovalent streptavidin was determined to be incongruent with our goals.

Latex microspheres, on the other hand, are cheap, available in many sizes, and have a wide variety of attachment chemistries. We choose to use 60 nm latex spheres having aldehyde functional groups. This size allowed us to maximize surface area while increasing the number of spheres that could be injected into the capillary for each run. The remainder of the surface was covered in sulfate groups, resulting in a high negative charge on the spheres, allowing for a greater separation. Displacement strands modified with a 3' C_6-NH_2 were synthesized and reductive amination was used to attach them to the microspheres. The functionalized microspheres were incubated with fluorescein la-

beled library and injected onto the capillary. Currently, we are exploring the effect of loading density on the separation of bound and unbound library. We anticipate that having the ability to control loading density of the displacement strands onto the latex microspheres will provide more precise control of separation and allow for higher ionic strengths to be used.

Conclusion

Much of our research has focused on development of an efficient selection procedure for reliably generating structure-switching DNA biosensors. This has proven to be the greatest hurdle for the integration of aptamers into our analytical applications. Our lab has focused on small-molecule selections, as these represent the most difficult targets for biosensor design. As such, we hypothesized that designing a robust selection method for small molecules would be more generalizable than methods for larger targets. The purpose of this chapter was to define the current limitations for selecting small-molecule aptamers and to provide alternative selection strategies. Clear evidence of the extent of these challenges in biosensor selection can be seen by the near exclusive use of the same handful of aptamer biosensors in the literature.

A practical application for these small-molecule biosensors is detailed in Chapter 2. Future work for (S)-CMA aptamers created in the Heemstra lab will be focused on the screening of P450 libraries to generate an enzyme that will produce 2-CMA with a commercially viable enantioselectivity. This will be accomplished by performing site-saturation mutagenesis on a variant of BM-3 reported by Arnold and coworkers.[9] The 9-10A-F87A mutant has been shown to hydroxylate substituted mandelic methyl esters. This mutant has high substrate specificity but only moderate enantioselectivity. The mutants would be screened for the stereochemistry of the alpha hydroxylation performed on 2-chlorophenylacetic methyl ester, producing 2-chloromandelic methyl ester, and the bi-

osensors being created would be used to measure the enantioselectivity of enzyme mutants. The use of aptamer-based screening methods will dramatically increase the number of mutants that can be screened, leading to enhanced efficiency and selectivity.

Materials and Methods

General methods

Unless otherwise noted, all starting materials were obtained from commercial suppliers and used without further purification. All DNA was purchased from the University of Utah DNA/Peptide Synthesis Core Facility. All absorbance and fluorescence values were recorded using a Biotek Synergy Mx microplate reader. All DNA sequences used in Chapter 3 can be found in Table 3.1. All buffers used in Chapter 3 can be found in Table 3.2.

Modifiers used for DNA synthesis

Fluorescein was installed using phosphoramidites obtained from Glen Research. Black Hole quencher 1, biotin, and C_6-NH_2 modifiers were installed using CPG cartridges from Glen Research.

PCR conditions

PCR1-87 [5 min 95 ºC,20x (1 min 94 ºC, 1 min 47 ºC, 1 min 72 ºC) 10 min 72 ºC]

Primers (jh0614-2 and jh0614-5)

PCRSSS [3 min 95 °C,15x (1 min 95 °C, 1 min 51 °C, 1 min 72 °C) 10 min 72 °C]

Primers (AP60 and Ter-AP20)

PCRSSS2 [3 min 95 °C,15x (30 sec 95 °C, 30 sec 60 °C, 45 sec 72 °C) 2 min 72 °C]

Primers (FP-II-30 and RP-II-30)

Table 3.1. Nucleic acid sequences and modifications used throughout Chapter 3. Where X= Fluorescein Y= PEG_6 Z= C_6-NH_2

JH0614-1	X-ATACCAGCTTATTCAATTN_{40}AGATAGTAAGTGCAATCT
JH0614-5	A_{20}-Y-AGATTGCACTTACTATCT
JH0614-2	X-ATACCAGCTTATTCAAT
TMC-II-2-N40	ATACCAGCTTATTCAATTN_{10}TGAGGCTCGATCN_{30}AGATAG
	TAAGCAATCT
AP60	X-ACCAGCTTATTCAATT
TER-AP20	A_{20}-Y-AGATTGCACTTACTATCT
TMC-3-I-ODN2SP	Biotin-GTC-Y-GATCGAGCCTCA
TMC-II-30-N_{30}	GGAGGCTCTCGGGACGACN_{30}GTCGTCCCGATGCTGCA
	ATCGTAA
FP-II-30	X-GGAGGCTCTCGGGACGAC
RP-II-30	A_{20}-Y-TTACGATTGCAGCATCGGGACGAC
CS-II-30	GTCGTCCCGAGAGCCATA-Biotin
TMC-II-69-2	T_{20}-Y-GATCGAGCCTCA
TMC-II-69-3	Biotin-TTTTT-YYY-GATCGAGCCTCA
TMC-II-70-1	X-GAATGGATCCACATCCATGGN_{40}TTCACTGCAGACTTGACGA
	AGCTTGACGAA
TMC-II-70-2	X-GGAATGGATCCACATCCATGG
TMC-II-70-3	T_{20}-Y-AAGCTTCGTCAAGTCTGCAGTGAA
TMC-II-70-4	GGATCCATTCC-Biotin
TMC-II-70-5	GTGGATCCATTCC-YYY-TTTTT-Biotin
TMC-II-72-1	GATCGAGCCTCA-YYY-T_{10}-Z

Table 3.2. All buffers used throughout Chapter 3

Binding buffer [BB1-9]	10 mM Tris-HCl, 100 mM NaCl, 5 mM KCl, 2 mM MgCl2, 1 mM CaCl2, pH 7.5
Wash conjugation buffer [WCB1-9]	0.1 M sodium phosphate, 0.15 M NaCl, pH 7.4
Elution buffer [EB1-74]	40 mM Tris-HCl, 10 mM EDTA, 3.5 M Urea, 0.02% tween 20
Reduction buffer [RB1-9]	5 M $NaCNBH_3$ in 1 M NaOH
Blocking agent [BA1-9]	0.1 M ethanolamine pH 7.4
Bind and Wash [B&W]	10 mM Tris-HCl, 1 mM EDTA, 2 M NaCl, pH 7.5
Crush and soak [C&S]	2 mM EDTA, 300 mM NaOAc
CE buffer [RB-69-10]	50 mM Tris-Borate, 10 mM NaCl, pH 7.4
Microsphere conjugation buffer [MSCB]	100 mM MES, 10 mM NaCl, pH 6
Microsphere reduction buffer [MSRB]	400 mM $NaCNBH_3$

FluMag magnetic bead preparation

M-270 amine functionalized magnetic beads were obtained from Invitrogen for all FluMag SELEX experiments. Bead conjugation was performed as follows; solutions of aldehyde modified (*S*)-CMA were made at 10 mg/mL in WCB1-9. 1 mL of M-270 beads were placed on a magnet for 4 minutes and the supernatant was removed. Beads were then resuspended in 1 mL of WCB1-9. This process was repeated 3 times followed by addition of 1 mL of the aldehyde modified (*S*)-CMA solution. 10 µL of RB1-9 was added and the solution was left to incubate for 2 hours on a nutating mixer at 25 °C. Following incubation, the beads were placed on a magnet and the supernatant was removed. 1 mL of BA1-9 was added and the solution was incubated for an additional 15 minutes on a nutating mixer at 25 °C. The beads were then washed 3 times with WCB1-9 followed by 3 washes with BB1-9. Beads were now ready for selection rounds and will be referred to as (FB-FM).

Structure-switching magnetic bead preparation

M-270 streptavidin functionalized magnetic beads were obtained from Invitrogen. 1 mL of beads were washed 3 times with B&W. On the final wash, B&W was added to produce a concentration 10^9 beads per mL. Next, 600 pmols of TMC-3-i-odn2sp capture strand was added per 10^8 beads. The resulting solution was incubated at room temperature for 1 hour on a nutating mixer. Beads were then washed 3 times with B&W followed by 3 times with BB1-9. Beads were now ready for selection rounds and will be referred to as (PB-SS).

Microsphere bead preparation

Aldehyde/sulfate 0.06 µm superactive latex beads were obtained from Life Technologies. Approximately 10^{12} latex beads were dialyzed 2 times for >3 hours with MSCB

using 20 kDa dialysis tubing. 50 nmols of TMC-II-72-1 was added to the equilibrated microspheres in 100 µL of MSCB. 5 µL of MSRB was added and the mixture was incubated at 37 ºC for 24 hours. The reaction was stopped through the addition of 0.1 mM ethanolamine and finally dialyzed 3 times for >3 hours with RB-69-10 using 20 kDa dialysis tubing. The microspheres were now ready for use.

FluMag SELEX general procedure

For the first round of selection, 6 nmols of jh0614-1 was snap cooled (heating to 90 ºC for 8 minutes, followed by 4 ºC for 10 minutes and finally equilibration at 25 ºC for 5 minutes) and then incubated for 2 hours on a nutating mixer with 50 µL of FB-FM in a total volume of 500 µL of BB1-9. Subsequent rounds used 200 pmols of the library from the previous round with a fresh 50 µL of FB-FM. The solution was then placed on a magnet for 4 minutes and the supernatant was removed. The beads were washed 5 times by adding 200 µL of BB1-9, briefly vortexing, magnetically separating, and removing the supernatant. If negative selections were performed, they were done at this stage by incubating the beads with the negative target for 30 minutes on a nutating mixer, magnetically separating, and removing of the supernatant. Next, 200 µL of BB1-9 containing the target of interest was added, briefly vortexed, and incubated at 25 °C for 30 minutes. Following the incubation, the solution was magnetically separated and the supernatant collected. The beads were then heat eluted to remove any library members that were tightly bound to the bead-bound targets. This was accomplished by the addition of 200 µL of EB1-74 and heating to 80 °C for 8 minutes. Before the solution was allowed to cool, it was magnetically separated, and the supernatant was removed.

The elutions were all quantified at this point using a 96 well plate and a fluorescence plate reader. The positive and the heat elutions were combined and PCR amplified in16 parallel 100 µL reactions using PCR1-87. The 16 reactions were pooled and

purified using a Qiagen minielute PCR clean up kit. The purified dsDNA was then separated using a 10% denaturing PAGE gel for ~60 minutes at 120 volts. Gels were then imaged on a UV transilluminator and the fluorescein bands were excised. The excised bands were crushed and placed in 500 µL of C&S and placed at -80 ºC for 1 hour and then immediately placed on a heat block at 90 ºC for 150 minutes. The gel fragments were then removed using a 0.2 µM spin filter. Purified library was concentrated using 10 kDa spin filters and used for the next round of selection.

Structure-switching SELEX general procedure

2.5 nmols of TMC-II-2-N40 was incubated with 10^9 of PB-SS for the first round. Subsequent rounds used an average of 200 pmol of library from the preceding round with 10^8 of fresh PB-SS. Library was suspended in BB1-9 and snap cooled (heating to 90 ºC for 8 minutes, followed by 4 ºC for 10 minutes and finally equilibration at 25 ºC for 5 minutes) and incubated with PB-SS for 18 hours at 25 ºC on a nutating mixer. Next, beads were stripped of nonbinding library members through a series of washing steps. This was accomplished by placing the tubes on a magnet for 4 minutes, then removing the supernatant and adding an equal volume of BB1-9. Time and quantity of washes varied between cycles and the specifics can be found within cycle descriptions. If negative selections were performed, they would be done at this point followed by washes. Finally, positive elutions were performed using target molecule in BB1-9. Tubes were placed on the magnet for 4 minutes and binding sequences were collected in the supernatant. Quantification of eluted library was carried out in a 96 well plate with a fluorescence plate reader.

Positive elutions were then PCR amplified in 16 parallel 100 µL reactions using PCRSSS for cycles 1, 4 and PCRSSS2 for cycles 2, 3, 5, and 6. The 16 reactions were pooled and purified using a Qiagen minielute PCR clean up kit. The purified dsDNA was

then separated using a 10% denaturing PAGE gel for ~60 minutes at 120 volts. Gels were then imaged on a UV transilluminator and the fluorescein bands were excised. The excised bands were crushed and placed in 500 µL of C&S and placed at -80 °C for 1 hour and immediately placed on a heat block at 90 °C for 150 minutes. The gel fragments were removed using a 0.2 µM spin filter, and purified library concentrated using a 10 kDa spin filter, and used for the next round of selection.

References

(1) Reetz, M. T. Controlling the Enantioselectivity of Enzymes by Directed Evolution: Practical and Theoretical Ramifications. *Proc. Natl. Acad. Sci. U.S.A.* **2004**, *101*, 5716-5722.

(2) Leung, D. W.; Chen, E.; Goeddel, D. V. A Method for Random Mutagenesis of a Defined DNA Segment Using a Modified Polymerase Chain Reaction. *Technique* **1989**, *1*, 11-15.

(3) Cadwell, C.; Joyce, G. F. Randomization of Genes by PCR Mutagenesis. *PCR Methods Appl.* **1992**, *2*, 28-33.

(4) Barettino, D.; Feigenbutz, M.; Valcárcel, R.; Stunnenberg, H. G. Improved Method for PCR-Mediated Site-Directed Mutagenesis. *Nucleic Acids Res.* **1994**, *22*, 541-542.

(5) Jung, S. T.; Lauchli, R.; Arnold, F. H. Cytochrome P450: Taming a Wild Type Enzyme. *Curr. Opin. Biotechnol.* **2011**, *22*, 809-817.

(6) Guengerich, F. P. Cytochrome P450 and Chemical Toxicology. *Chem. Res. Toxicol.* **2008**, *21*, 70-83.

(7) Pochapsky, T. C.; Kazanis, S.; Dang, M. Conformational Plasticity and Structure/Function Relationships in Cytochromes P450. *Antioxid. Redox Signal* **2010**, *13*, 1273-1296.

(8) Bloom, J. D.; Labthavikul, S. T.; Otey, C. R.; Arnold, F. H. Protein Stability Promotes Evolvability. *Proc. Natl. Acad. Sci. U.S.A.* **2006**, *103*, 5869-5874.

(9) Landwehr, M.; Hochrein, L.; Otey, C. R.; Kasrayan, A.; Backvall, J. E.; Arnold, F. H. Enantioselective Alpha-Hydroxylation of 2-Arylacetic Acid Derivatives and Buspirone Catalyzed by Engineered Cytochrome P450 Bm-3. *J. Am. Chem. Soc.* **2006**, *128*, 6058-6059.

(10) Tang, W. L.; Li, Z.; Zhao, H. Inverting the Enantioselectivity of P450pyr Monooxygenase by Directed Evolution. *Chem. Commun. (Camb)* **2010**, *46*, 5461-5463.

(11) Sulistyaningdyah, W. T.; Ogawa, J.; Li, Q. S.; Maeda, C.; Yano, Y.; Schmid, R. D.; Shimizu, S. Hydroxylation Activity of P450 Bm-3 Mutant F87v Towards Aromatic Compounds and Its Application to the Synthesis of Hydroquinone Derivatives from Phenolic Compounds. *Appl. Microbiol. Biotechnol.* **2005**, *67*, 556-562.

(12) Reetz, M. T. Laboratory Evolution of Stereoselective Enzymes: A Prolific Source of Catalysts for Asymmetric Reactions. *Angew. Chem. Int. Ed.* **2011**, *50*, 138-174.

(13) Romero, P. A.; Arnold, F. H. Exploring Protein Fitness Landscapes by Directed Evolution. *Nat. Rev. Mol. Cell Biol.* **2009**, *10*, 866-876.

(14) Dzik-Jurasz, A. S. K. Molecular Imaging in Vivo: An Introduction. *Brit. J. Radiol.* **2003**, *76*, S98-S109.

(15) (15) Jäckel, C.; Kast, P.; Hilvert, D. Protein Design by Directed Evolution. *Annu. Rev. Biophys.* **2008**, *37*, 153-173.

(16) Ellington, A. D.; Szostak, J. W. In Vitro Selection of RNA Molecules That Bind Specific Ligands. *Nature* **1990**, *346*, 818-822.

(17) Tuerk, C.; Gold, L. Systematic Evolution of Ligands by Exponential Enrichment: RNA Ligands to Bacteriophage T4 DNA Polymerase. *Science* **1990**, *249*, 505-510.

(18) Zuker, M. Mfold Web Server for Nucleic Acid Folding and Hybridization Prediction. *Nucleic Acids Res.* **2003**, *31*, 3406-3415.

(19) North, M.; Usanov, D. L.; Young, C. Lewis Acid Catalyzed Asymmetric Cyanohydrin Synthesis. *Chem. Rev.* **2008**, *108*, 5146-5226.

(20) Stoltenburg, R.; Reinemann, C.; Strehlitz, B. Flumag-Selex as an Advantageous Method for DNA Aptamer Selection. *Anal. Bioanal. Chem.* **2005**, *383*, 83-91.

(21) Stoltenburg, R.; Nikolaus, N.; Strehlitz, B. Capture-Selex: Selection of DNA Aptamers for Aminoglycoside Antibiotics. *J. Anal. Met. Chem.* **2012**, *2012*, 14.

(22) Morse, D. P. Direct Selection of RNA Beacon Aptamers. *Biochem. Biophys. Res. Commun.* **2007**, *359*, 94-101.

(23) Mosing, R. K.; Mendonsa, S. D.; Bowser, M. T. Capillary Electrophoresis-Selex Selection of Aptamers with Affinity for Hiv-1 Reverse Transcriptase. *Anal. Chem.* **2005**, *77*, 6107-6112.

CHAPTER 4

CONVENIENT AND SCALABLE SYNTHESIS OF FMOC-PROTECTED PEPTIDE NUCLEIC ACID BACKBONE*

Introduction

Peptide nucleic acid (PNA) has recently emerged as a promising alternative to the native nucleic acids DNA and RNA (Figure 4.1) for a wide variety of applications including antisense therapy and gene diagnostics.[1-3] The key advantages of PNA over DNA and RNA are its resistance to degradation by cellular nucleases and its relatively higher binding affinity and mismatch selectivity in duplex formation.[4-5] PNA can be generated by Fmoc- or Boc-solid phase peptide synthesis,[6] and Fmoc-protected monomers bearing each of the four canonical nucleobases are commercially available. Recently, the incorporation of modified nucleobases into PNA has been shown to enable synthesis of nucleic acids having unique physicochemical properties.[7] However, PNA monomers bearing modified nucleobases are not commercially available, and must instead be synthesized in the laboratory. Suitable reactions have been reported for preparation of modified nucleobases and coupling of these nucleobase acetic acids to the PNA backbone (Figure 4.2).[7-8] However, to our knowledge, a scalable and cost-effective synthesis for the protected *N*-[2-(Fmoc)aminoethyl]glycine benzyl ester (Fmoc-AEG-OBn) back-

---

* Adapted under the terms of the Creative Commons Attribution License from Feagin, T. A.; Shah, N. I.; Heemstra, J. M. Convenient and Scalable Synthesis of Fmoc-Protected Peptide Nucleic Acid Backbone. *J. Nucleic Acids*. **2012**, 2012, 354549.

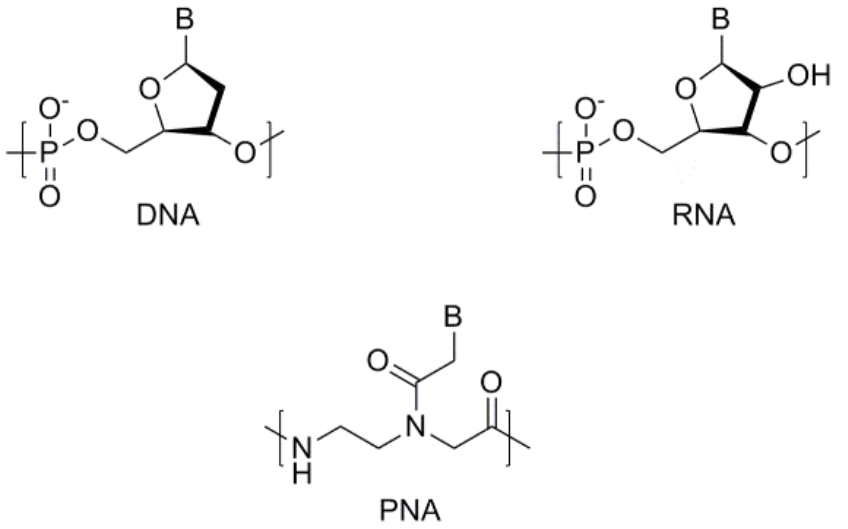

Figure 4.1. Chemical structure of DNA, RNA, and PNA.

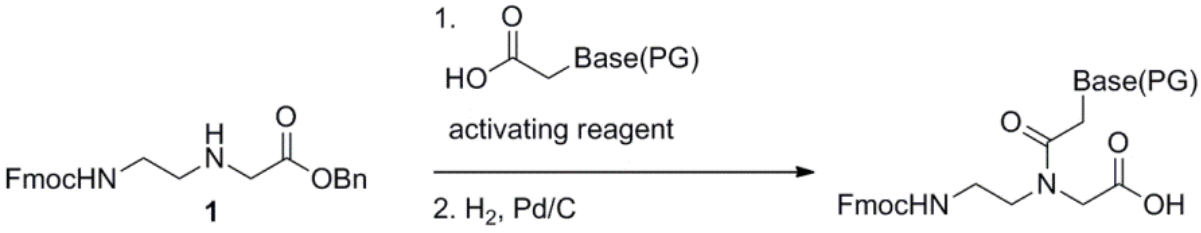

Figure 4.2. Synthesis of Fmoc-protected PNA monomers.

bone **1** has yet to be reported.[9] Here we describe a synthesis of **1** that proceeds in four steps with an overall yield of 32%, utilizes inexpensive reagents, and can be scaled to produce large quantities of final product in a single batch with only minimal purification.

Results and Discussion

An extensive literature search reveals only one published route to **1**, as shown in Figure 4.3a. This route, reported by Hudson and coworkers, proceeds in three steps with an overall yield of 81%, but requires the use of costly *N*-(2-aminoethyl)glycine as the starting material.[8] Furthermore, in our hands, this synthetic route has proven difficult to reproduce. Alternatively, Porcheddu and coworkers have described a synthesis of Fmoc-AEG-OMe **2** that proceeds in three steps with an overall yield of 66% (Figure 4.3b), but requires three equivalents of IBX to accomplish the oxidation step.[9] Thomson and coworkers have described a synthesis of Fmoc-AEG-O*t*-Bu·HCl **3·HCl** that proceeds in two steps with 46% overall yield from inexpensive starting materials (Figure 4.3c), but does not produce analytically pure material.[10-13] Furthermore, the exocyclic amines of the PNA nucleobases are typically protected with acid-labile Boc or Bhoc protecting groups. Deprotection of the *tert*-butyl ester requires strongly acidic conditions, making **3** unsuitable for use with Boc- or Bhoc-protected nucleobases.

Inspired by the ease and cost-effectiveness of the Thomson route, we first envisioned synthesis of **1** by alkylation of ethylenediamine with benzyl bromoacetate, followed by reaction with Fmoc *N*-hydroxysuccinimide ester (Fmoc-OSu). Unfortunately, after alkylation and aqueous workup, only benzyl alcohol was recovered. We hypothesize that alkylation product **4** rapidly cyclizes to give benzyl alcohol and water soluble cyclic piperazinone **5** (Figure 4.4a), and that this undesired cyclization can only be suppressed by the use of a bulky ester such as a *tert*-butyl ester. In fact, this cyclization has been demonstrated previously using the analogous methyl ester.[14] We next considered

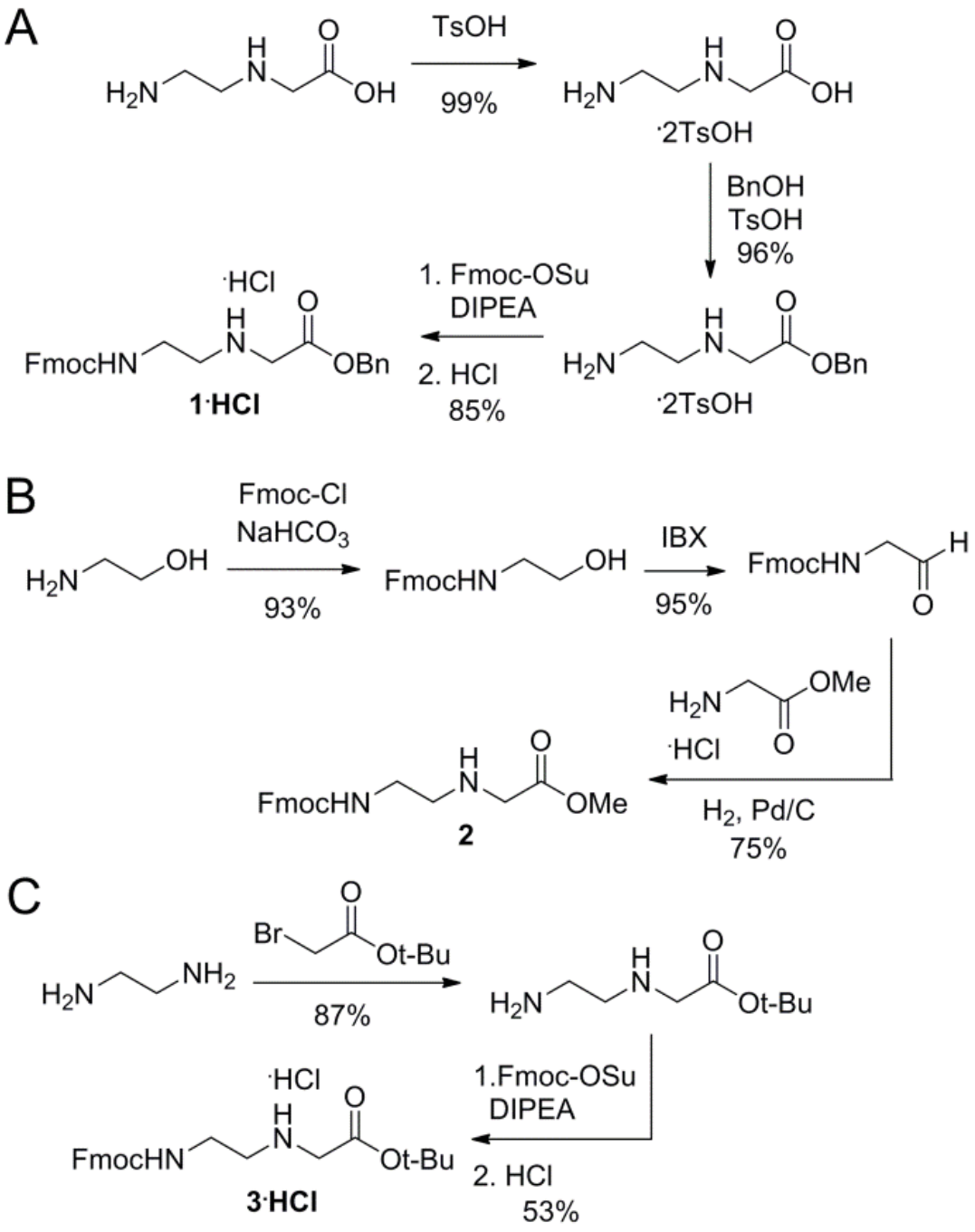

Figure 4.3. Reported synthetic routes to the Fmoc-AEG-OR backbone.

reversing the order of the two reactions such that ethylenediamine would first be mono-protected with Fmoc-OSu, then alkylated with benzyl bromoacetate to give **1**. However, Fmoc-ethylenediamine cannot be directly prepared by the reaction of ethylenediamine with Fmoc-Cl or Fmoc-OSu. Rather, a three-step process is required in which ethylene-diamine is mono-Boc protected (**6**), then Fmoc protected (**7**), and finally the Boc group removed under acidic conditions to give **8** as the TFA salt.[15] Unfortunately, our attempts to alkylate **8**·**TFA** with benzyl bromoacetate failed to yield the desired product **1**, likely due to the instability of the free base of **8** (Figure 4.4b).

Fortunately, we were able to obtain Boc-ethylenediamine **6** in 80% yield from ethylenediamine and Boc anhydride using a modified version of a reported procedure, and this was successfully alkylated with benzyl bromoacetate to give **9** in 72% yield.[16] We then deprotected the Boc group using trifluoroacetic acid (TFA) to give a quantitative yield of free amine, which was importantly found to be stable to cyclization when isolated as the TFA salt. In the final step, we combined the amine TFA salt with Fmoc-OSu prior to adding base, so that protection of the primary amine could compete with cyclization to give the desired product **1** in 55% yield. Starting with 50g of Boc anhydride, we were able to generate 31g of analytically pure **1** in a single batch using inexpensive reagents (Figure 4.4c).[17]

A key to the scalability of our synthetic route is the relatively facile purification of the synthetic intermediates and final product. The Boc protection step to give **6** requires only aqueous workup, and the deprotection step requires simple concentration and re-moval of TFA via formation of an azeotrope with toluene. The alkylation to produce **9** and the Fmoc protection to give **1** require flash column chromatography, but a large dif-ference in R_f between the products and impurities makes purification possible using only a silica plug.

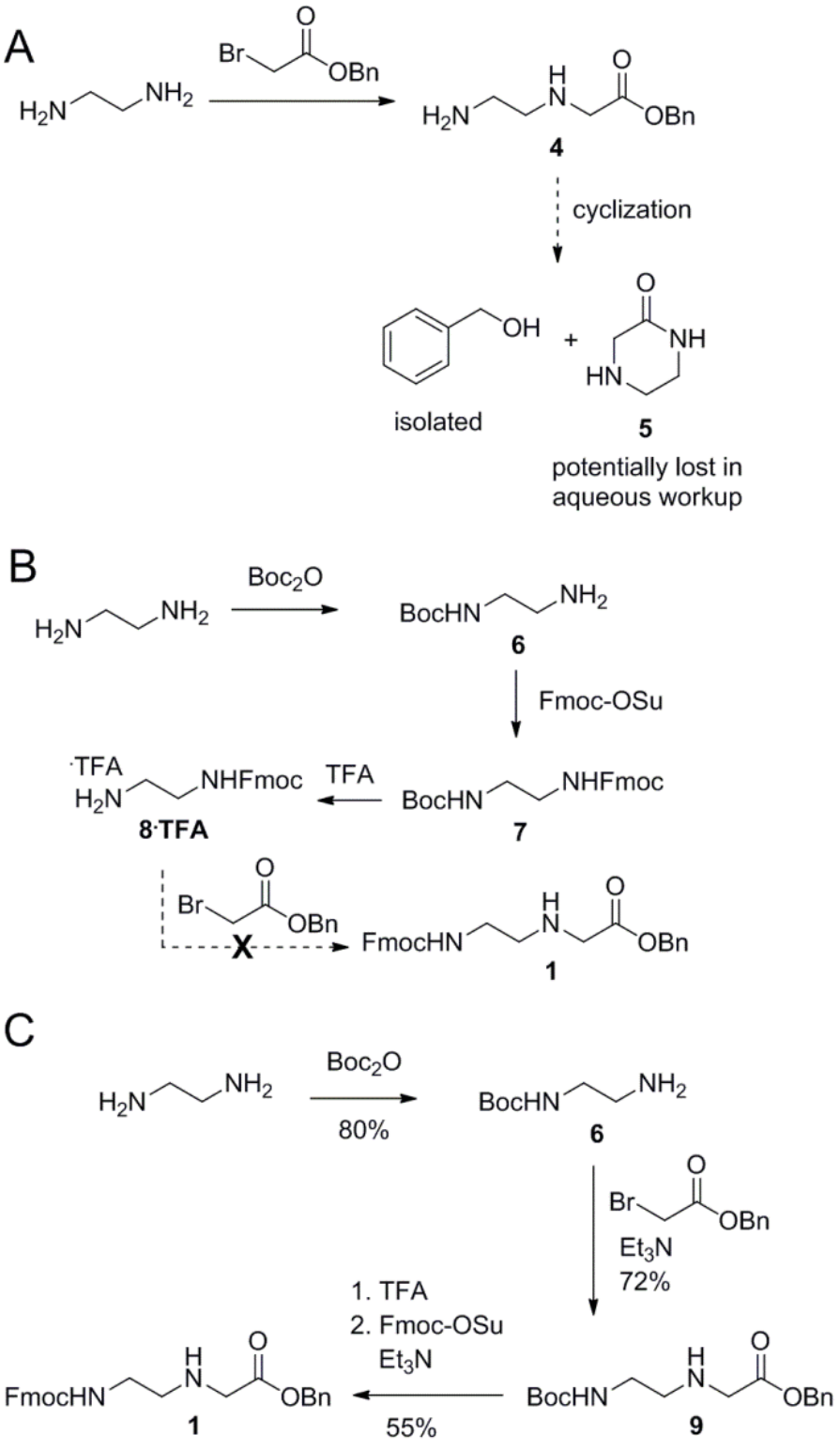

Figure 4.4. Synthetic route to Fmoc-AEG-OBn 1.

Fmoc-protected PNA backbone **1** is a key intermediate in the synthesis of Fmoc-protected PNA monomers having modified nucleobases. However, to date, a scalable and cost-effective synthetic route to this molecule has yet to be reported in the literature. An efficient synthesis of the Boc-protected backbone has been reported, but our attempts to utilize this synthetic route with Fmoc in place of Boc failed to give product, likely due to the instability of synthetic intermediate **8**. Rather, synthesis of **1** can be initiated using a Boc protecting group, followed by a protecting group swap to provide the Fmoc-protected product. The first two steps of our synthetic route mirror those of the published synthesis for the Boc-protected monomer.[18] However, replacement of the Boc group with Fmoc poses a significant challenge, as this step proceeds through unstable intermediate **4**. We were able to perform this transformation by generating the free base of **4** at reduced temperature and in the presence of Fmoc-OSu, enabling Fmoc-protection to effectively compete with cyclization, providing **1** in moderate yield.

Conclusion

In summary, we describe here a novel route to the PNA backbone Fmoc-AEG-OBn **1**. Using this route, we have rapidly synthesized 31g of **1** using inexpensive starting materials and only minimal purification. The overall yield for our synthetic route is modest at 32%; however, the low cost of starting materials and ease of purification enable this synthesis to be tractable on a large scale. Having a convenient route to access **1** is anticipated to ease the synthesis of new Fmoc-protected PNA monomers, presumably furthering the exploration of PNA having unique modified nucleobases.

Materials and Methods

General methods

Unless otherwise noted, all starting materials were obtained from commercial suppliers and were used without further purification. Flash column chromatography was carried out using silica gel 60 (230-400 mesh). ^{1}H and ^{13}C NMR chemical shifts are expressed in parts per million (δ) using residual solvent protons as internal standard (δ 7.26 ppm (1H) and 77.16 ppm (^{13}C) for $CHCl_3$). Coupling constants, *J*, are reported in Hertz (Hz), and splitting patterns are designated as s (singlet), d (doublet), t (triplet), q (quartet), m (multiplet), br (broad), and app (apparent). Mass spectra were obtained through the Mass Spectrometry Facility, University of Utah.

tert-Butyl (2-aminoethyl)carbamate (6)

A 2 L round bottom flask was charged with ethylenediamine (306.5 mL, 4.58 mol) and tetrahydrofuran (600 mL). Boc anhydride (50.0 g, 229 mmol) was dissolved in 400 mL tetrahydrofuran and added to the solution of ethylenediamine via addition funnel over 45 minutes with vigorous stirring. After 18 hours, the reaction was quenched by addition of 500 mL H_2O. The aqueous phase was saturated with solid K_2CO_3, then the phases separated and the organic phase dried over Na_2SO_4, filtered, and concentrated to give a pale yellow oil. The oil was dissolved in 700 mL toluene and concentrated to azeotrope remaining ethylenediamine, yielding 29.24 g of pale yellow oil (80%). ^{1}H NMR (300 MHz, $CDCl_3$) δ 4.90 (br s, 1H), 3.16 (q, *J* = 5.8 Hz, 2H), 2.78 (t, *J* = 5.9 Hz, 2H), 1.43 (s, 9H), 1.09 (br s, 2H). ^{13}C NMR (75 MHz, $CDCl_3$) δ 156.3, 79.1, 43.3, 41.8, 28.4. HRMS (ESI) *m/z* 161.1295 (calcd $[M+H]^+$ = 161.1290).

Benzyl 2-((2-((tert-butoxycarbonyl)amino)ethyl)amino)acetate (9)

A 2 L round bottom flask was charged with **6** (29.24 g, 183 mmol), triethylamine (25.5 mL, 183 mmol), and acetonitrile (450 mL). The reaction mixture was stirred and ethyl bromoacetate (28.9 mL, 182 mmol) added via syringe over 2 minutes. After 100 minutes, the reaction mixture was diluted with 500 mL EtOAc and washed with 500 mL 2M K_2CO_3 (aq.), then 500 mL brine. The organic phase was dried over Na_2SO_4, filtered, and concentrated to a pale yellow oil, which was purified by flash column chromatography, (70 mm diameter column, 285 g silica gel, 1:1 hexanes:EtOAc, 99:1 EtOAc:Et_3N) to give 40.56 g of pale yellow oil (72%). ^{1}H NMR (300 MHz, $CDCl_3$) δ 7.38-7.33 (m, 5H), 5.17 (s, 2H), 4.99 (br s, 1H), 3.45 (s, 2H), 3.20 (q, *J* = 5.7 Hz, 2H), 2.74 (t, *J* = 5.8 Hz, 2H), 1.59 (br s, 1H), 1.44 (s, 9H). ^{13}C NMR (75 MHz, $CDCl_3$) δ 172.3, 156.1, 135.5, 128.6, 128.4, 128.3, 79.0, 66.5, 50.4, 48.7, 40.1, 28.4. HRMS (ESI) *m/z* 331.1640 (calcd $[M+Na]^+$ = 331.1634).

Benzyl 2-((2-((((9H-fluoren-9-yl)methoxy)carbonyl)amino)ethyl)amino)acetate (Fmoc-AEG-OBn 1)

To a 2 L round bottom flask was added **9** (40.46 g, 131 mmol) and dichloromethane (200 mL). The reaction mixture was stirred in an ice bath and 200 mL trifluoroacetic acid added. The ice bath was removed and the reaction mixture stirred for 20 minutes, then concentrated to a yellow oil. The oil was dissolved in 400 mL toluene and concentrated to azeotrope remaining trifluoroacetic acid. The resulting yellow oil was dissolved in 700 mL dichloromethane and stirred under N_2 in an ice bath. Fmoc-OSu (44.26 g, 131 mmol) was added all at once, then triethylamine (54.8 mL, 393 mmol) added dropwise via addition funnel over 5 minutes. The ice bath was removed and the reaction mixture stirred for 2 hours, then washed with 500 mL 1M K_2CO_3 (aq.), dried

over Na_2SO_4, filtered, and concentrated to a yellow oil. The oil was purified by flash column chromatography, (70 mm diameter column, 250 g silica gel, 1:1 hexanes:EtOAc, 98:2 EtOAc:MeOH) to give 31.04 g of pale yellow oil that crystallized into a white solid upon standing (55%). ^{1}H NMR (300 MHz, $CDCl_3$) δ 7.76 (d, *J* = 7.4 Hz, 2H), 7.61 (d, *J* = 7.3 Hz, 2H), 7.42-7.28 (m, 9H), 5.29 (br s, 1H), 5.18 (s, 2H), 4.40 (d, *J* = 7.0 Hz, 2H), 4.22 (t, *J* = 6.8 Hz, 1H), 3.47 (s, 2H), 3.29 (q, *J* = 5.4 Hz, 2H), 2.78 (t, *J* = 5.6 Hz, 2H), 1.58 (br s, 1H). ^{13}C NMR (75 MHz, $CDCl_3$) δ 172.3, 156.6, 144.0, 141.3, 135.5, 128.6, 128.5, 128.4, 127.6, 127.0, 125.1, 120.0, 66.6, 66.4, 50.4, 48.6, 47.3, 40.6. HRMS (ESI) *m/z* 431.1972 (calcd $[M+H]^+$ = 431.1971).

References

(1) Nielsen, P. E.; Egholm, M.; Berg, R. H.; Buchardt, O. Sequence-Selective Recognition of DNA by Strand Displacement with a Thymine-Substituted Polyamide. *Science* **1991**, 254, 1497-1500.

(2) Good, L.; Nielsen, P. E. Antisense Inhibition of Gene Expression in Bacteria by PNA Targeted to mRNA. *Nat. Biotechnol.* **1998**, 16, 355-358.

(3) Nielsen, P. E. Peptide Nucleic Acid: A Versatile Tool in Genetic Diagnostics and Molecular Biology. *Curr. Opin. Biotechnol.* **2001**, 12, 16-20.

(4) Gambacorti-Passerini, C.; Mologni, L.; Bertazzoli, C.; LeCoutre, P.; Marchesi E, E.; Grignani, F.; Nielsen, P. E. In Vitro Transcription and Translation Inhibition by Anti-Promyelocytic Leukemia (PML)/Retinoic Acid Receptor Alpha and Anti-PML Peptide Nucleic Acid. *Blood* **1996**, 88, 1411-1417.

(5) Egholm, M.; Buchardt, O.; Christensen, L.; Behrens, C.; Freier, S. M.; Driver, D. A.; Berg, R. H.; Kim, S. K.; Norden, B.; Nielsen, P. E. PNA Hybridizes to Complementary Oligonucleotides Obeying the Watson-Crick Hydrogen-Bonding Rules. *Nature* **1993**, 365, 566-568.

(6) Braasch, D. A.; Nulf, C. J.; Corey, D. A. Synthesis and Purification of Peptide Nucleic Acids. *Curr. Protocols Nucleic Acid Chem.* **2002**, 4.11.1-4.11.18.

(7) Wojciechowski, F.; Hudson, R. H. E. Nucleobase Modifications in Peptide Nucleic Acids. *Curr. Top. Med. Chem.* **2007**, 7, 667-679.

(8) Wojciechowski, F.; Hudson, R. H. E. A Convenient Route to N-[2-(Fmoc)aminoethyl]glycine Esters and PNA Oligomerization Using a Bis-N-Boc Nucleobase Protecting Group Strategy. *J. Org. Chem.* **2008**, 73, 3807-3816.

(9) Porcheddu, A.; Giacomelli, G.; Piredda, I.; Carta, M.; Nieddu, G. A Practical and Efficient Approach to PNA Monomers Compatible with Fmoc-Mediated Solid-Phase Synthesis Protocols. *Eur. J. Org. Chem.* **2008**, 34, 5786-5797.

(10) Lioy, E.; Suarez, J.; Guzmàn, F.; Siegrist, S.; Pluschke, G.; Patarroyo, M. E. Synthesis, Biological, and Immunological Properties of Cyclic Peptides from *Plasmodium Falciparum* Merozoite Surface Protein-1. *Angew. Chem. Int. Ed.* **2001**, 40, 2631-2635.

(11) Coull, J. M.; Egholm, M.; Hodge, R. P.; Ismail, M.; Rajur, S. B. Synthons for the Synthesis and Deprotection of Peptide Nucleic Acids Under Mild Conditions. U.S. Patent 6,172,226, 2001.

(12) Debaene, F.; Da Silva, J. A.; Pianowski, Z.; Duran, F. J.; Winssinger, N. Expanding the Scope of PNA-Encoded Libraries: Divergent Synthesis of Libraries Targeting Cysteine, Serine and Metalloproteases as well as Tyrosine Phosphatases. *Tetrahedron* **2007**, 63, 6577-6586.

(13) Altenbrunn, F.; Seitz, O. *O*-Allyl Protection in the Fmoc-Based Synthesis of Difficult PNA. *Org. Biomol. Chem.* **2008**, 6, 2493-2498.

(14) Thomson, S. A.; Josey, J. A.; Cadilla, R.; Gaul, M. D.; Hassman, C. F.; Luzzio, M. J.; Pipe, A. J.; Reed, K. L.; Ricca, D. J.; Wiethe, R. W.; Noble, S. A. Fmoc Mediated Synthesis of Peptide Nucleic Acids. *Tetrahedron* **1995**, 51, 6179-6194.

(15) Hay, R. W.; Basak, A. K.; Pujari, M. P. Kinetics and Mechanism of the Copper(II) Promoted Hydrolysis of the Methyl Ester of Ethylenediaminemonoacetate. *Transit. Metal Chem.* **1986**, 11, 27-30.

(16) Kocis, P.; Issakova, P.O.; Sepetov, N. F.; Lebl, M. Kemp's Triacid Scaffolding for Synthesis of Combinatorial Nonpeptide Uncoded Libraries. *Tetrahedron Lett.* **1995**, 36, 6623-6626.

(17) Xu, P.; Zhang, T.; Wang, W.; Zou, X.; Zhang, X.; Fu, Y. Synthesis of PNA Monomers and Dimers by Ugi Four-Component Reaction. *Synthesis* **2003**, 34, 1171-1176.

(18) Fader, L. D.; Boyd, M.; Tsantrizos, Y. S. Backbone Modifications of Aromatic Peptide Nucleic Acid (APNA) Monomers and Their Hybridization Properties with DNA and RNA. *J. Org. Chem.* **2001**, 66, 3372-3379.

CHAPTER 5

CONCLUSION AND FUTURE DIRECTIONS

Enzyme Evolution

The field of enzyme screening and evolution has been advanced recently by a number of research labs who have shown that enzymes can be adapted to perform conversions similar to many exotic chiral catalysts at a fraction of the cost.[1-8] Through their work, enzyme mutation has been made trivial, allowing massive libraries of mutant enzymes to be created within a matter of days. As such, the limitation of enzyme evolution has become screening these vast libraries. Reetz has developed powerful HPLC methods for screening the libraries for enantioselectivity. However, these techniques are still only capable of screening a few thousand samples per day, severely limiting the selection process. Other groups have also worked to increase the throughput of enantiopurity screening.[9-17] Anslyn and coworkers have shown that the use of supramolecular sensors can increase the efficiency of screening, demonstrating the ability to analyze greater than 4000 samples per day.[18] The limitations of this system originate from the need to independently measure concentration prior to gaining knowledge of enantiopurity. Therefore, while this method represents a step forward in developing high-throughput methods, it does not approach the necessary efficiency for screening the massive libraries generated in enzyme evolution.

The Heemstra lab has shown a strong dedication to advancing aptamer technologies, and has pioneered a method for using aptamers to measure concentrations of

enantiomers in solution. We hypothesized that by using an enantioselective aptamer and its Speigelmer, orthogonal biosensors could be created to provide accurate concentration and enantiopurity information for a mixture of enantiomers. We demonstrated this concept using a previously reported tyrosinamide aptamer[19] as described in Chapter 2, and showed that our orthogonal biosensors could accurately discriminate complex mixtures of L- and D-Tym. Our system rivals HPLC in accuracy, showing < 1.7% error for complex reaction mixture, and has the ability to work in near real-time. Additionally, this method demonstrates exceptionally high-throughput, allowing for mixtures to be screened in a few minutes as opposed to the > 17 hours that would be required using HPLC.

One hurdle to widespread adoption of this technology for enzyme evolution is the ability to obtain aptamers that are highly enantioselective. While it is often difficult to select aptamers with extremely high enantioselectivities (~10,000:1), we derived a mathematical equation that allows for aptamers with even modest enantioselectivity (i.e. ~10:1 for our model system) to be used for determining enantiopurity. This greatly increases the practicality of our method, as it is considerably easier to select for moderate enantioselectivity, even without the use of negative selections, as shown by our work in Chapter 3. The one limitation to the equation arises from the loss of information regarding concentration, since the equation can only provide a ratio of the two enantiomers. This limitation is acceptable because in screening of enantioselective enzyme mutants, a ratio of enantiomers is sufficient to determine the best mutant. Therefore, we envision that our approach will be amenable to screening the products of enzyme-mediated reactions.

Nucleic acid aptamers show tremendous potential with wide applicability in many fields due to their unrivaled specificity, low cost, and ability to be generated by *in vitro* selection. Many powerful new technologies are being improved through the use of these versatile affinity reagents. However, we recognize the greatest limitation of integrating

aptamers into applications such as our enantiopurity analysis method is the difficulties associated with obtaining sequences having a privileged architecture that can be easily converted to a biosensor. This obstacle is evident in researchers' continued use of the same handful of aptamers, which have already been established in their compatibility with a variety of different detection platforms. Our focus has shifted accordingly to address this growing problem through the design of new aptamer selection techniques.

Aptamer Biosensor Selection

Traditional bead-based selections, like FluMag, work very well for selecting affinity reagents, as demonstrated by our selection of the highly enantioselective (*S*)-CMA aptamer, BH6*t*. As shown in Chapter 3, this aptamer performs well as an affinity reagent, demonstrating excellent specificity and enantioselectivity (>100:1). However, attempts to convert BH6*t* into a structure-switching biosensor were unsuccessful. This is likely due to the fact that this biosensor format typically requires a large conformational change upon target binding, and small molecules like 2-CMA often produce only small perturbations in the structure of the aptamer. Therefore, the displacement event must be part of the selection process to ensure that the small change will displace the strand efficiently. This is a major problem within the field and is being vigorously pursued by many groups, including our own. We seek to address this challenge through development of methods for the direct selection of aptamer biosensors. This dissertation discusses our methods and future goals to advance new technologies in the selection and applications of aptamer biosensors for small molecules.

Towards these goals, we have explored several methods, both established and novel, for directly selecting the privileged displacement strand architecture required for structure-switching biosensors. We have found that while many traditional methods are successful in generating aptamers that can easily be converted to biosensors for larger

targets, such as proteins, they are far from generalizable and often fail when challenged with small-molecule targets. Incorporating the requirement of a large conformational change within the selection process for small-molecule-binding has shown promise for many groups. We tested two of the leading structure-switching SELEX methods to evaluate their ability to successfully select for a 2-CMA structure-switching biosensor. Unfortunately, our six different structure-switching SELEX trials were unsuccessful in producing a high affinity biosensor for 2-CMA. We hypothesize that this may be due to the well-known issues of structure-switching methods which rely on the use of a solid support, typically magnetic beads. We have found that magnetic bead-based selections generate high levels of nonspecific background and reason that this leads to poor enrichment, lower affinity aptamers, and/or failed selections. Therefore, our current efforts aim to design a generalizable structure-switching SELEX approach that does not require a solid support and will be compatible with targets of any size. We hypothesize that capillary electrophoresis (CE) will provide the level of partitioning and lack of matrix effects necessary for the rational design of a rapid and generalizable structure-switching SELEX method.

Bowser and coworkers have demonstrated the power of CE as a selection platform for traditional aptamers, obtaining high-affinity sequences in as little as one round of selection.[20] Several groups have worked on advancing CE-SELEX methods, but these methods all hinge upon the target being large enough to cause a change in electrophoretic mobility of the library upon binding. Unfortunately, small molecules are not of a sufficient size to induce a considerable migration shift upon binding to the library. Therefore, the generation of small-molecule aptamers requires a CE method that must be designed to allow for a significant change in mobility regardless of target size. We envision that an approach that requires a displacement event to occur upon binding will effectively modu-

late the mobility of bound and unbound library members and thus allow for the direct selection of small-molecule structure-switching biosensors.

As a proof of concept, our current work is focused on optimizing a novel CE structure-switching SELEX method for the aminoglycoside tobramycin. Tobramycin was chosen because, while it contains a high level of functionality, allowing for ease of selection, it is still small enough to result in little to no change in migration under normal CE-SELEX conditions. To induce a migration shift, we have incorporated a structure switching element that is dependent upon tobramycin binding. This is accomplished through the use of a short capture strand with bulky drag tag that is complementary to a short docking region contained in the random library. Upon binding to tobramycin, the target-bound library members that undergo a structural change that displaces them from the capture strand will be considerably smaller as a result of separation from the bulky drag tag. This results in a large change in the migration, allowing for efficient partitioning of bound and unbound library members. While use of streptavidin and PEG as drag tags failed to provide sufficient separation, preliminary work using latex microspheres has shown high levels of partitioning. In addition, the use of latex microspheres as the drag tag has resulted in lower background binding when compared to magnetic bead-based methods. We envision that this will provide a novel method to produce high affinity small-molecule structure-switching biosensors.

Our results provide insight into potential solutions to biosensor engineering, which is what we regard as currently the greatest limitation within the aptamer field. We anticipate that our extensive work into the direct selection of aptamer biosensors will help to drive an expansion of the known small-molecule aptamers that can function as displacement strand biosensors. Aptamer technology is at a crucial phase where new uses for aptamer biosensors are far outpacing the creation of new sensors for unique

targets. The integration of these new technologies therefore hinges upon the discovery of a robust, rapid, and generalizable method for selecting biosensors for new targets.

Upon realization of a generalizable structure-switching SELEX method, the future direction of this research is expected to drive enzyme evolution through the use of aptamer biosensors. We anticipate that our high-throughput enantioselective enzyme screening technique, described in Chapter 2, can be used to rapidly screen large enzyme libraries and determine the best mutant enzymes for nearly any reaction. This will greatly increase the speed of enantioselective enzyme evolution as well as the quality of the biocatalysts that are discovered.

References

(1) Reetz, M. T. Controlling the Enantioselectivity of Enzymes by Directed Evolution: Practical and Theoretical Ramifications. *Proc Natl Acad Sci U S A* **2004**, *101*, 5716-5722.

(2) Reetz, M. T.; Daligault, F.; Brunner, B.; Hinrichs, H.; Deege, A. Directed Evolution of Cyclohexanone Monooxygenases: Enantioselective Biocatalysts for the Oxidation of Prochiral Thioethers. *Angew Chem Int Ed Engl* **2004**, *43*, 4078-4081.

(3) Reetz, M. T. Directed Evolution of Enantioselective Enzymes as Catalysts for Organic Synthesis. *Adv. Catal.* **2006**, *49*, 1-69.

(4) Reetz, M. T. Laboratory Evolution of Stereoselective Enzymes: A Prolific Source of Catalysts for Asymmetric Reactions. *Angew. Chem. Int. Edit.* **2011**, *50*, 138-174.

(5) Schmidt-Dannert, C.; Arnold, F. H. Directed Evolution of Industrial Enzymes. *Trends Biotechnol* **1999**, *17*, 135-136.

(6) Bloom, J. D.; Labthavikul, S. T.; Otey, C. R.; Arnold, F. H. Protein Stability Promotes Evolvability. *Proc Natl Acad Sci U S A* **2006**, *103*, 5869-5874.

(7) Romero, P. A.; Arnold, F. H. Exploring Protein Fitness Landscapes by Directed Evolution. *Nat Rev Mol Cell Biol* **2009**, *10*, 866-876.

(8) Jung, S. T.; Lauchli, R.; Arnold, F. H. Cytochrome P450: Taming a Wild Type Enzyme. *Curr Opin Biotechnol* **2011**, *22*, 809-817.

(9) Gubitz, G.; Schmid, M. G. Chiral Separation by Chromatographic and Electromigration Techniques. A Review. *Biopharm. Drug Dispos.* **2001**, *22*, 291-336.

(10) Kang, J.; Wistuba, D.; Schurig, V. Recent Progress in Enantiomeric Separation by Capillary Electrochromatography. *Electrophoresis* **2002**, *23*, 4005-4021.

(11) Subramanian, G., *Chiral Separation Techniques: A Practical Approach. 3rd Ed.* Wiley-VCH: Weinheim, 2006.

(12) Zhu, Z.; Ravelet, C.; Perrier, S.; Guieu, V.; Roy, B.; Perigaud, C.; Peyrin, E. Multiplexed Detection of Small Analytes by Structure-Switching Aptamer-Based Capillary Electrophoresis. *Anal. Chem.* **2010**, *82*, 4613-4620.

(13) Drake, A. F.; Gould, J. M.; Mason, S. F. Simultaneous Monitoring of Ligh-Absorption and Optical Activity in the Liquid Chromatography of Chiral Substance. *J. Chromatogr. A* **1980**, *202*, 239-245.

(14) Sawada, M.; Takai, Y.; Yamada, H.; Hirayama, S.; Kaneda, T.; Tanaka, T.; Kamada, K.; Mizooku, T.; Takeuchi, S. Chiral Recognition in Host-Guest Complexation Determined by the Enantiomer-Labeled Guest Method Using Fast Atom Bombardment Mass Spectrometry. *J. Am. Chem. Soc.* **1995**, *117*, 7726-7736.

(15) Abato, P.; Seto, C. T. Emdee: An Enzymatic Method for Determining Enantiomeric Excess. *J. Am. Chem. Soc.* **2001**, *123*, 9206-9207.

(16) Reetz, M. T.; Hermes, M.; Becker, M. H. Infrared-Thermographic Screening of the Activity and Enantioselectivity of Enzymes. *Appl. Microbiol. Biot.* **2001**, *55*, 531–536.

(17) Schrader, W.; Eipper, A.; Pugh, D. J.; Reetz, M. T. Second-Generation MS-Based High-Throughput Screening System for Enantioselective Catalysts and Biocatalysts. *Can. J. Chemistry* **2002**, *80*, 626-632.

(18) Shabbir, S. H.; Regan, C. J.; Anslyn, E. V. Molecular Recognition and Self-Assembly Special Feature: A General Protocol for Creating High-Throughput Screening Assays for Reaction Yield and Enantiomeric Excess Applied to Hydrobenzoin. *P. Natl. Acad. Sci. USA* **2009**, *106*, 10487-10492.

(19) Vianini, E.; Palumbo, M.; Gatto, B. In Vitro Selection of DNA Aptamers That Bind L-Tyrosinamide. *Bioorgan. Med. Chem.* **2001**, *9*, 2543–2548.

(20) Yang, J.; Bowser, M. T. Capillary Electrophoresis-Selex Selection of Catalytic DNA Aptamers for a Small-Molecule Porphyrin Target. *Anal Chem* **2013**, *85*, 1525-1530.

APPENDIX A

TABULAR AND OMITTED DATA OF CHAPTER 2

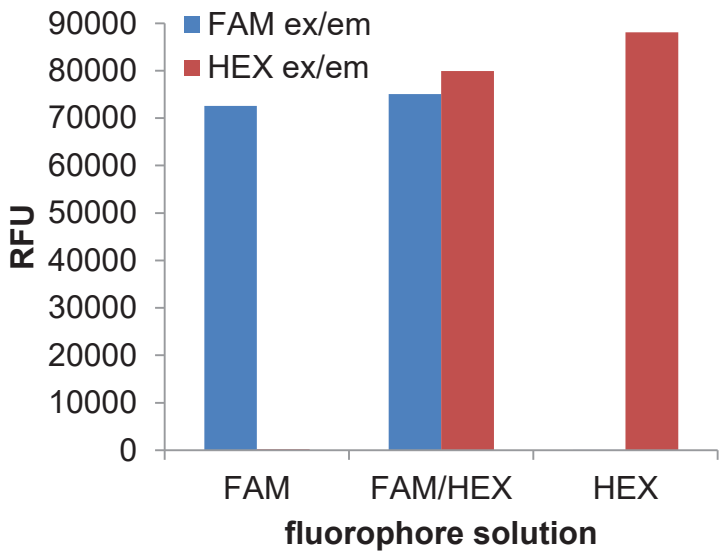

excitation/emission wavelength	FAM	FAM/HEX	HEX
490/520 nm	72589	75052	81
524/572 nm	228	79944	88050

Figure A1: Demonstrating orthogonality of FAM and HEX. Table shows values for relative fluorescence intensity.

Table A1: Tabular data for Figure 2.3

aptamer:complementary strand ratio	1000 μM	100 μM	10 μM	1 μM
1:3	15108	12750	12943	12773
1:2.5	24884	17645	13813	12986
1:2	42292	22919	16094	13748
1:1.5	79129	42881	20352	15382
1:1	82378	42292	22919	19112

Table A2: % Displacement in calibration curve experiments Figure 2.7a. Error represents the standard deviation of three independent trials.

% L-Tyr	% Displacement (D-DNA)	error (D-DNA)	% Displacement (L-DNA)	error (L-DNA)
100	23.36	0.43	0.00	0.29
99	22.83	0.46	0.15	0.27
98	22.99	0.57	0.84	0.36
97	23.02	0.59	0.95	0.44
96	22.71	0.63	1.54	0.33
95	22.60	0.66	1.99	0.25
94	22.14	0.58	2.08	0.37
93	22.22	0.75	2.36	0.33
92	21.40	0.46	2.73	0.26
91	21.67	0.48	3.06	0.34
90	21.59	0.80	3.57	0.37
80	20.96	0.89	6.22	0.19
70	19.01	0.58	8.30	0.17
60	17.47	0.42	10.50	0.25
50	16.27	0.46	12.07	0.15
40	13.24	0.44	12.41	0.33
30	10.12	0.30	14.13	0.27
20	7.22	0.29	14.77	0.29
10	4.16	0.40	16.30	0.44
9	3.90	0.38	16.51	0.44
8	4.32	0.42	16.60	0.62
7	3.68	0.34	17.24	0.54
6	2.87	0.40	16.78	0.79
5	2.67	0.21	16.87	0.42
4	2.47	0.40	16.68	0.30
3	1.01	0.27	17.29	0.31
2	0.94	0.45	17.26	0.43
1	0.56	0.29	17.41	0.38
0	0.00	0.41	17.99	0.49

Equations from non-linear fit analysis:

D-DNA %D = $\frac{52.2*x}{41.5+x}$ $R^2 = 0.9979$

L-DNA %D = $\frac{60.7*x}{39.0+x}$ $R^2 = 0.9989$

Table A3. Comparison of actual vs measured % L-Tym Figure 2.7b. Deviation is the difference between actual and measured and error is represents the standard deviation of three independent trials.

Actual % L-Tym	Measured % L-Tym	Error	Deviation
100	99.56	0.37	0.44
99	98.81	0.67	0.19
98	98.00	1.03	0.00
97	97.86	0.62	0.86
96	93.78	1.07	2.22
95	93.95	0.81	1.05
94	93.75	0.77	0.25
93	92.09	0.59	0.91
92	90.08	1.64	1.92
91	91.05	0.54	0.05
90	90.22	0.60	0.22
80	80.22	0.65	0.22
70	71.13	0.17	1.13
60	57.30	0.67	2.70
50	49.14	0.83	0.86
40	41.05	0.55	1.05
30	30.26	0.66	0.26
20	20.04	1.07	0.04
10	10.94	0.67	0.94
9	9.32	0.64	0.32
8	8.90	0.52	0.90
7	6.88	0.55	0.12
6	6.06	0.78	0.06
5	5.66	0.44	0.66
4	4.31	0.74	0.31
3	2.60	1.18	0.40
2	2.30	0.98	0.30
1	0.62	0.47	0.38
0	0.37	0.26	0.37

Table A4. Tabular data for % yield of L- and D-Tym in reaction monitoring experiments Figure 2.8.

Time (min)	10° L-Tym	10° D-Tym	20° L-Tym	20° D-Tym	30° L-Tym	30° D-Tym	50° L-Tym	50° D-Tym
2	-0.140	0	0	0	0	0	0	0
4	-0.216	0.756	0.60	2.28	0	0.82	1.79	0.27
6	-0.710	2.81	0	4.48	0	2.56	0.45	2.42
8	-0.76	4.22	1.20	6.85	1.74	4.10	1.39	5.50
10	-1.35	4.77	1.06	8.64	1.84	7.23	3.08	11.42
20	-2.45	12.03	3.14	18.87	3.55	16.90	5.42	29.23
30	-2.55	12.50	6.52	23.88	3.41	24.09	11.29	30.66
40	-2.08	17.52	2.91	31.34	4.00	28.55	9.57	41.36
50	0.847	27.34	4.80	31.03	4.46	33.16	9.28	53.14
60	-1.25	29.35	5.73	39.64	5.13	42.05	11.03	63.80
70	0.763	33.23	6.64	44.14	4.82	40.29	10.43	67.30
80	0.755	38.33	6.41	52.93	7.43	47.94	13.13	67.08
90	-1.85	35.56	6.23	48.76	8.40	48.38	12.79	68.02
100	-1.64	42.83	8.64	50.46	9.80	54.55	14.98	68.17
110	0.382	38.96	8.63	54.77	10.04	61.84	16.58	77.60
120	0.717	40.40	7.80	59.24	10.24	57.31	16.86	74.38

APPENDIX B

SPECTRAL DATA OF CHAPTER 3

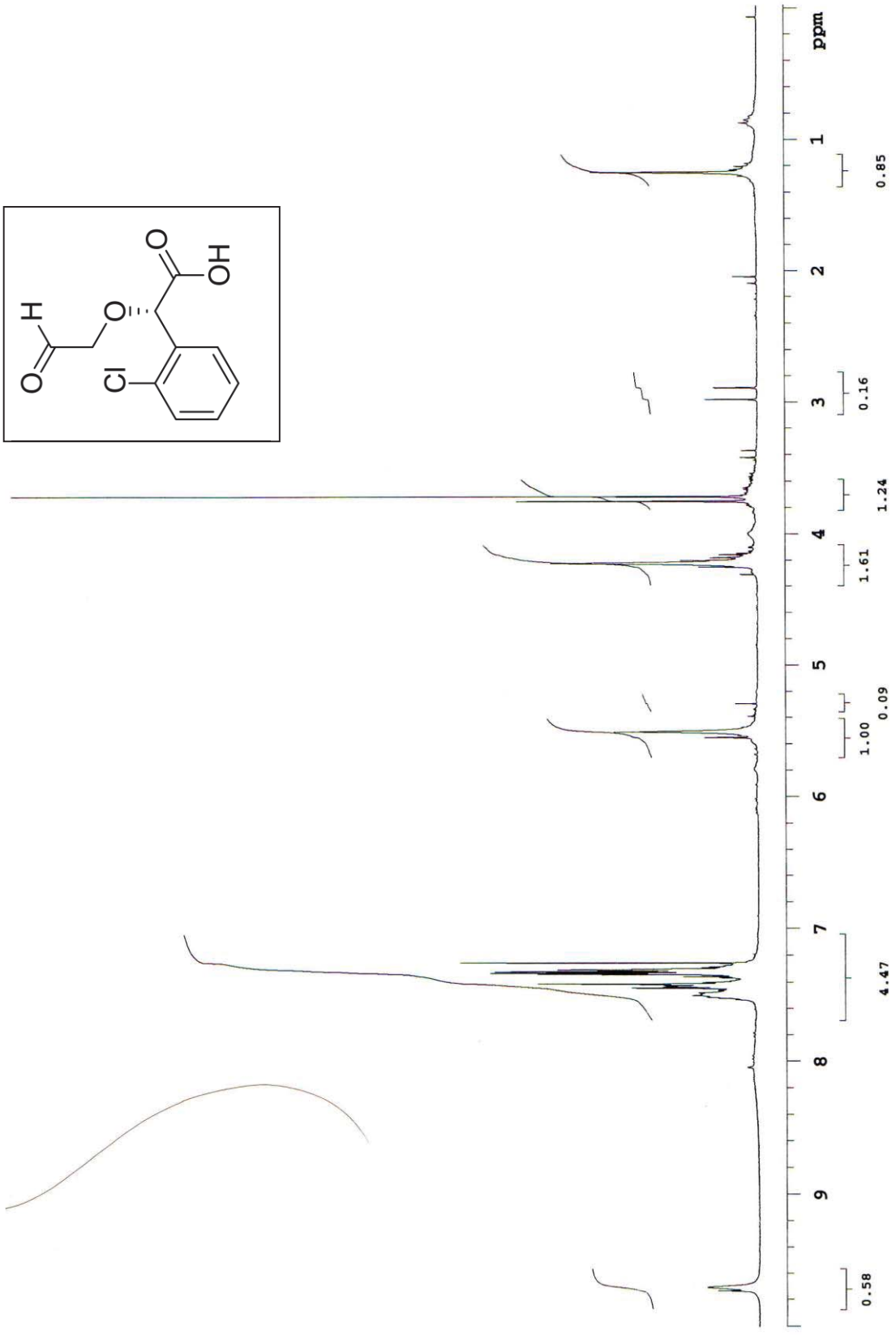
O
OH
O
H
O
Cl
ppm
1
2
3
4
5
6
7
8
9
0.85
0.16
1.24
1.61
1.00
0.09
4.47
0.58

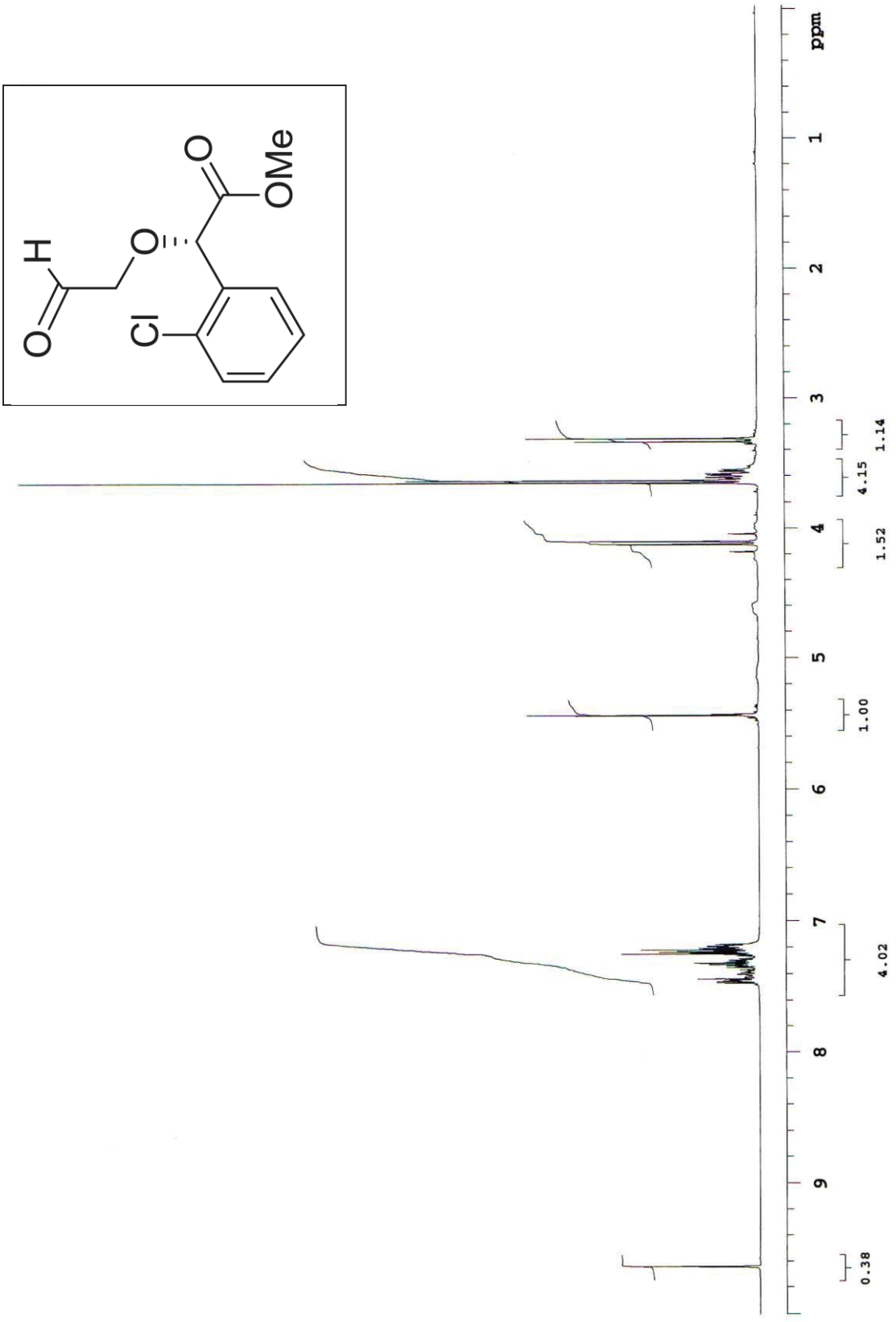
O
H
O
Cl
O
OMe
ppm
1
2
3
4
5
6
7
8
9
0.38
4.02
1.00
1.52
4.15
1.14

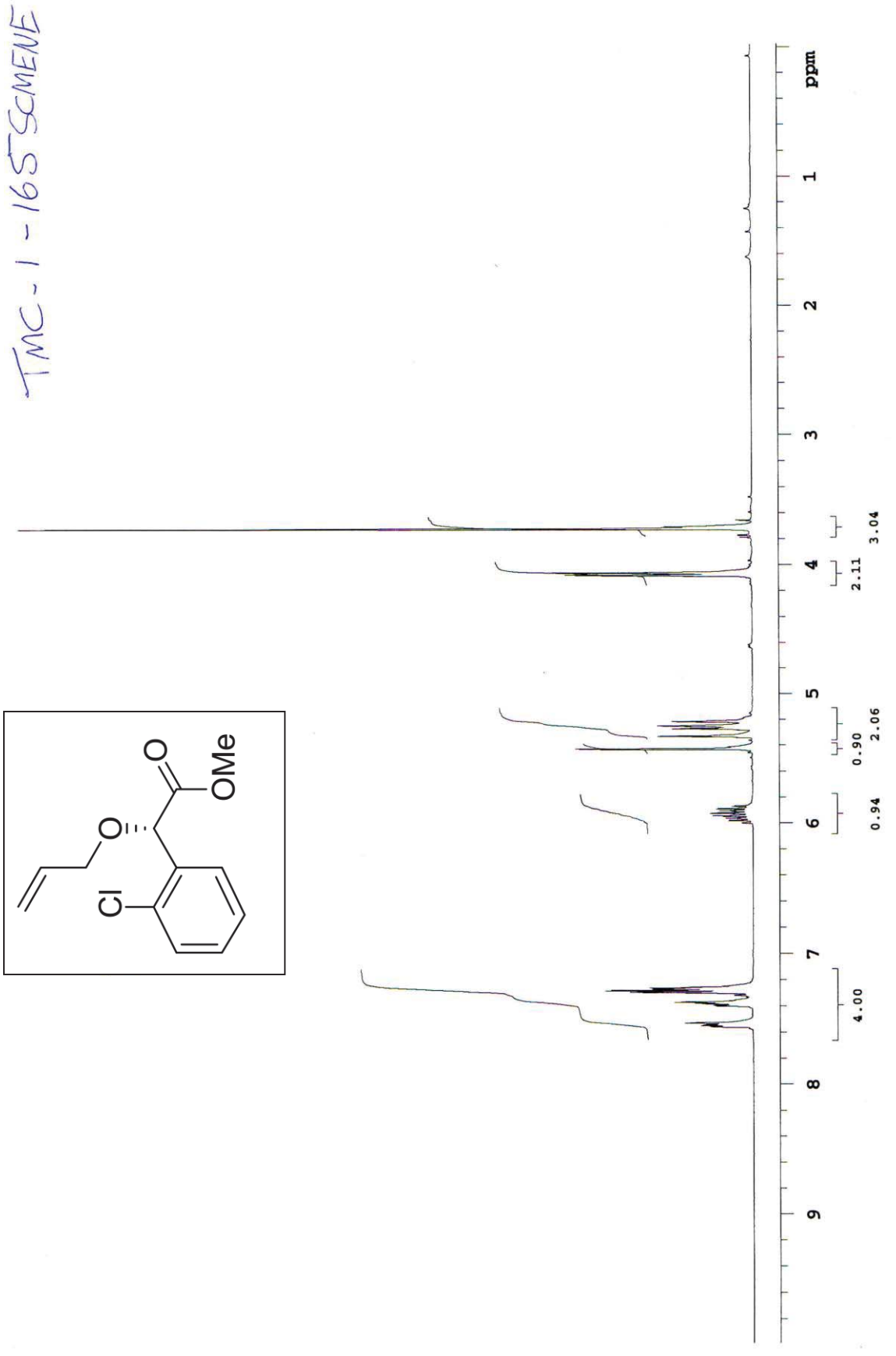
TMC-1-165 SCMENE
O
OMe
O
Cl
ppm
1
2
3
4
5
6
7
8
9
4.00
0.94
0.90
2.06
2.11
3.04

APPENDIX C

SPECTRAL DATA OF CHAPTER 4

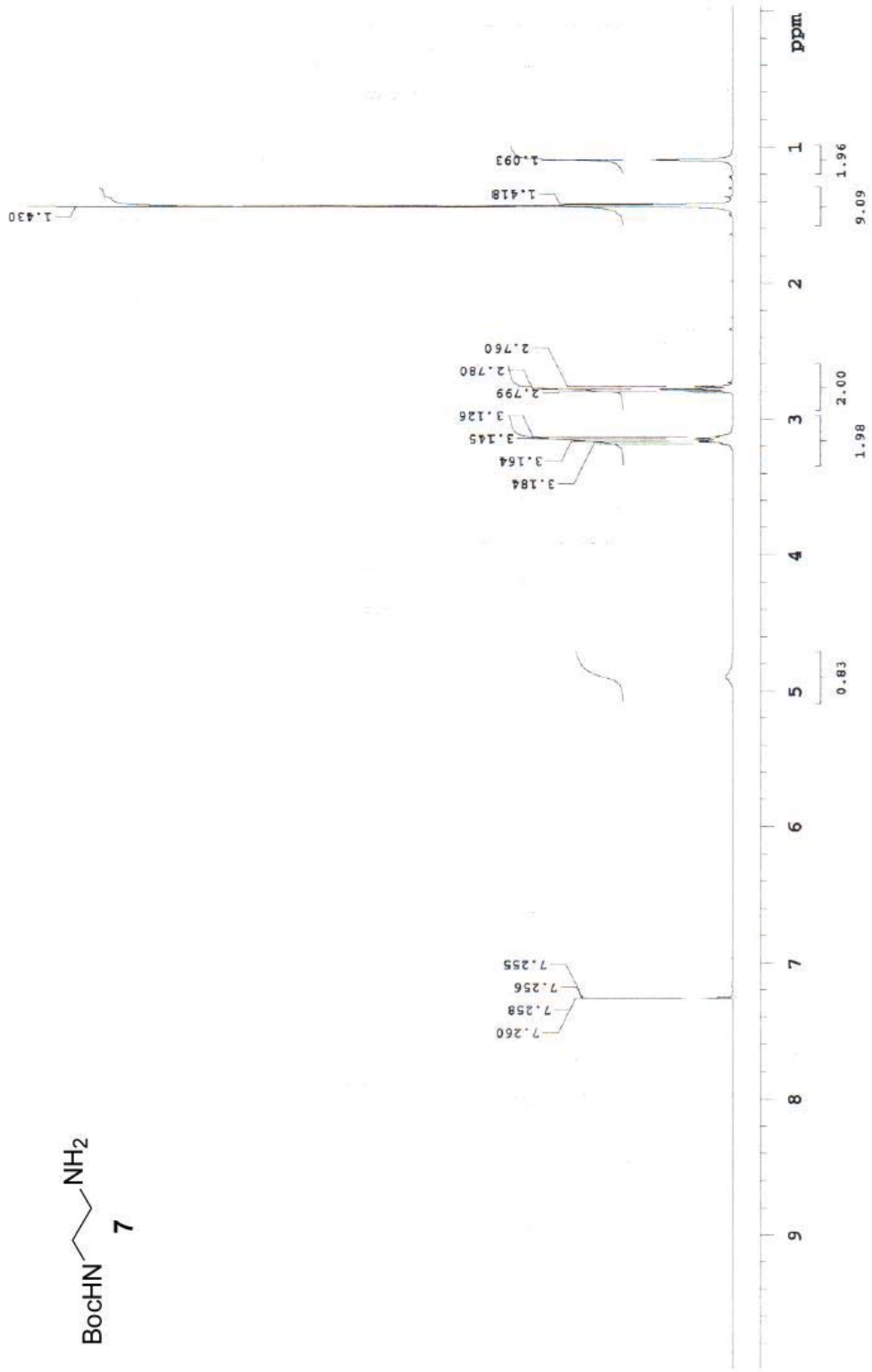
BocHN
NH2
7
ppm
1.430
1.418
1.093
2.760
2.780
2.799
3.126
3.145
3.164
3.184
7.255
7.256
7.258
7.260
1.96
9.09
2.00
1.98
0.83

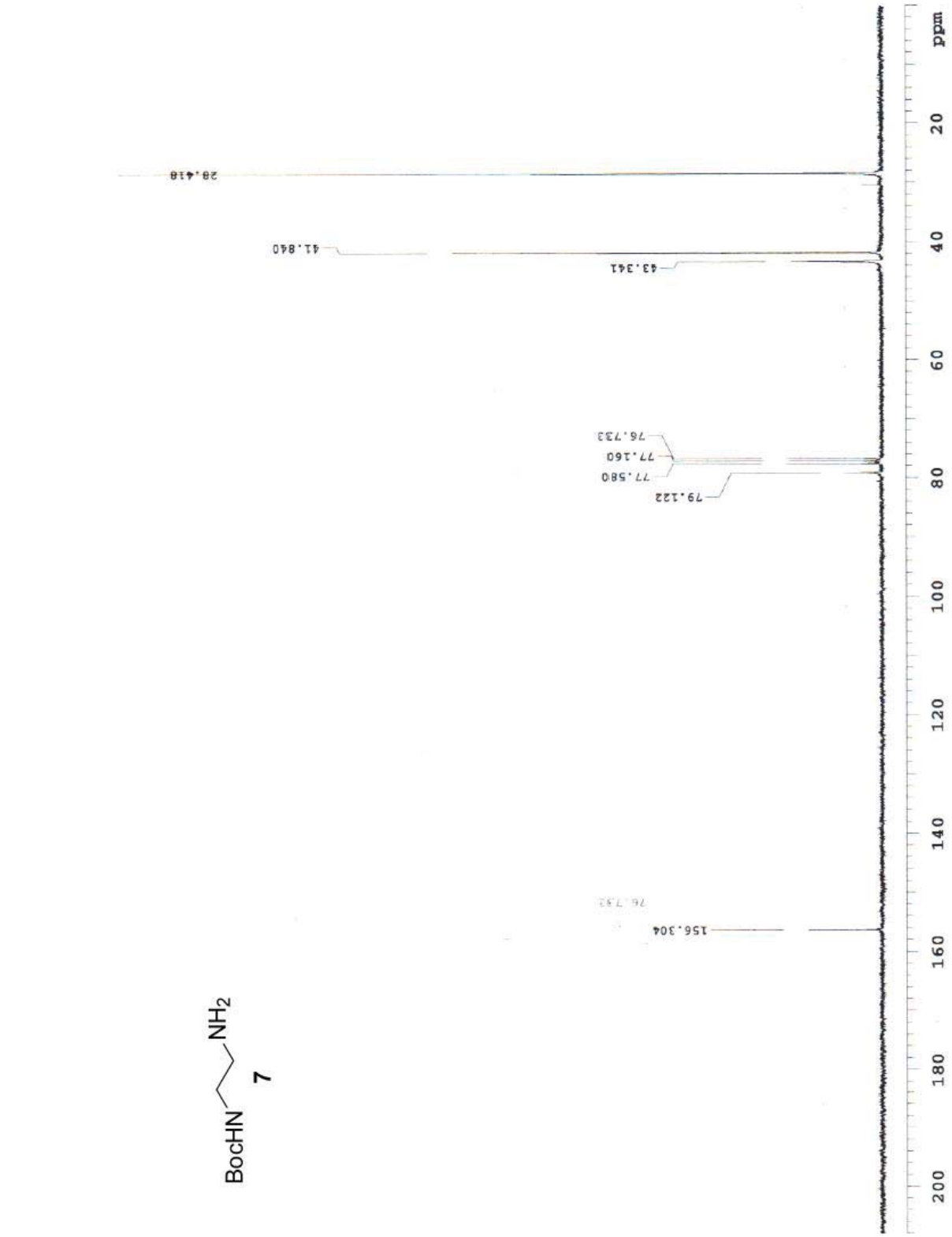
BocHN
NH2
7
156.304
79.122
77.580
77.160
76.733
43.341
41.840
28.418
ppm
200
180
160
140
120
100
80
60
40
20

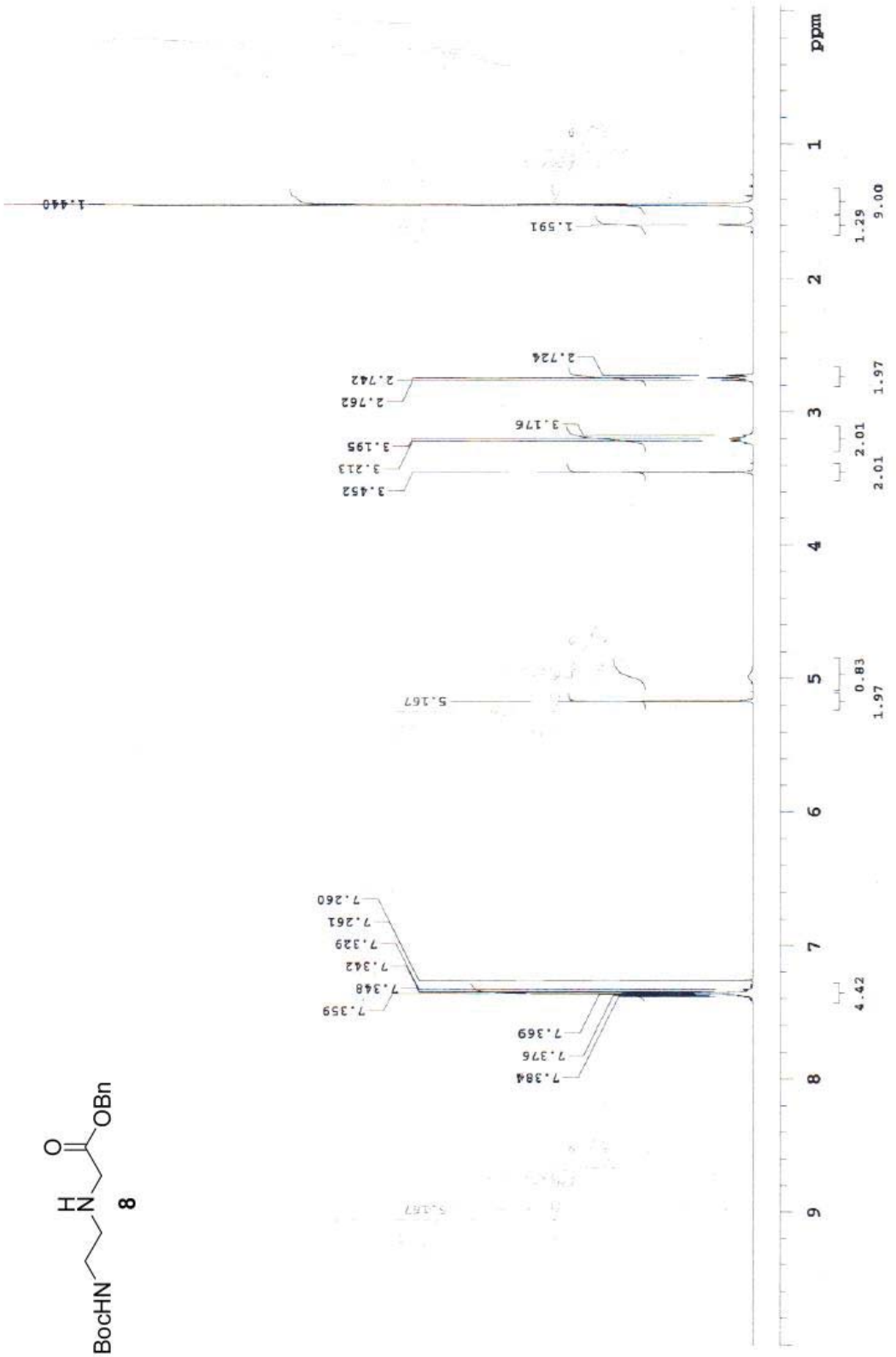
BocHN
N
H
O
OBn
8
1.440
1.591
2.724
2.742
2.762
3.176
3.195
3.213
3.452
5.167
7.260
7.261
7.329
7.342
7.348
7.359
7.369
7.376
7.384
ppm
1
2
3
4
5
6
7
8
9
9.00
1.29
1.97
2.01
2.01
0.83
1.97
4.42

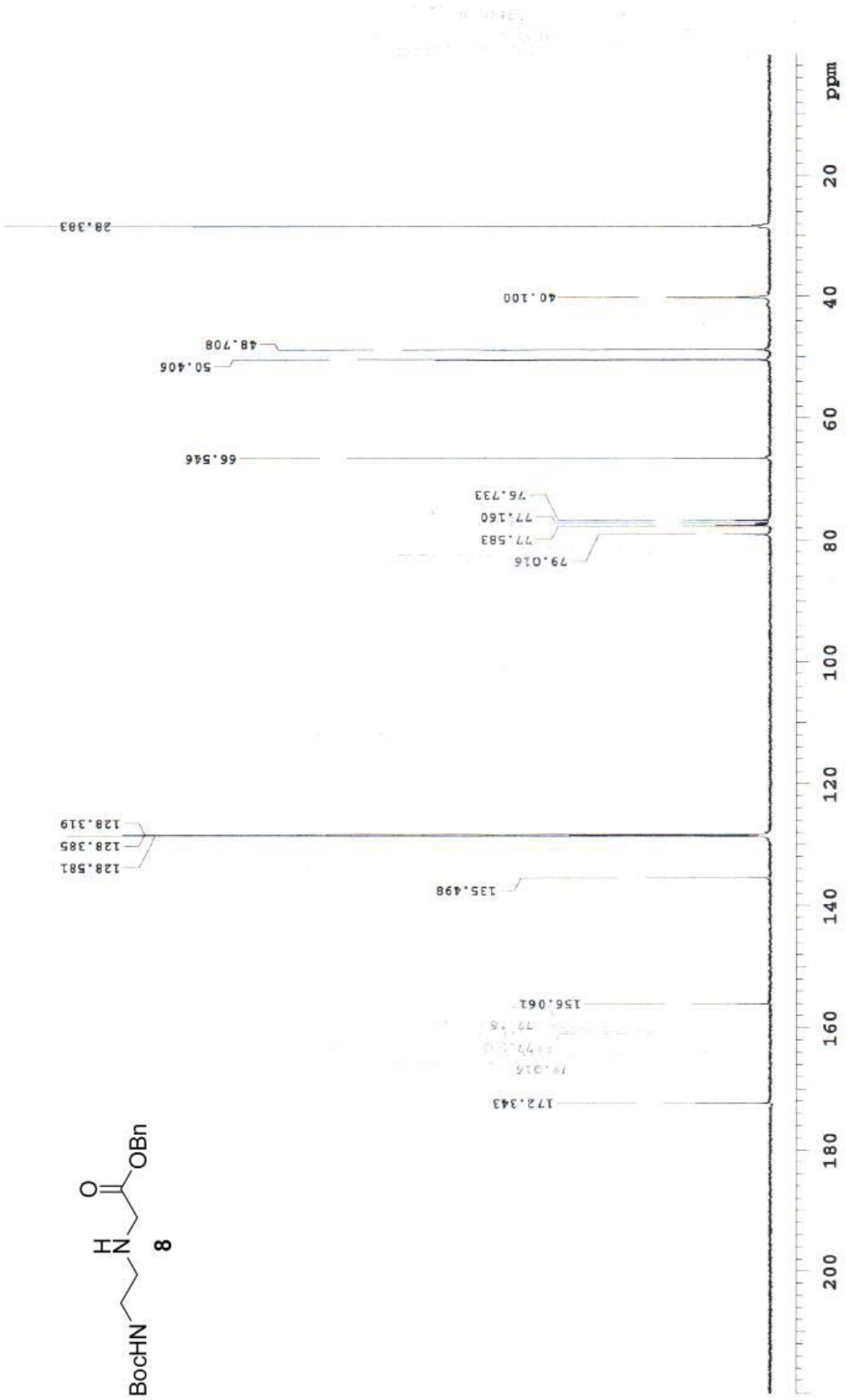
ppm
20
40
60
80
100
120
140
160
180
200
28.383
40.100
48.708
50.406
66.546
76.733
77.160
77.583
79.016
128.319
128.385
128.581
135.498
156.061
172.343
BocHN
N
H
O
OBn
8

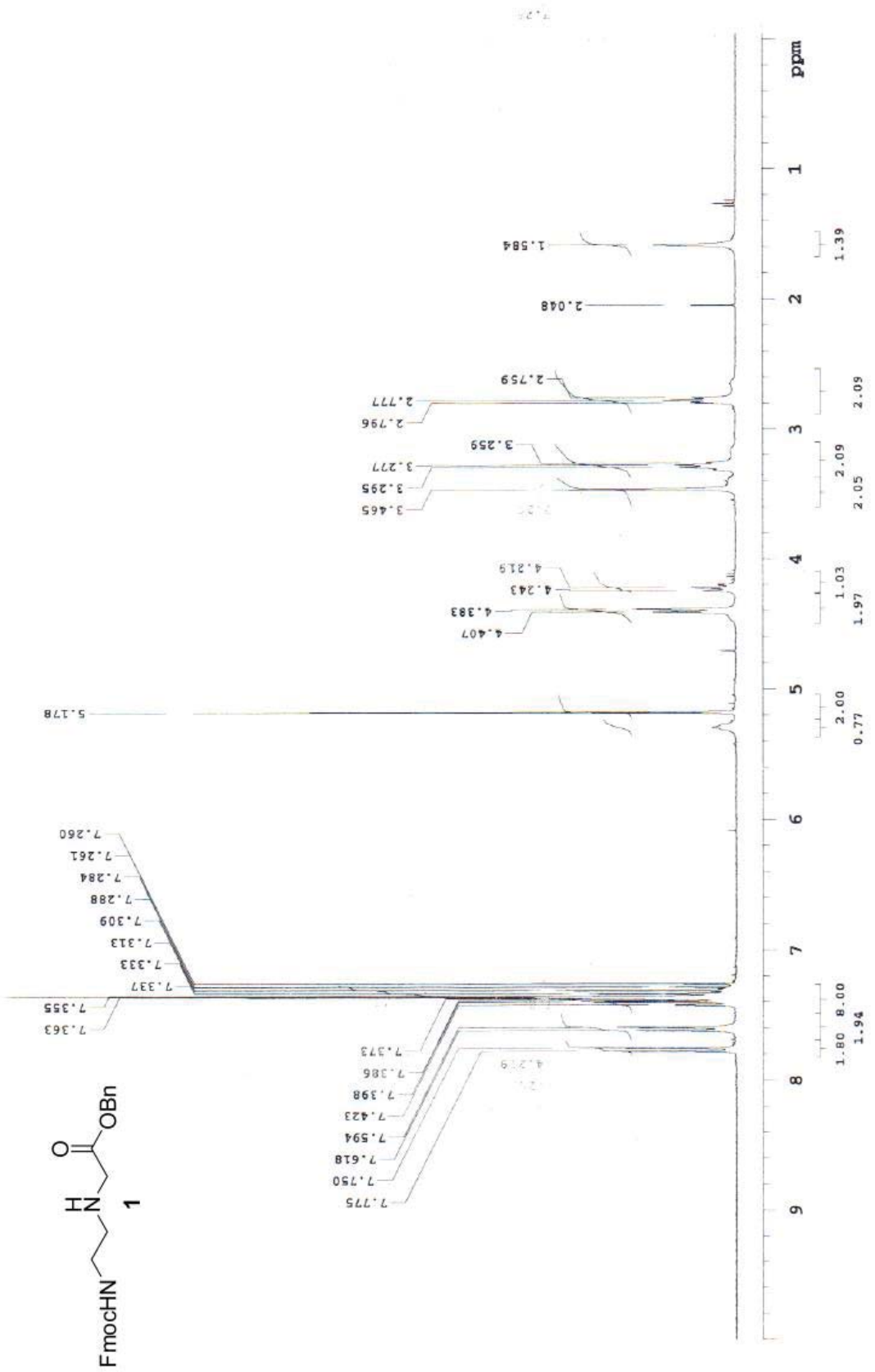
FmocHN
H
N
O
OBn
1
ppm
1.80
8.00
1.94
2.00
0.77
1.03
1.97
2.09
2.05
2.09
1.39
7.775
7.750
7.618
7.594
7.423
7.398
7.386
7.373
7.363
7.355
7.337
7.333
7.313
7.309
7.288
7.284
7.261
7.260
5.178
4.407
4.383
4.243
4.219
3.465
3.295
3.277
3.259
2.796
2.777
2.759
2.048
1.584

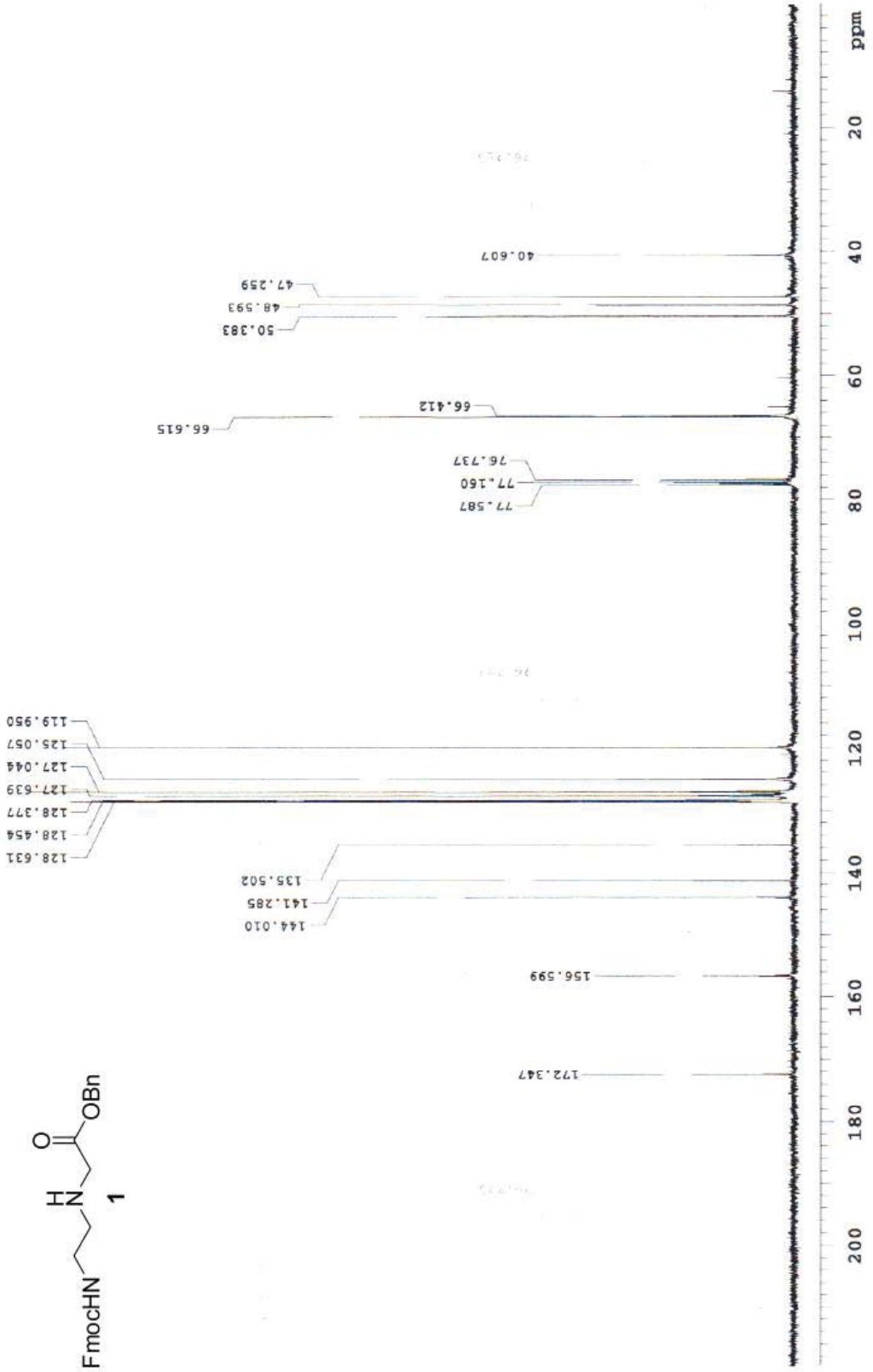
FmocHN
H
N
O
OBn
1
ppm
20
40
60
80
100
120
140
160
180
200
172.347
156.599
144.010
141.285
135.502
128.631
128.454
128.377
127.639
127.044
125.057
119.950
77.587
77.160
76.737
66.412
66.615
50.383
48.593
47.259
40.607